Northward drift of the Burma Terrane with India during the Cenozoic and implications for the India–Asia collision

Jan Westerweel, Pierrick Roperch, Zaw Win, Guillaume Dupont-Nivet

Northward drift of the Burma Terrane with India during the Cenozoic and implications for the India–Asia collision

Jan Westerweel[1], Pierrick Roperch[1]*, Zaw Win[2] and Guillaume Dupont-Nivet[1,3]

[1]Geosciences Rennes, CNRS, University of Rennes, Rennes, France

[2]Department of Geology, University of Shwebo, Shwebo, Myanmar

[3]Helmholz Center, GeoForschungZentrum (GFZ), Potsdam, Germany

PR, 0000-0002-1145-6658

*Correspondence: pierrick.roperch@univ-rennes1.fr

Abstract: The past location of the Burma Terrane during the convergence of the Indian and Asian tectonic plates is key to unravelling the regional geodynamic, palaeoenvironmental and palaeobiogeographical history of the eastern edge of the Himalayan orogen. Palaeomagnetic data provide the ability to constrain the location of the Burma Terrane, but it has been very difficult to find rocks with palaeomagnetic records of primary characteristic remanent magnetizations. We present here new palaeomagnetic results spanning the Paleocene to late middle Eocene within the Burma Terrane, complementing palaeolatitudes previously established from Late Cretaceous intrusive rocks and late middle Eocene sedimentary rocks. Our palaeomagnetic data indicate that the Burma Terrane remained at equatorial latitudes during the Paleocene and early Eocene, at a considerable distance from the South Asian margin. In addition, palaeomagnetic results from mid- to late Eocene sedimentary rocks yield a predominantly north–south orientation of the Burma Terrane over the past 45 Myr, showing that it was not part of the NW–SE-oriented Sundaland margin before its collision with India. Our results support collision models involving a Trans-Tethyan subduction system during the Late Cretaceous and early Paleocene. We propose that this system incorporated the Burmese volcanic arc and continental fragments of Argoland before drifting north with India towards Asia. The new palaeogeographical model considers a reduced amount of oblique subduction of the Indian plate below Burma during the Cenozoic. A possible source of sediments filling the thick Myanmar basins from the Gangdese belt during the Eocene supports the hypothesis of an India–Asia collision around ~50 Ma. The new palaeogeography supporting the formation of the Myanmar Cretaceous amber on an isolated Trans-Tethyan Arc is also a key element in discussions of the palaeobiogeographical evolution of the numerous faunas it contains.

Supplementary material: A detailed description of the palaeomagnetic data (location and magnetic properties) and an analysis of the U–Pb age data from detrital zircons are available at https://doi.org/10.6084/m9.figshare.c.7291282

The India–Asia tectonic convergence is widely regarded as the quintessential continental collision example for investigating deep to surface processes, the formation of an orogen (Fig. 1) of extensive scale and elevation, the propagation of regional thrust and strike-slip systems, as well as widespread volcanism and metamorphism. Despite over a century of focused geological research, the fundamental questions of how and when the collision occurred remain highly debated with ongoing and contentious discussions regarding the palaeogeography, chronology and significance of the various tectonic elements, arcs, sutures and exotic terranes during the convergence between the Indian and Asian plates (e.g. Royden *et al.* 2008; van Hinsbergen *et al.* 2011). Generally, three main classes of India–Asia collision models have been proposed (Kapp and DeCelles 2019). The first considers a simple collision involving a very large northward extent of India (aka 'Greater India') coming into contact with Asia during the Paleocene (e.g. Shen *et al.* 2001; Replumaz *et al.* 2010, 2013; Hu *et al.* 2015). The second involves a double collision: first, India with a Trans-Tethyan Arc and, second, India and this arc with the southern Asian margin (e.g. Jagoutz *et al.* 2015; Kapp and DeCelles 2019; Westerweel *et al.* 2019). The third invokes the northward drift of a continental fragment of Greater India involving the Tethys Himalayas coming into collision with the southern Asian margin during the Paleocene, before a final collision of India with Asia at the end of the Oligocene (van Hinsbergen *et al.* 2019). In these models, the Burma Terrane (hereafter BT; also called the West Burma Block, mainly lying within the borders of Myanmar today) was originally of minor importance in the elements used for the discussion,

From: Dupont-Nivet, G., Jonell, T. N., Dommain, R. and Clift, P. D. (eds) *Asian Geodynamics, Climate and Biodiversity*. Geological Society, London, Special Publications, **549**,
https://doi.org/10.1144/SP549-2024-18

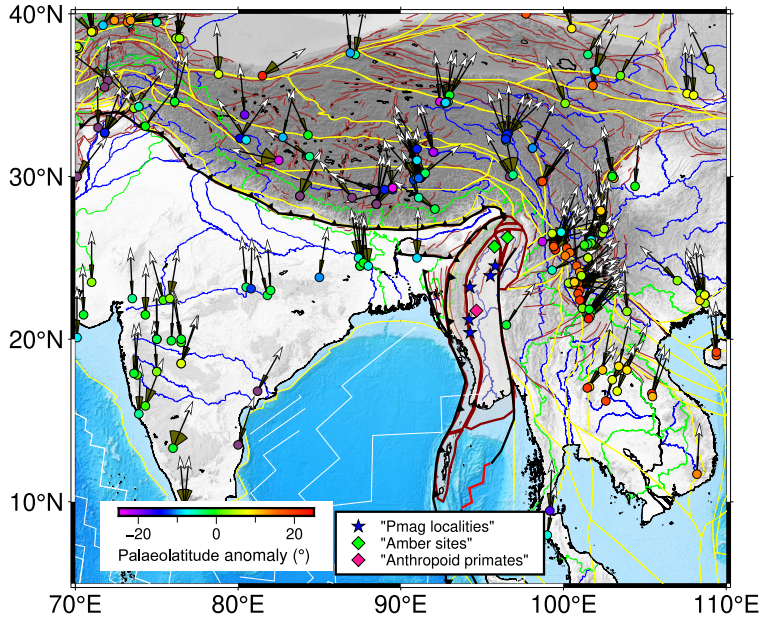

Fig. 1. Regional topographic map showing the location and tectonic setting of the BT. Palaeomagnetic sampling localities in the BT are indicated by blue stars while the two main amber localities are shown with green diamonds. The area where anthropoid primates (Khin Zaw *et al.* 2014; Jaeger *et al.* 2019) have been found in the middle Eocene Pondaung Formation is marked with a pink diamond. A summary of the palaeomagnetic results obtained from Cretaceous to Paleogene rocks from India and Asia is shown, with the angle of the white arrows relative to the north indicating tectonic rotations and associated errors at 95% (brown pie), while palaeolatitude anomalies are determined from the observed palaeomagnetic inclination relative to that expected from the global apparent polar wander curve (Torsvik *et al.* 2012). The length of the arrows is arbitrary. Figure created with GMT software (Wessel *et al.* 2019). Source: data mainly from the compilation of Cogne *et al.* (2013) and Tong *et al.* (2021).

although it constitutes the major microplate at the eastern edge of the Himalayan collision zone (Fig. 1).

Until recent palaeolatitude constraints were obtained from palaeomagnetic data (Westerweel *et al.* 2019, 2020), the BT was usually placed close to its present-day location (~20° N) and mostly considered stable throughout the India–Asia collision (e.g. Replumaz and Tapponnier 2003; Royden *et al.* 2008; Replumaz *et al.* 2013; van Hinsbergen *et al.* 2019), with the notable exception of the reconstructions of Rangin (2017), who suggested a very different plate configuration with the BT attached to India during the Paleogene. Subduction below the BT throughout the Cenozoic constituted an essential element to justify these traditional collision models, mainly because the magmatic Wuntho–Popa Arc (WPA) of the BT (Fig. 2) was usually seen as the eastward continuation of the Gangdese Arc on the Lhasa Terrane (e.g. Mitchell *et al.* 2012; Lin *et al.* 2019; Zhang *et al.* 2019*b*), while the Western Belt Ophiolite (WBO) west of the BT has been correlated with the Yarlung–Tsangpo Suture Zone (YTSZ; Mitchell 1993; Liu *et al.* 2016). However, palaeomagnetic data recently yielded southern hemisphere to near-equatorial latitudes for the BT from the early Late Cretaceous (~95 Ma) up until the late Eocene (~40 Ma) with a large magnitude rotation of ~60° clockwise sometime within this time window (Westerweel *et al.* 2019). These results showed that the BT was initially thousands of kilometres away from the Asian margin, and were interpreted as evidence that the BT was part of an isolated near-equatorial Trans-Tethyan subduction system before moving northward as part of the Indian Plate (Westerweel *et al.* 2019). These constraints are consistent with a two-stage India–Asia collision, with India first colliding with this Trans-Tethyan Arc sometime in the early Paleogene, and then colliding with Asia together, as previously proposed for the Kohistan Arc as part of the Trans-Tethyan Arc (Hall 2012; Jagoutz *et al.* 2015; Zahirovic *et al.* 2016; Westerweel *et al.* 2019).

This new palaeogeographic context for the BT on the Indian Plate during the Cenozoic calls for a fundamental revision of many aspects of the evolution of the BT, the eastern Himalayan collision zone and SE Asia. The required reappraisal of the correlations of geological belts along the East Asian margin

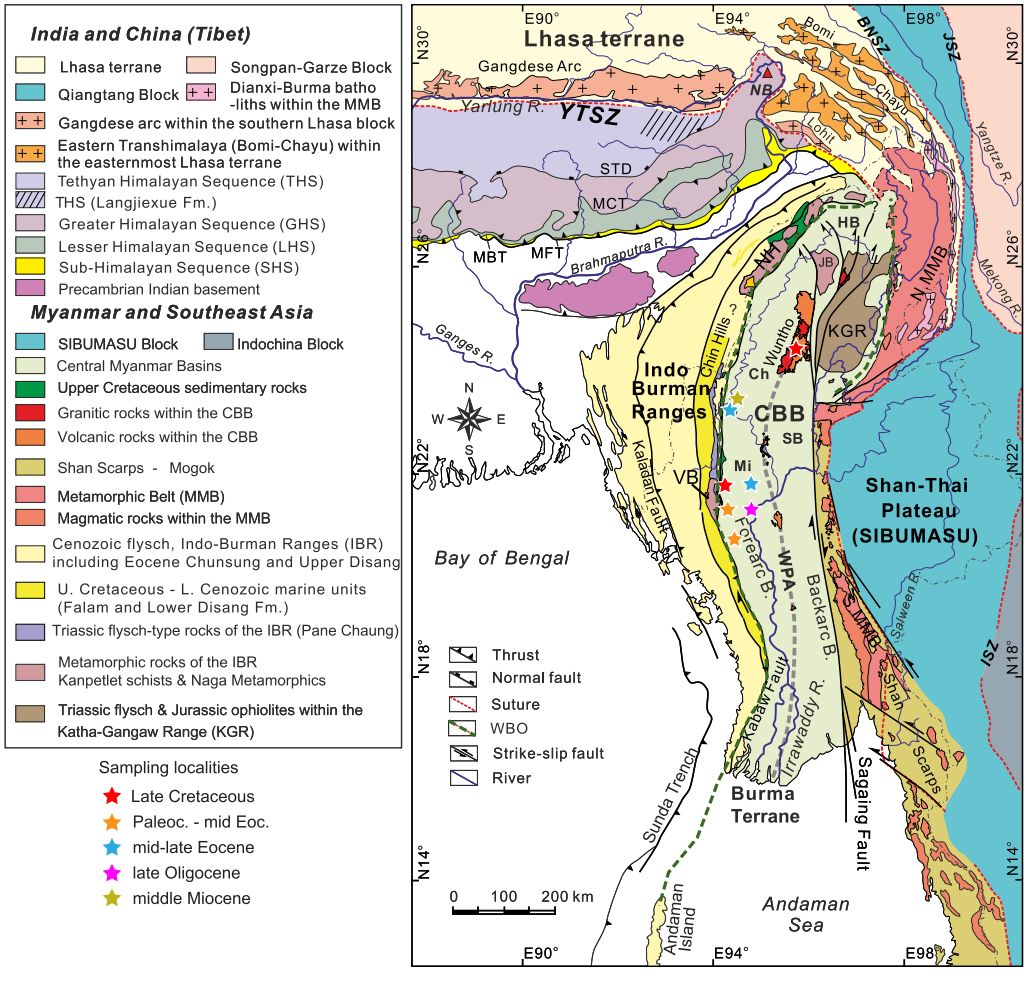

Fig. 2. Regional geological map centred on Myanmar. Abbreviations: CBB, Central Basins Block; Ch, Chindwin Basin; HB, Hukawng Basin; JB, Jade Belt Ophiolite; KGR, Katha–Gangaw Range; Mi, Minbu Basin; MMMB, Mogok–Mandalay–Mergui Belt; NH, Naga Hills; SB, Shwebo Basin; SF, Sagaing Fault; VB, Victoria Block; WBO, Cretaceous Western Belt Ophiolite; WPA, Wuntho–Popa Arc; YTSZ, Yarlung–Tsangpo Suture Zone. Stars mark the palaeomagnetic sampling localities of this study and Westerweel *et al.* (2019). Source: modified after Mitchell *et al.* (2012) and Najman *et al.* (2022).

and their role in the India–Asia collision raises new questions. The first concerns the timing of the different collisions and their palaeogeographical configurations. What were the timing and location of (1) the collision of India with the Trans-Tethyan Arc, (2) the incorporation of the BT on to the northward-moving Indian Plate and (3) the collision of the BT with Asia? Were there separate collisions or a joint collision of the BT and (Greater) India with Sibumasu on the Asian margin (Licht *et al.* 2013, 2019; Zhang *et al.* 2019*a*; Cai *et al.* 2020)? Westerweel *et al.* (2019) suggested a collision of the BT with Sumatra before 40 Ma. A more western position of the BT closer to India during its northward motion was later proposed (Westerweel *et al.* 2020; Morley *et al.* 2021) based mainly on geological constraints because palaeomagnetism does not provide information on longitude. More data are needed to test these models and propose alternatives. Another major unknown in the tectonic history of the BT is its origin. Contrasting Gondwanan, Cathaysian (i.e. correlated to Indochina) or intra-oceanic origins have been postulated (Metcalfe 2013; Sevastjanova *et al.* 2016; Yao *et al.* 2017; Licht *et al.* 2020; Morley *et al.* 2020) and several reconstructions have suggested that the BT is a part of Argoland, a collection Gondwanan crustal ribbon fragments that rifted from northern Australia in the Late Jurassic (Heine *et al.*

2004; Advokaat and Van Hinsbergen 2024). Licht *et al.* (2020) have given a detailed overview of these different origins for the BT and attempted to reconcile these apparently contrasting origins by proposing that the BT consists of several rifted crustal fragments of different origins that were amalgamated when the BT was part of the Trans-Tethyan subducting system. The origin and palaeogeographical evolution of the BT are also of considerable interest for understanding Asian palaeobiodiversity, because it hosts one of the most diverse and largest known records of Cretaceous fossil biota preserved in amber, including plants, insects and vertebrates. These amber biota commonly display a Gondwanan affinity, providing further evidence that the BT travelled across the Tethys Ocean (Grimaldi *et al.* 2002; Poinar 2018; Rasnitsyn and Öhm-Kühnle 2018; Zheng *et al.* 2018; Jouault *et al.* 2021).

To answer these questions, we have obtained new Campanian–Maastrichtian, latest Paleocene–middle Eocene, late Eocene, middle Oligocene and middle Miocene palaeomagnetic data from the BT in addition to our previously published early Late Cretaceous and late Eocene data (Westerweel *et al.* 2019). This dataset provides new constraints on the latitudinal motion of the BT, which are then compared to relevant geological data and integrated into a plate tectonic model of the India–Asia collision, allowing us to discuss the geodynamic, palaeoenvironmental and sedimentary provenance data of the BT and the eastern Himalayan orogen in this updated context.

The BT

Tectonic regime

The BT is the major microplate at the southeastern margin of the Himalayan orogen, comprising much of western and central Myanmar (Figs 1 and 2). Its present tectonic regime is controlled by hyper-oblique convergence between India and Indochina, resulting in a general northward transcurrent motion. Subduction of the Indian Plate is well illustrated by the present distribution of seismicity from southern Myanmar to the Imphal valley in Northeastern India (Mon *et al.* 2023).

The BT northward motion has been largely accommodated by large-scale dextral strike-slip displacements along the Sagaing Fault, which separates the BT from the Shan Plateau (Sibumasu) to the east (e.g. Mitchell 1981; Vigny *et al.* 2003; Tun and Watkinson 2017; Panda *et al.* 2018). In addition to the dextral displacement along the Sagaing Fault, geodetic data demonstrate dextral movement between India and Sibumasu across the Indo-Burman Ranges (IBR), mainly via the Churachandpur-Mao and Kaladan Faults (Panda *et al.* 2020) and the Kabaw Fault (Oryan *et al.* 2023). However, there is no quantitative estimate of dextral displacements between India and the BT across the IBR in the geological record (Rangin *et al.* 2013; Rangin 2018). It is important to note that the Sagaing Fault juxtaposes two crustal blocks with very different geological histories, and crustal and lithospheric characteristics. Tibetan crustal flow around the Eastern Himalayan Syntaxis, well observed in geodetic data, may have given the convexity to the west of the Sagaing Fault (Rangin *et al.* 2013). The entire region in between the Sagaing Fault (Bertrand *et al.* 2001), the Gaoligong–Mogok belt (Zhang *et al.* 2012) and the Ailao Shan–Red River shear zone (Leloup *et al.* 1995) is also affected by numerous well-dated shear zones (Wang *et al.* 2022), demonstrating the eastward extrusion of the Indochina block. Palaeomagnetic studies (Tong *et al.* 2013; Li *et al.* 2018) have shown that the largest clockwise rotations occurred in the vicinity of the Tengchong and Baoshan blocks (Fig. 1), with a minor clockwise rotation of the Indochina block.

Dextral displacement along the Sagaing Fault has been estimated to be about 400 km since the Neogene from observations of structural geology (Maung 1987; Socquet *et al.* 2006; Maurin and Rangin 2009; Rangin *et al.* 2013; Morley 2017*b*). Late Eocene palaeomagnetic constraints from the BT show that it moved northward from a near-equatorial position with little rotation, suggesting that the dextral displacement of the BT relative to Indochina may have exceeded 2000 km (Westerweel *et al.* 2019). These late Eocene palaeomagnetic data further suggest that there has been no significant relative latitudinal motion between the BT and India since the Eocene and within the uncertainties of the palaeomagnetic method, suggesting that strike-slip motions were almost exclusively concentrated on the eastern margin of the BT (Westerweel *et al.* 2019), along a precursor of the Sagaing Fault (Morley and Arboit 2019; Morley *et al.* 2020).

Geological setting

The BT is a composite terrane with several ophiolite belts (Searle *et al.* 2023) and we refer readers to Morley *et al.* (2021) for a more complete description. The WBO divides the BT longitudinally along the eastern border of the IBR and extends from the Andaman Sea in the south to the Hukawng Basin in the north (Fig. 2). The western sub-terrane of the BT is constituted by the IBR. The eastern sub-terrane, east of the WBO, consists of an early Late Cretaceous magmatic arc (the WPA) with thick, mainly Cenozoic, sedimentary basins on both sides of the magmatic belt. To simplify the discussion, we refer to this subterrane as the Central Basins Block (CBB). Previously published palaeomagnetic results are only

from the main CBB units, including the WPA (Westerweel *et al.* 2019), and upper Eocene sedimentary sections from the Chindwin Basin west of the WPA (Westerweel *et al.* 2020), described in more detail below.

The WBO (Fig. 2) includes ophiolites exposed in the Chin Hills of Myanmar and the Nagaland ophiolites of India with late Early Cretaceous zircon ages (Acharyya 2007, 2015; Liu *et al.* 2016; Singh *et al.* 2017; Morley *et al.* 2020). Liu *et al.* (2016) determined a mid-Cretaceous U–Pb zircon age of *c.* 127 Ma from the Kaleymyo ophiolite. Singh *et al.* (2017) reported $^{206}Pb/^{238}U$ zircon ages of 116.4 $\pm$ 2.2 Ma and 118.8 $\pm$ 1.2 Ma from the Nagaland–Manipur ophiolite just across the border in eastern India.

The eastern boundary of the BT with Sibumasu is mainly defined by the presently active dextral Sagaing Fault (Socquet *et al.* 2006), which cuts and displaces the eastern ophiolite belt (Tagaung–Myitkyina belt) and central ophiolite belt (Jades belt) (Morishita *et al.* 2023; Searle *et al.* 2023). The western boundary of Sibumasu is characterized by the Mogok–Mandalay–Mergui Belt (MMMB), which is predominantly composed of Paleogene granulite–upper amphibolite facies rocks and Jurassic to Cretaceous S-type intrusions with generally negative zircon ε_{Hf} values (Lamont *et al.* 2021). These rock types contrast sharply with the concurrent formation of thick Cenozoic sedimentary basins within the BT. The MMMB records several major metamorphic events, beginning with a latest Cretaceous to early Paleocene phase of metamorphism and partial melting. This was followed by a phase of high-temperature metamorphism during the late Eocene–Oligocene, interpreted as reflecting the collision of India with the Asian margin (Searle *et al.* 2007, 2017, 2020; Lamont *et al.* 2021). This high-grade metamorphic phase was followed by an Oligocene to early Miocene phase of rapid exhumation and uplift related to strike-slip deformation and extrusion of the MMMB (Bertrand *et al.* 2001; Bertrand and Rangin 2003). This exhumation phase is coeval with the timing of southeastward extrusion of the MMMB from the Eastern Himalayan Syntaxis and a significant phase of uplift and exhumation across the Eastern Himalayan orogen in the early Miocene (Vannay *et al.* 2004; Godin *et al.* 2006; Kellett *et al.* 2013; Garzanti 2019; Haproff *et al.* 2019; Najman *et al.* 2019).

At the northern edge of the Sagaing Fault, the Jade Belt is exposed (Fig. 2) and has an unclear emplacement age (Yui *et al.* 2013; Searle *et al.* 2017, 2023). A possible correlation of the Jade Belt with sporadic dismembered ophiolitic fragments on the trace of the Sagaing Fault has been proposed, together forming the Central Belt Ophiolite (Htay *et al.* 2017).

Despite being located to the east of the main segment of the Sagaing Fault, we consider the Katha–Gangaw Range and the Tagaung–Myitkina belt (Mitchell 2018*e*) as also belonging to the CBB block and the MMMB to be the main eastern boundary of the BT. The Myitkina belt has been relatively displaced relative to the CBB during the late Neogene.

The Sagaing Fault merges to the south with the transtensional setting of the Andaman Sea. The Andaman Sea represents a complex and partitioned back-arc basin, which developed mostly in the Neogene along the oblique convergent margin of Sibumasu and Sundaland (Morley 2017*a*; Morley *et al.* 2023).

The western limit of the BT is the present-day subduction system of the oceanic Indian Plate north of Sumatra (Andaman trench) merging to the north with the Indo-Burman fold and thrust belt (Steckler *et al.* 2016) related to the underthrusting of India below the BT. This western boundary of the BT with the Indian continent (Fig. 2) mainly consists of thick Mesozoic to Cenozoic flysch deposits and associated ophiolitic material (Maurin and Rangin 2009; Bannert *et al.* 2012; Rangin *et al.* 2013; Rangin 2018; Morley *et al.* 2020). Transpressional deformation has affected the IBR since the late Oligocene–early Miocene (Rangin 2018).

Traditionally, the IBR are divided into an Inner and Outer Wedge (United Nations 1978; Maurin and Rangin 2009). The Outer Wedge consists of a fold and thrust belt deforming the Neogene clastic sediments of the Bengal fan with Himalayan affinity (Allen *et al.* 2008; Rangin 2018; Najman *et al.* 2020). By contrast, the geology of the Inner Wedge is more complex; it comprises in its Core the Pane Chaung Formation, Kanpetlet Schists and the WBO. The first two have potentially separate histories from the CBB as part of the Mount Victoria Block (Fig. 2). The origin and emplacement direction of the WBO remain unclear, as well as its role in the potential suture of the CBB with the Mount Victoria Block (see reviews in: Searle *et al.* 2017; Morley *et al.* 2020).

The northern boundary of the BT coincides with the southeastern boundary of the Eastern Himalaya Syntaxis. The Naga Hills ophiolite belt is usually represented as the northwestern limit of the BT. However, a narrow belt of thrust slices in the southeastern boundary of the Imphal valley and west of the Naga Hills, known as the Naga Schuppen Belt, can be traced to the south with the IBR of central Myanmar.

BT basement

Many aspects of the complex geological history of the BT remain controversial (Morley *et al.* 2021).

Because the BT is longitudinally divided by the WOB, we first describe the basement within the IBR and then in the CBB.

The IBR are an asymmetric mountain chain with Triassic turbidites of the Pane Chaung Formation and the Kanpetlet Schists mainly outcropping on its eastern side in Myanmar and forming the Core including the WBO (Brunnschweiler 1966; Morley *et al.* 2020). The youngest U–Pb detrital zircon ages (DZA) of numerous samples (Sevastjanova *et al.* 2016; Yao *et al.* 2017) are consistent with the Late Triassic fossils (Halobia) found in Pane Chaung sandstones.

In the Chin Hills, the Kanpetlet Schists within the IBR Core are often considered to correspond to metamorphosed Triassic turbidites of the Pane Chaung Formation (United Nations 1978; Maurin and Rangin 2009; Bannert *et al.* 2012; Morley *et al.* 2020), as evidenced by similar U–Pb age distributions (Zhang *et al.* 2017*a*; Najman *et al.* 2020). Metamorphism in the greenschist facies is described by Socquet *et al.* (2002) but the age of this metamorphism is not well constrained. Recent zircon fission-track data do not provide a clear constraint on the age of the metamorphism (Najman *et al.* 2020, 2022). The relationship between the Triassic flysch and the Kanpetlet Schists remains unresolved (Mitchell 2018*f*) as the metamorphic Kanpetlet Schists are mainly in fault contact with the Pane Chaung (Brunnschweiler 1966).

U–Pb age distributions of the Pane Chaung Formation were initially correlated with Sibumasu, suggesting that the BT was part of Indochina before the Mesozoic (Sevastjanova *et al.* 2016). More detailed results from recent studies show that the main age peaks of detrital zircons in the Pane Chaung Formation more closely resemble the Langjiexue Formation of the NE Himalayan collision zone, suggesting that it was deposited adjacent to the Indian area of northern Gondwana (NW Australia) during the Triassic (Cai *et al.* 2016, 2020; Wang *et al.* 2016; Yao *et al.* 2017; Naing *et al.* 2023). This correlation suggests that the BT separated from Gondwana after the Triassic.

Several studies have proposed that the Mount Victoria Block forms a separate tectonic unit, which was accreted to the CBB east of the WBO in the Cretaceous or early Paleogene time (Acharyya 2007; Barber and Crow 2009; Metcalfe 2013; Rangin *et al.* 2013; Searle *et al.* 2017; Zhang *et al.* 2017*b*). In the northern IBR, the oldest unit is the Naga metamorphics with Early Ordovician schists and gneisses (Aitchison *et al.* 2019). In contrast to the Kanpetlet Schists and although usually interpreted as part of the IBR, the Naga Metamorphics overthrust the ophiolite belt to the west.

Exposures of the oldest known units within the CBB are limited and are mainly found in the least-documented areas of northern Myanmar, in the Jade Belt (Mitchell 2018*b*), Kumon Range (Mitchell 2018*c*) and Katha–Gangaw Range rocks (Mitchell 2018*e*; Aung *et al.* 2022). Mitchell (2018*d*) describes several lines of evidence suggesting a crust with a continental component; however, detrital zircons from the internal drainage system of the WPA lack evidence for an older crustal component (Licht *et al.* 2020). East of the WPA, the Minwun Range rocks crop out along the northern strands of the Sagaing Fault, consisting of metamorphic rocks, serpentinites and deformed carbonate rocks (United Nations 1978; Thein 2015; Mitchell 2018*g*). Some of these middle Permian carbonate rocks have been described as having a putative Cathaysian affinity (i.e. correlated with warm-water faunas of Indochina and the South China Block; Oo *et al.* 2002; Barber and Crow 2009; Ueno *et al.* 2016), suggesting that at least part of the BT is Cathaysian in origin (Licht *et al.* 2020). However, this affinity is challenged by new descriptions of middle Permian fusulines from the Thitsipin Formation of the Shan State (Zhang *et al.* 2020). Permian fusilinids are widely distributed around the Paleotethys and limited palaeomagnetic data constrain the Permian palaeogeography of all the blocks that are now merged in Asia. Furthermore, the relationship of these carbonate rocks to the BT remains ambiguous (Metcalfe 2017), as they are located in strands of the Sagaing Fault and thus could represent displaced slices of Sumatra or Sibumasu.

The WPA

During the early Late Cretaceous, subduction began along the present-day western margin of the BT, evidenced by the timing of ophiolite formation and emplacement of the WOB dated to ~125–130 Ma (Fareeduddin 2015; Liu *et al.* 2016; Htay *et al.* 2017; Singh *et al.* 2017; Zhang *et al.* 2017*a*). This was followed by magmatic activity along the WPA, and the low latitude determined from palaeomagnetic data was interpreted as evidence that the BT was a segment of a near-equatorial Trans-Tethyan Arc (Westerweel *et al.* 2019). The main phase of magmatic activity in the WPA was dated to ~110–90 Ma in the Wuntho Ranges (Licht *et al.* 2020). On the one hand, dated volcanic rocks suggest sporadic activity in the Late Cretaceous, late Eocene and Neogene (Crow and Khin Zaw 2017). On the other hand, U–Pb DZA from the CBB sedimentary basins have been interpreted as evidence of a more continuous magmatic activity, assuming that the Paleogene sedimentary rocks were mainly derived from the WPA (Wang *et al.* 2014; Licht *et al.* 2016).

Late Cretaceous–Paleogene sedimentary basins

The thick sedimentary basins within the BT are the main source of information on the geological evolution of the BT since the Late Cretaceous. These basins have been the subject of numerous studies in recent years, particularly with the contribution of extensive databases on U–Pb DZA (Allen *et al.* 2008; Wang *et al.* 2014; Licht *et al.* 2016, 2019; Zhang *et al.* 2017*a*, 2019*a*, 2023; Najman *et al.* 2020, 2022; Arboit *et al.* 2021; Naing *et al.* 2023). However, observations from sedimentary basins in the northern IBR (the belt of Schuppen in the Nagaland region of India) are rarely compared with those from the BT central basins (Aitchison *et al.* 2019; Betka *et al.* 2021; Ding *et al.* 2022).

The CBB hosts numerous basins in so-called forearc and back-arc locations, subdivided by the WPA (Fig. 2), as the Myanmar margin was traditionally considered to be the consequence of the subduction of the Indian oceanic crust resulting in the formation of an accretionary wedge, a forearc basin and a volcanic arc (Gardiner *et al.* 2015). Although this subdivision between forearc and back-arc might be outdated, we will retain the terms in the following for clarity. The Burmese back-arc basins comprise the northern Shwebo Basin and the southern Pegu Basin. Throughout the Neogene, both basins were characterized by southward-prograding fluvial and tidally influenced estuarian sequences; the Paleogene and older deposits of the back-arc basins remain poorly documented (Bender 1983; Pivnik *et al.* 1998; Khin and Myitta 1999; Thein and Maung 2017). In the Quaternary, the Shwebo and Pegu basins were unconformably overlain by the fluvial Irrawaddy Formation (Bender 1983).

The Burmese forearc is usually divided into two main basins, the southern Minbu (or Salin) Basin and the northern Chindwin Basin, separated by a topographic high called the Pondaung Ranges (Bender 1983; Rangin 2018; Licht *et al.* 2019; Westerweel *et al.* 2020). The sedimentary rocks of the Burmese forearc were sampled for this study, so their stratigraphy is described in more detail below.

The oldest sedimentary rocks are the poorly exposed Paung Chaung limestones unconformably overlying the BT basement in the CBB and IBR, which are Aptian–Cenomanian in age based on biostratigraphic constraints from *Orbitolina* fossils, planktonic foraminiferas and ammonites (Mitchell 2018*g*). The Paung Chaung sedimentary rocks contain clasts of the IBR basement (e.g. Pane Chaung Formation, Western Belt ophiolite and Kanpetlet Schists). Mitchell (2018*a*) infer that these *Orbitolina* limestones were widely deposited over most of the BT.

The Minbu Basin

The Albian–Maastrichtian Kabaw Formation is the second Cretaceous unit of the Burmese forearc, consisting of marine limestones, mudstones, sandstones and occasional conglomerates with clasts derived from the Kanpetlet Schist (Bender 1983; Cai *et al.* 2020). Detrital zircons from the Kabaw Formation yielded maximum depositional ages of ~82–70 Ma (Cai *et al.* 2020). Tuffaceous layers (later simply referred to as 'tuffs') overlying amber-bearing sediments of the Kabaw Formation near the village of Tilin yielded an age of 72.1 ± 0.3 Ma (Zheng *et al.* 2018).

The Cretaceous sequence is unconformably overlain by a Paleocene to middle Eocene sedimentary sequence (United Nations 1978; Cai *et al.* 2020), which consists of four sedimentary formations. Unfortunately, these formations have poorly defined stratigraphic boundaries and only sporadic geochronological constraints. The first formation within this sequence is the Paunggyi Formation (or Paunggyi conglomerates), which consists of conglomerates, tuffs, sandstones, mudstones and limestones (United Nations 1978; Cai *et al.* 2020). The Paunggyi Formation covers most of the Paleocene, based on foraminifera (United Nations 1978), ~65 Ma dated tuffs and ~70–62 Ma maximum depositional U–Pb DZA (Cai *et al.* 2020). The Paunggyi Formation grades into the finer-grained Laungshe Formation, composed of marine mudstones and rarer sandstones (Cai *et al.* 2020). This formation is poorly dated; foraminifera fossils yield a lower to middle Eocene age at one locality north of the town of Kyauktu, with occasional Paleocene components identified at other localities (Bender 1983). The middle Eocene Tilin Formation sandstones and the fine-grained marine shales of the Tabyin Formation (Bender 1983) have few geochronological constraints, from foraminifera (Nagappa 1959) and one sample yielding a maximum depositional age (MDA) of ~47 Ma based on U–Pb DZA (Cai *et al.* 2020); with MDA determined by calculating the weighted mean of the youngest normally distributed age population of three or more grains that overlap within 2σ uncertainty (Dickinson and Gehrels 2009). Due to its proximity to the IBR, this Cretaceous to middle Eocene sedimentary sequence is relatively more deformed than younger deposits. Locally, there are complex folding and numerous faults, although continuous sequences following the general north–south trend of the Burmese forearc occur as well (Fig. S1; Pivnik *et al.* 1998). The sedimentary provenance of the Cretaceous to middle Eocene formations was interpreted to be derived from both volcanic arc and recycled uplifted sedimentary sources (Cai *et al.* 2020), as indicated by U–Pb age distributions with ~100–60 Ma peaks and positive ε_{Hf} values similar to the

WPA (Gardiner *et al.* 2015, 2017; Zhang *et al.* 2017*b*; Lin *et al.* 2019), as well as significant populations of pre-Cretaceous zircons with age spectra similar to the BT basement (Allen *et al.* 2008; Naing *et al.* 2014; Najman *et al.* 2020).

Overlying the Cretaceous to middle Eocene units is the late middle Eocene Pondaung Formation, dated at ~40 Ma (Khin Zaw *et al.* 2014; Jaeger *et al.* 2019). The Pondaung Formation is composed of westward directed, fluvio-deltaic sediments with a continental upper member containing carbonate-bearing palaeosols, stacked channels, fossil vertebrates and freshwater gastropods. The upper Eocene Yaw Formation overlies the Pondaung Formation and consists of shallow-marine, fine-grained sediments containing nummulites. All subsequent formations, the lower Oligocene Shwezetaw, middle Oligocene Padaung and upper Oligocene Okhmintaung Formations, conformably overlie the Yaw Formation (Pivnik *et al.* 1998; Gough *et al.* 2020). They are composed of fluvio-deltaic to increasingly marine deposits towards the south (Bender 1983; Gough *et al.* 2020). These units are followed by the lower to middle Miocene fluvio-deltaic sediments of the Pyawbwe, Kyaukkok and Obogon Formations. Finally, the middle Miocene–Pliocene Irrawaddy Formation unconformably covers the sequence in most of the CBB lowlands.

The Chindwin Basin

The sedimentary sequence of the Chindwin Basin is similar to the Minbu Basin up until the upper Eocene Yaw Formation, which is shallow marine in the Minbu Basin, but is characterized by shallow marine to estuarian/fluvio-deltaic sediments in the Chindwin Basin (Licht *et al.* 2019; Gough *et al.* 2020).

The Yaw Formation is overlain by the exclusively fluvial deposits of the upper Oligocene Tonhe Formation and lower Miocene Letkat Formation (Bender 1983; Licht *et al.* 2019; Westerweel *et al.* 2020). In contrast to continuous deposition in the Minbu Basin, the late Eocene to early Miocene of the Chindwin Basin is characterized by large depositional hiatuses, which are contemporaneous with basin-wide unconformities. These were linked to major uplift and exhumation phases in the northernmost BT, which eventually entered the Eastern Himalayan collision zone during the late Oligocene–early Miocene (Westerweel *et al.* 2020).

Overlying the Letkat Formation are the thick Natma and Shwethamin formations, which consist of non-fossiliferous fluvial sandstones interbedded with abundant palaeosols (United Nations 1978; Bender 1983). These formations are middle Miocene age, younger than the Letkat Formation, which has yielded ~19–16 Ma maximum depositional ages from U–Pb DZA and Apatite Fission Track detrital ages (Westerweel *et al.* 2020), and older than the overlying base of the Irrawaddy Formation (locally called Mingin Gravels), which has yielded 14–11 Ma fossiliferous mammals (*Tetralophodon* cf. *Falconeri, Bunolophodon* cf *pandionis, Bunolophodon angust. palaeoindicus*, *Listriodon pentapotamiae*) coeval to the Chinji fauna of Pakistan (Bender 1983). Similar to the Minbu Basin, the Irrawaddy Formation ends the Chindwin Basin sedimentary sequence; see Jonell *et al.* (2022) for a detailed description of the Neogene evolution of the CBB basins.

Hukawng Basin

The Hukawng Basin, located north of the Chindwin basin and east of the Naga Hills, is an understudied region (Mitchell 2018*a*). The basin is bounded on the NW by the Naga Metamorphic Complex, on the north and NE by the Upper Triassic Nyu Hka Formation and minor ophiolite fragments, and on the east by metamorphic rocks of the Kumon Range. To the SW, the Jade Mines Uplift forms the basin's southern border (Mitchell 2018*a*). The Hukawng Basin is home to the most famous Cretaceous Kachin amber mines, whose fossil assemblages provide insight into the origin of the BT (Grimaldi *et al.* 2002). The sedimentary sequence that the amber mines excavate consists mainly of occasionally folded clastic sedimentary rocks, alternated with thin limestone beds, and abundant carbonaceous material (Grimaldi *et al.* 2002; Cruickshank and Ko 2003). Mitchell (2018*a*) indicates that the Cretaceous limestones in the amber mines are also equivalent to the Albian–Cenomanian Namakauk Limestone found east of Pinlebu on the western flank of the WPA, to the *Orbitolina* Limestone in the jade mines areas, to the *Orbitolina* limestone widespread in the Tagaung–Myitkyina belt and to the Paung Chaung Limestone in the IBR. It is of significant importance to note that an additional significant amber site (Khamti amber) is situated to the SW of the Jade Mines Uplift. The ambers are found in *Orbitolina* limestone and interbedded sandstones, which are slightly older (~109 Ma; Xing and Qiu 2020) than the Kachin amber site.

Sedimentary deposits of the IBR

Thermochronological data from the central IBR (Najman *et al.* 2020, 2022) provide late Oligocene–early Miocene zircon U–Th/He (ZHe) cooling ages in late Cretaceous to Eocene sandstones and late Middle Miocene apatite fission track ages, indicating a major exhumation phase of the mountain range that began mainly during the latest Oligocene–Miocene, with a possible precursory event in the late Eocene (Najman *et al.* 2020). The late

Cretaceous to Eocene basins have thus been strongly eroded, especially considering that the resetting of the ZHe ages of the detrital zircons is due to burial, suggesting the IBR was covered by a thick late Cretaceous to Eocene cover. U–Pb DZA in late Cretaceous (Falam Fm) to Eocene sandstones (Chunsung Fm) from the IBR share a similar distribution to those of the BT central basins, mainly suggesting the same source for the sediments (Allen *et al.* 2008; Naing *et al.* 2014, 2023; Najman *et al.* 2022).

Methods

Palaeomagnetic sampling

Conventional palaeomagnetic core samples were obtained from several localities with different rock types in the Burmese forearc in western Myanmar, in both the Minbu and Chindwin Basins (Fig. 2 and Fig. S1). In addition, six sites were sampled in Paleogene sediments of the IBR along the road from Kalemyo to Falam and six sites were drilled in ophiolitic rocks. The locations of all sites are given in a supplementary Google Earth archive (Supplementary Material S1). Sampling and sample orientation were done using standard palaeomagnetic field equipment and procedures with both magnetic and sun compasses. In the field, it is often difficult to identify a specific formation in the Paleocene–Eocene sections.

Palaeomagnetic sampling in the Minbu Basin

Three sites were located around the Sidotkaya Township (ST), in the southwestern Minbu Basin in close proximity to the IBR. Local faulting is present in this area due to its proximity to the IBR (Fig. S1). Site ST01 is a ~65 m thick section of sandstones and mudstones of the Paleocene to lower Eocene Laungshe Formation, exposed in a ~200 m long roadcut to the SE of Sidoktaya. The sedimentary bedding is largely continuous, following the general north–south trend and eastward dip of the basin, and the section is not overturned based on observations from cross-bedding orientation. However, small-scale thrusts are present at the bottom of the section. Site ST01 corresponds to 44 collected samples in grey-brown to blue-grey mudstones (Fig. 3a). Eleven samples were drilled at site ST02 in grey and white tuffs of the Paunggyi Formation, near the dam north of Sidoktaya (Fig. 3b). The tuffs at this location are undoubtedly contemporaneous with those, farther south, recently dated by Cai *et al.* (2020) and Gentis *et al.* (2023) at ~66–61 Ma. This provides unquestionable evidence for an early Paleocene age for the upper part of the Paunggyi Formation. Unlike ST01, the bedding of this site is not parallel to the general trend of the basin, and is internally deformed with local folding and faulting. Nearby site ST02, no significant results were obtained in the deformed and weathered siltstones of site ST03.

Eight sites were sampled around the town of Saw (SW) farther to the north in the Minbu Basin. Similar to the Sidoktaya sites, local faulting is present here due to proximity to the IBR (Fig. S1). Sampled rocks here are grey mudstones and siltstones. Two of these sites (SW02 and SW04) are from the Laungshe Formation, similar to site ST01. SW02, located south of the Laungshe town, is a long continuous type section of the Laungshe Formation, from which we collected 31 samples (Fig. 3c). It follows the general ~north–south trend and eastward dip of the Minbu Basin, although there are occasional small-scale faults and slumps that were avoided during sampling. SW04 is a smaller site of 10 samples. It is located along a strike-slip fault (Fig. S1). Siltstones of the Laungshe Formation were also sampled at two nearby sites, SW01 and SW05, which did not provide palaeomagnetic results. Two other sites near Saw are from the Tilin Formation (SW03 and SW07). SW03 is located on the same strike-slip fault as SW04, and provided eight samples. By contrast, site SW07 again follows the general ~north–south trend of the basin with a steep eastward dip and yielded 14 samples. Site SW08, with 16 samples, was obtained in the younger Tabyin Formation. It also follows the general ~north–south trend of the basin. At site ST04, 13 samples were drilled in vertical beds of the Tabyin Formation near a fault zone.

The 20 samples taken at site SW09 were drilled in mudstones of the Upper Cretaceous Kabaw Formation that is exposed farther north, near the town of Tilin, close to the Kabaw fault. Amber mines proximal to Tilin have yielded geochronological constraints from dated tuff layer (72.1 ± 0.1 Ma, in Zheng *et al.* 2018) that provided Campanian–Maastrichtian ages for the Kabaw Formation in this area, consistent with maximum depositional ages from Cai *et al.* (2020). Site SW09 is therefore probably Campanian–Maastrichtian in age, although it should be noted that the exact coordinates of these Tilin amber mines have not been published.

Our samples from the upper middle Eocene Pondaung Formation were collected from nine sites (PD01–PD09) with variable bedding around the towns of Bahin and Pangan. These are part of the Pondaung Ranges, an anticlinal topographical high on the northern edge of the Minbu Basin separating it from the Chindwin Basin. The 89 samples from these nine sites consist of fine-grained red to brown and purple palaeosols (Fig. 3d).

In the ~north–south trending rollover anticline of the Yenangyat–Chauk Thrust (Pivnik *et al.* 1998) at the Tantkyitaung Pagoda, west of Bagan (Supplementary Fig. S1), we sampled three sites (TP) in the middle Oligocene Padaung Formation, two on the western limb of the anticline near the fold axis

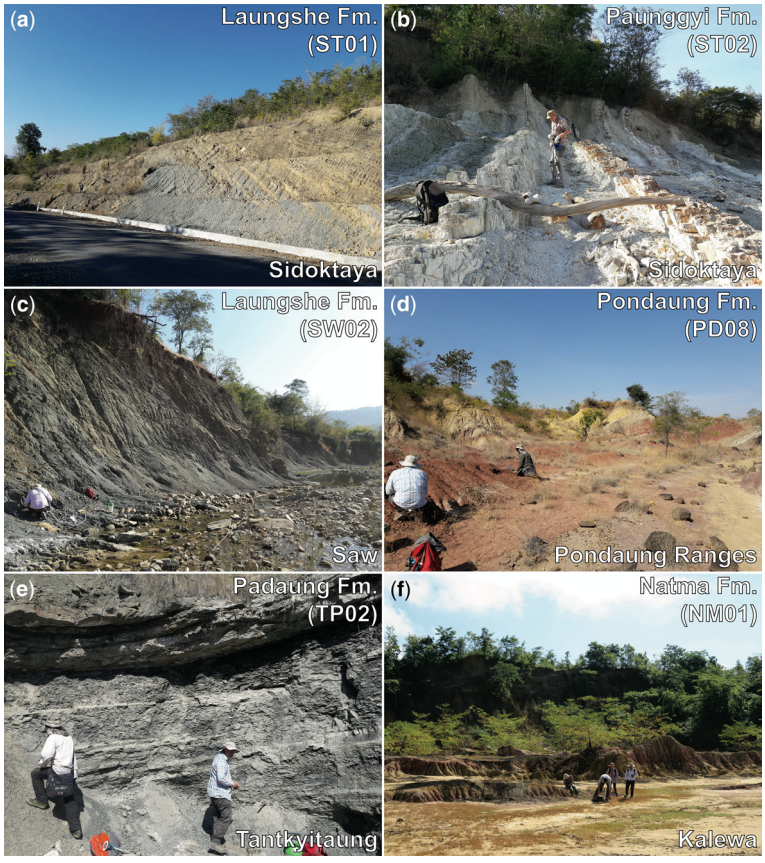

Fig. 3. Representative outcrops and lithologies related to this study. The site names, lithologies and localities are indicated in each photograph.

(TP01 and TP02) and the third on the eastern limb but with a brownish colour indicating some weathering (TP03). The grey to beige fine-grained sandstones and siltstones of these sites yielded 31 samples (Fig. 3e).

The remaining localities in the Minbu Basin did not provide reliable results (Supplementary Material S2). These are two sedimentary sections in the upper Eocene Yaw (YP) and lower Oligocene Shwezetaw Formations (SP) near the Shwezetaw Pagoda. Seven sites were drilled in the Dakton area, especially near the Dam north of the Ngape town, where fresh outcrops of tuffs, siltstones and sandstones are exposed. Although palaeomagnetic results from the same location have been reported by Li *et al.* (2020), our own study casts doubt on the reliability of these results.

Palaeomagnetic sampling in the Chindwin Basin

In the Chindwin Basin, we sampled 27 sites in the middle Miocene Natma Formation (NM), located in badlands around the road north of the town of Kalewa to Mawlaik in the western Chindwin Basin. In this area, the Natma Formation is part of a large north–south-trending, ~35° east-dipping, monoclinal sedimentary section, where 219 samples were drilled at 27 sites in fine-grained red to brown and purple palaeosols. The yellow-brown colour of some samples is interpreted as evidence for recent incipient weathering (Fig. 3f).

Immediately west of the Chindwin Basin and WBO, sampling of the Triassic basement rocks and Paleogene turbiditic sediments within the IBR (PC) did not provide interpretable results (Supplementary Material S2).

Palaeomagnetic analysis

The natural remanent magnetizations (NRMs) of the collected samples were measured on a 2G cryogenic magnetometer located in a magnetically shielded room at Geosciences Rennes. Stepwise thermal demagnetization with increments of 20–50°C up to

680°C, and three-axis alternating field (AF) demagnetization with increments of 2.5–10 mT up to 120 mT were used to isolate the characteristic remanent magnetization (ChRM) of each sample. Subsequently, the ChRM directions of interpretable samples were obtained using principal component analysis (Kirschvink 1980) and, in a few cases, a great-circle approach (McFadden and McElhinny 1988). Great circles are often useful in lightning-affected volcanic rocks where the great circles are controlled by the ChRM and secondary magnetizations due to lightning that should have different directions between samples drilled several metres apart. The intersection of the great circles is then clearly the ChRM for the site. In sediments where the secondary magnetization is a viscous overprint in the present-day field, great circles between this secondary and primary magnetization should all be parallel at the site level, and it is not possible or tricky to use great-circle intersection. The determination of the site-mean direction cannot be done unless there are already numerous well-defined characteristic vectors at the site. The other possibility is to have great circles from different sites with significant variation in bedding direction and great circles from different sites will intersect after tilt correction to provide the pre-tectonic characteristic direction. However, this is not often the case, so we have been very cautious and often discarded such data. Well-determined ChRM directions from the same locality and age were grouped, after which mean directions and corresponding statistical parameters could be calculated (Fisher 1953; Butler 1992).

To better constrain the origin of magnetization, we investigated the magnetic properties of our samples using several methods. Before demagnetization, the anisotropy of magnetic susceptibility (AMS) of each sample was measured on a KLY3S AGICO Kappabridge to determine the magnetic fabric in every locality. In sediments, the minimum axis is typically orthogonal to the bedding and the maximum axis (K_{max}) of the AMS ellipsoid will gradually be aligned with the fold axis in compressive regimes (Hrouda 1982; Kissel *et al.* 1986). After each thermal demagnetization step, the bulk magnetic susceptibility of each sample was measured to monitor chemical changes during heating. Furthermore, magnetic hysteresis loops were obtained for samples from different localities and lithologies. Finally, acquisition of isothermal remanent magnetization (IRM) was done up until 2400 mT for selected samples to evaluate differences in mineralogy. For several samples, the acquired IRM was then thermally demagnetized by increments of 20–50°C up to 680°C to further characterize the magnetic carriers.

Raw demagnetization data of all samples are accessible in the MAGIC palaeomagnetic database. Several sites did not yield reliable palaeomagnetic results. These sites are not presented as part of our main palaeomagnetic analysis, but are presented in Supplementary Material S3. Given the difficulties in obtaining interpretable data, we feel it is important to provide this information to guide future sampling in the region. All sites are used to discuss rock magnetic properties, especially the magnetic susceptibility, observed across the BT.

Results

Rock magnetism

Magnetic susceptibility

Bulk magnetic susceptibility provides first-order information on the basic magnetic properties of the sedimentary rocks sampled in this study, especially when compared with values observed in the igneous rocks of the Wuntho Ranges (Westerweel *et al.* 2019) and in the Yaw and Letkat sedimentary rocks from the Chindwin Basin (Westerweel *et al.* 2020). On average, the bulk magnetic susceptibility in the sediments is two orders of magnitude lower than in the igneous rocks (Fig. 4 and Fig. S2). Hysteresis plots indicate a large paramagnetic component (>90% of the high field magnetization) in most sampled rocks, preventing even an accurate paramagnetic correction (Fig. S3). The large paramagnetic content further corroborates the low concentrations of detrital magnetite in samples with magnetic susceptibility below $\sim 4 \times 10^{-4}$ SI. The wider scatter in NRM intensity than in magnetic susceptibility (Fig. S2) reflects a strong control of paramagnetic minerals on the bulk magnetic susceptibility as well. The low concentrations of detrital magnetite could be related to an initial low magnetite content of the source rocks or intense chemical weathering of the sedimentary sources, possibly enhanced by sediment reworking or prolonged sediment transport, and diagenesis (Roberts 2015), as indicated by previously reported intense mineral alteration in these formations (Garzanti *et al.* 2016; Jonell *et al.* 2022). There are a few exceptions to this general trend. Detrital magnetite is found in some layers of volcaniclastic sandstones of the Paunggyi Formation, several red palaeosols layers from the Pondaung Formation and, notably, in the sandstones of the Letkat Formation (Westerweel *et al.* 2020).

Magnetic properties of yellowish to red palaeosols

The IRMs of many samples from palaeosols of the Pondaung (PD) and Natma (NM) Formations are not yet fully saturated at 2300 mT, suggesting that high coercivity phases such as hematite play an

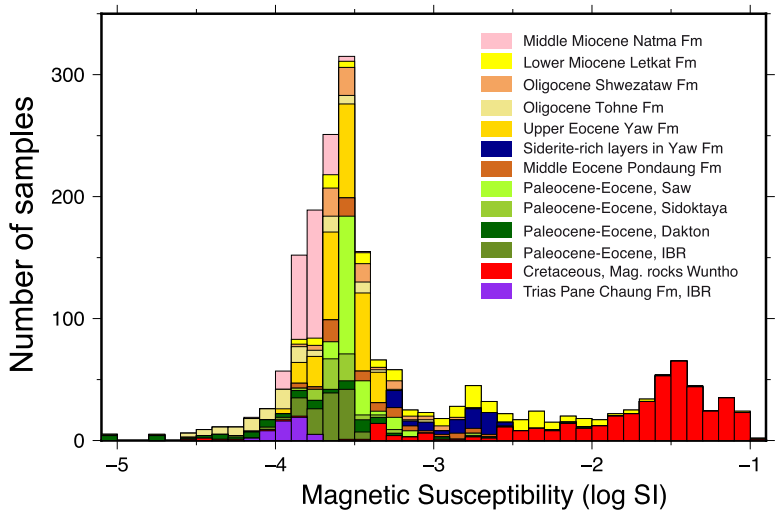

Fig. 4. Histograms of volume magnetic susceptibilities (in log-transformed SI units) observed in the various lithological units of the BT. Locations and raw palaeomagnetic data for all of these sampled units are given in Supplementary Material S1 and S2. See also Westerweel *et al.* (2019, 2020).

important role alongside magnetite. This is further illustrated by the fact that the many samples from these localities show demagnetization of the IRM up to 680°C (Fig. 5f). Higher bulk magnetic susceptibilities in some layers of the Pondaung Formation are due to a higher detrital magnetite content (Fig. 4). Samples from the Natma Formation have generally lower bulk magnetic susceptibilities despite their apparently similar lithology to the Pondaung Formation, representing differences in sedimentary provenance. The low magnetite content of samples from the Natma Formation contrasts especially with the magnetite-rich underlying sandstones of the Letkat Formation, and this suggests a difference in provenance or exhumation rates at the source location.

Magnetic properties of marine shales and siltstones

Here we include all sites in Late Cretaceous and Paleogene formations except the Ponduang Ranges. IRM acquisition (Fig. 5a) shows that magnetite is the major remanent magnetic carrier in most marine shale and siltstone samples. This is further supported by thermal demagnetizations of IRM up to 580°C (Fig. 5f). However, laboratory experiments, especially high field experiments such as hysteresis cycles (Fig. S3), IRM (Figs S4 and S5) or ARM acquisition (Fig. S6) were often not pertinent to distinguish samples that were either good or poor recorders of well-defined characteristic magnetizations. At site ST01, near Sidoktaya, the marine shales also have a high-coercivity phase, probably hematite, as ∼5–15% of the IRM is acquired above 250 mT (Figs S4 and S5) and demagnetized above 580°C. This specific mineralogy is probably the reason for the excellent palaeomagnetic demagnetization data from this site, as the samples with evidence of weathering have the lowest hematite content.

During thermal demagnetization, the magnetic susceptibility increases above ∼400°C (Fig. S7), possibly due to the transformation of pyrite to magnetite during heating, which favours the formation of spurious magnetizations in the laboratory. For this reason, data from demagnetization steps above 400°C were often not included in the analyses, especially for samples with relatively low natural remanent magnetizations.

Magnetic viscous overprint and weathering

Samples were stored in the shielded room several days or weeks before remanent magnetization measurements. This procedure often reduces the importance of short-term viscous remanent magnetization (VRM). Yet, persistent magnetic overprints acquired *in situ* in the recent past are common in many samples at different locations, generally in more brownish rocks affected by recent weathering (Fig. S8).

Recent weathering is a major problem in the palaeomagnetic study of these rocks and it is more problematic with increasing grain size, especially in siltstones to sandstones. We carried out a two-week viscosity test in the laboratory field (Prévot 1981) on seven samples from the marine shales of

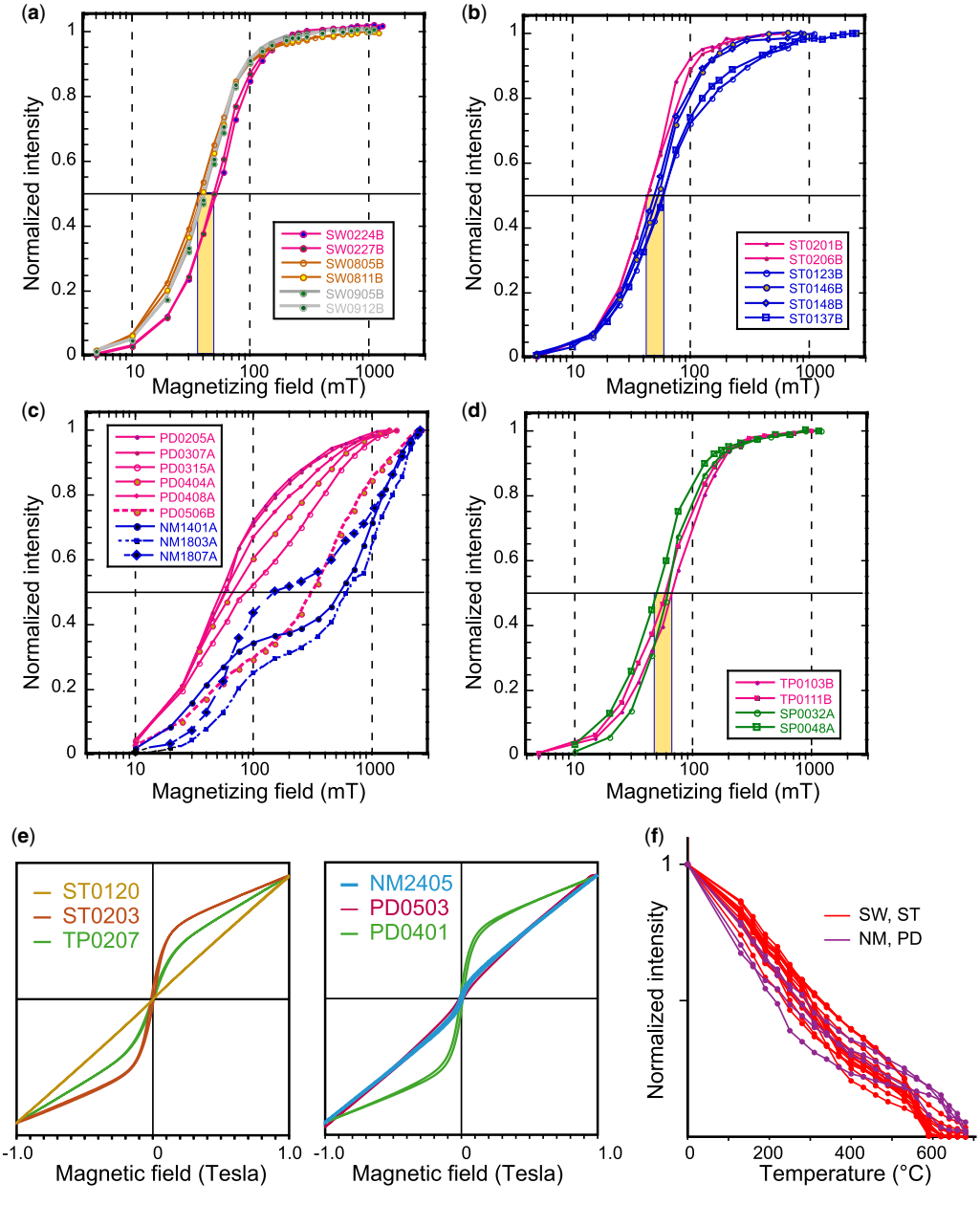

Fig. 5. Plots of isothermal remanent magnetization (IRM) acquisition for marine mudstone samples from (**a**) the Saw area and (**b**) the Sidoktaya area and samples from (**c**) palaeosols of the Pondaung and Natma Formations and (**d**) mudstones from the Padaung Formation. (**e**) Normalized hysteresis loops of representative samples from all localities. (**f**) Thermal demagnetization of IRM up to 680°C. Hematite-bearing samples from the Pondaung (PD) and Natma (NM) Formations are shown in purple.

the Shwezetaw and Yaw Formations of the Minbu Basin. The short-term VRM acquired during two weeks ranged from 30 to 136% of the NRM in these samples. In samples previously demagnetized at 150°C, the VRM acquisition is almost twice as high as in unheated samples (Fig. S9), highlighting the high capacity to acquire VRM in the low-temperature range (<200°C). Because of the

logarithmic variation with time, for a total VRM acquired during the last normal Brunhes Chron (0.78 Myr), about one-third of the VRM could be short term (weeks), about one-third acquired during the past 400 years and the last third for the rest of the Brunhes period. However, it is difficult to extrapolate with time the short-term VRM acquisition in the laboratory over time. Although this low-temperature component is often presented as a viscous magnetization acquired in the present-day field or in long-term normal field during the last normal Brunhes Chron, our data from Myanmar provide evidence that such an overprint may be acquired over the last centuries.

In outcrops from recent road cuts, the fresh mudstones present a blue-grey colour, and the weathered material often has grey to brown colours. In some natural outcrops, such as in small streams with lower erosion rates, weathering may be more pronounced. For example, several siltstone samples were drilled from a stream exposure of Oligocene Shwezataw Formation. A well-defined low unblocking temperature ChRM component is resolved (Fig. S8) and it has shallower inclinations than expected by the present-day field or the normal dipole field. The global secular variation of the Earth's magnetic field is well established for the last four centuries (GUFM model; Jackson *et al.* 2000). The geomagnetic inclination over Myanmar has been low over the last centuries. The low-temperature component may be the result of VRM acquisition under a weathering process over four to five centuries that likely stabilized these VRMs. At other sites in the sandstones (such as site MY31; Fig. S8) the overprint has slightly higher unblocking temperatures and a direction closer to the long-term dipole field. These samples have no short-term viscous magnetization and weathering likely hardened a Brunhes VRM as suggested for a maghemitization process (Jackson and Worm 2001). These two examples illustrate the importance of recognizing such secondary magnetizations. Strong overprint in the Brunhes normal field is also observed in red palaeosoils from the Pondaung Formation containing detrital magnetite. In these cases, oxidation of large magnetite grains may even lead to more resistant magnetic overprints.

In the marine shales, weathering either reduces or increases NRM intensities and high-field magnetic properties do not provide relevant information to classify such samples. For example, sample 20SW0706 has a strong NRM with a single component in the present-day field and the AF demagnetization of a 1.0 T IRM indicates a high magnetic coercivity (see Fig. S5 and the next section for further details on the palaeomagnetic analyses). The resistance of magnetizations during AF demagnetizations does not guarantee a primary magnetization. However, magnetizations with low unblocking temperatures are always suspected of being a recent overprint.

Anisotropy of magnetic susceptibility

AMS data show a magnetic fabric related to compaction as the minimum susceptibility is perpendicular to the bedding (Fig. 6). The magnetic lineation is best observed in samples from the middle Miocene Natma Formation in the Chindwin basin. The anisotropy is significant at Sidoktaya, Saw and Tantkyitaung Pagoda, and up to 1.2 for site SW08 in the Tabyin Formation.

Characteristic remanent magnetizations

In general, the magnetic properties of our sampled rocks in the Burmese forearc appear to be affected by a degree of alteration that typically increases with grain size, but most fresh outcrops of fine-grained rocks retain a primary or early diagenetic magnetic signal. AF demagnetization was significantly less efficient than thermal methods in separating components of magnetization, particularly in removing large overprints in the recent field as discussed above. AF demagnetization was mainly used to check the magnetic properties or when the same magnetization component could be unambiguously determined by both methods. During AF demagnetization, we also often observed gyroremanent magnetizations (GRMs) above 30–40 mT and these GRMs were cancelled by measuring the remanent magnetization after each axis of AF demagnetization (x, y, z) (Dankers and Zijderveld 1981; Roperch and Taylor 1986) (examples are shown in Fig. S10).

Campanian–Maastrichtian (Kabaw Formation at Saw)

Twenty mudstone samples were drilled from the Kabaw Formation at site SW09 near Saw. The NRM intensity is low (2×10^{-4} A m^{-1}) and there are chemical changes above 400°C. Seventeen samples yielded apparent ChRMs in the temperature range 250–430°C with magnetite as the most likely carrier (Fig. 7e). In geographical coordinates, the remanent magnetization above 250°C tends to cluster around a south declination and a positive inclination of about 40°, far from the present-day field (Fig. S11). The bedding follows the overall north–south trend of the Minbu Basin with no evidence for overturning. After bedding correction, the SW09 mean direction becomes declination (D) = 149.7°/inclination (I) = 17.9°, Fisher cone of 95% confidence ($\alpha 95$) = 8.3° (Fig. 8; Table 1). However, the stability of the remanent magnetization is low and further

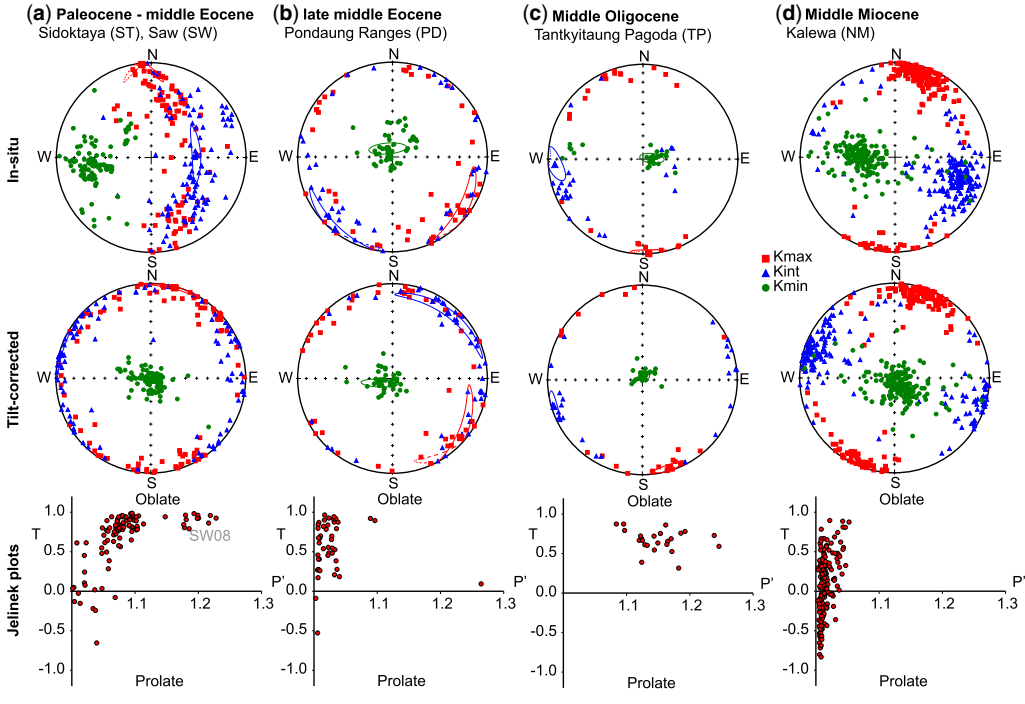

Fig. 6. Equal-area lower-hemisphere plots of the anisotropy of magnetic susceptibility (AMS) of all samples for the (**a**) Paleocene−middle Miocene, (**b**) late middle Miocene, (**c**) middle Oligocene and (**d**) Middle Miocene. The top row shows *in situ* data and the middle row data after bedding correction. Plots of the shape (T) of the anisotropy ellipsoid v. the corrected degree of anisotropy (P') (Jelinek 1981). Sorted by locality and age are shown in the bottom row.

work would be required to obtain a robust palaeolatitude for the Kabaw Formation.

Paleocene to early Eocene (Sidoktaya and Saw)

SE of Sidoktaya (ST), we obtained the most stable ChRMs in 27 blue-grey mudstone samples out of 27 thermally and 17 AF demagnetized samples along the road cut section of site ST01. The samples with the well-defined ChRMs have an average NRM intensity of 10^{-3} to 2×10^{-3} A m^{-1} while the rejected samples show evidence of weathering with lower intensity of NRM $\sim 2 \times 10^{-4}$ A m^{-1}. The thickness of the section providing useful palaeomagnetic results is about 50 m.

The remanent magnetization is especially stable upon AF or thermal demagnetization up to 580°C (Fig. S12). The ChRMs were anchored to the origin in the temperature range (220–580°C) (14 samples) and above 20 mT for AF demagnetization (13 samples) (Fig. 7a, b), providing a well-grouped mean direction. The mean direction is $D = 253.8°$, $I = -22.8°$, $\alpha 95 = 4.1°$, $k = 46$ and $D = 253.7°$, $I = 35.1°$, $\alpha 95 = 4.1°$, $k = 46$ after bedding correction (Fig. 8; Fig. S4; Table 1). The rejected samples with less accurate ChRM vectors support the same result but were not taken into account because the number of high-quality samples is already sufficiently high. Both the univectorial magnetization and the presence of magnetite as the main magnetic carrier support the interpretation of a primary magnetization. In IRM acquisition experiments, there is evidence for a high coercivity phase above 250 mT. This may be evidence for some oxidation during early diagenesis that somehow made the remanent magnetization more stable as there is no evidence for a different ChRM carried by hematite. We have not found evidence supporting a late secondary magnetization for these rocks and we therefore consider that the magnetization was acquired before tilting of the strata.

The 12 samples from site ST02, from the grey and white tuffs of the Paunggyi Formation, present a larger overprint and more site-level scatter than ST01 (Figs 7a–c & 8). Following the removal of an overprint in the present-day field, the ChRMs show well-defined directions with southward declinations at temperatures up to 580°C (Fig. 7c and Fig. S13). The mean inclination after tilt correction of ST02 is $I = -2.7°/\alpha 95 = 11.2°$.

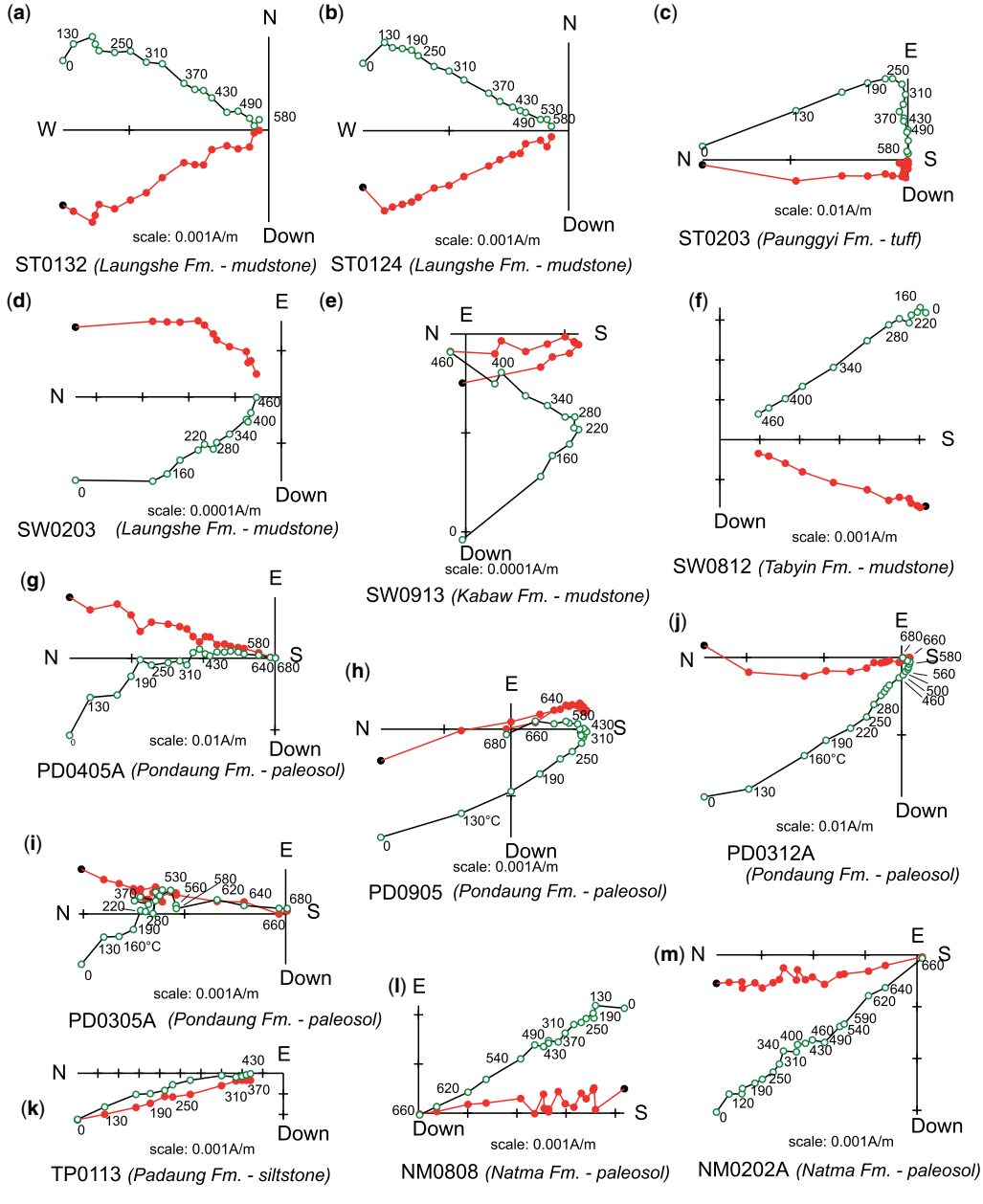

Fig. 7. Representative orthogonal demagnetization plots in geographical coordinates for samples from the different localities in this study (a–m). Open green circles (filled red circles) are the vertical (horizontal) component. Demagnetization steps given on each plot are in °C.

The other early Paleogene sites from Saw (SW) provide stable ChRMs up to 460°C far from the present-day field direction, although with generally more scatter compared with site ST01 (Fig. 8; Fig. S4; Table 1). Site SW02 was sampled along a ~200 m long continuous section of the Laungshe Formation with some synsedimentary deformation, but we did not sample the most deformed sedimentary beds. Deformation is not visible in the AMS results (Fig. 6). The magnetic fabric is controlled by compaction. Samples with stable magnetization from site SW02 are of normal polarity, suggesting

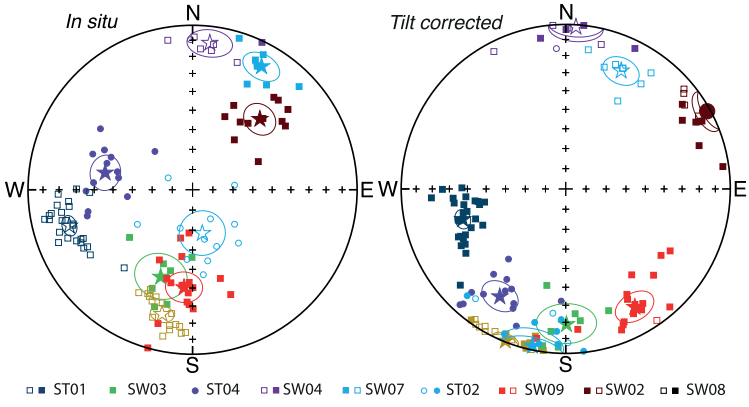

Fig. 8. Equal-area projections of interpretable palaeomagnetic results from this study and Westerweel *et al.* (2019) before (*in situ*) and after tilt correction. The estimated mean direction for each site is shown with a star and the associated 95% angle of confidence by the coloured outline. Open (filled) symbols are for negative (positive) inclinations.

a latest early Eocene age during an interval when normal polarity chrons become more common. Twelve reliable samples with stable demagnetizations and coherent ChRM directions away from the present-day field (Fig. 7d; Fig. S14) yield a mean direction of $D = 61.2°$, $I = 2.2°$, $\alpha95 = 7.8°$ after bedding correction.

Site SW07 in the Tilin Formation gives interpretable results from eight samples, providing a mean direction of $D = 25.1°$, $I = -21.7°$, $\alpha95 = 7.8°$ after tilt correction (Fig. 8, Fig. S15). Sites SW03 (Tilin Formation, seven samples; Fig. S16) and SW04 (Laungshe Formation, eight samples; Fig. 8 and Fig. S17) exhibit mean directions of $D = 179.7°$, $I = 18.8°$, $\alpha95 = 12.1°$ and $D = 3.6°$, $I = -1.5°$, $\alpha95 = 9.7°$, respectively.

At site ST04, and in the Tabyin Formation, the ChRMs shown by *in situ* coordinates are steep and different from the present-day field (Fig. 8; Fig. S18) with a tilt-corrected direction with a south declination. The geometric mean intensity of the NRM is greater than 1.0 mAm^{-1} and only a single component of magnetization was identified.

Samples from site SW08 in the Tabyin Formation have a stronger input of magnetite as shown by higher magnetic susceptibility of 500×10^{-6} SI and an NRM intensity about 5×10^{-3} Am^{-1}. There is no secondary overprint in the present-day field and the 16 samples yielded very well-defined ChRMs (Fig. 7f; Figs S10 & S19), resulting in a well-determined mean direction of $D = 201.7°$, $I = 0.7°$, $\alpha95 = 4.9°$.

In summary, sites ST01 and SW08 have very well-defined ChRMs. The other sites show more complexity in demagnetization but a reliable ChRM is always clearly distinguishable from an overprint of present-day direction.

Late middle Eocene (Pondaung Ranges)

In contrast to the marine mudstones discussed above, these samples are in yellow to red claystones from palaeosols of the Pondaung Formation (PD). Sampling was particularly challenging, because it was usually necessary to remove a 20–50 cm thick cover of recent soils due to weathering to reach fresh outcrops. The remanent magnetization is carried by magnetite and hematite. A normal overprint was not always fully removed in many samples, either by thermal (Fig. 7j; Fig. S20) or AF demagnetization (Fig. S20). Twenty-eight samples provided demagnetization paths on great circles showing a reverse polarity component at high temperatures. Unfortunately, the intersections of great circles are mainly constrained by the recent *in situ* overprint and the variation in bedding attitude is not large enough to secure the use of great circles after bedding correction. We observe that the directions in the high-temperature interval (460–640°C) are distributed in two opposite clusters and not in the present-day field (Fig. S21). Taking into account the scatter and the difficulty to fully remove the overprint, ChRM vectors were determined from 28 samples with normal or reverse polarity (Fig. 7g–I; Fig. S20) and we do not determine a mean direction per site but for the area. These normal and reversed polarity magnetizations were identified stratigraphically at different locations and not in the same beds. The obtained ChRMs carried by hematite at high temperatures are interpreted to be acquired during sedimentation or early diagenesis in the palaeosols and it is not a late magnetization. Previous magnetostratigraphic results in the Pondaung Formation of only normal polarity (Benammi *et al.* 2002) are likely the consequence of a poorly

Table 1. Palaeomagnetic mean directions from this study and Westerweel *et al.* (2019)

Name	Locality	Formation	Lithology	Sites	$N/n/s$	IS				TC			
						D	I	α95	k	D	I	α95	k
Late Cretaceous													
MY*	Wuntho Ranges	Wuntho volcanic complex	intrusives, extrusives, volcaniclastics, clastics	16		69.2	−9.8	10.1	14.2	–	–	–	–
SW09	Saw Township	Kabaw Formation	mudstones, siltstones	1	17/20/29	185	40.1	8.3	19.3	149.7	17.9	8.3	19.3
Paleocene–middle Eocene													
ST01	Sidoktaya Township	Laungshe Formation	mudstones, siltstones	1	27/43/45	253.7	−23.0	4.3	44.2	253.6	35.0	4.3	44.2
ST02	Sidoktaya Township	Paunggyi Formation	tuffs	1	12/11/15	167.4	−67.9	11.2	15.9	192.0	2.7	11.2	15.9
SW02	Saw Township	Laungshe Formation	mudstones, siltstones	1	12/31/37	43.6	40.4	7.8	31.6	61.2	2.2	7.8	31.6
SW03	Saw Township	Tilin Formation	mudstones, sandstones	1	7/8/10	200.1	43.0	12.1	25.9	179.7	18.8	12.1	25.9
SW04	Saw Township	Laungshe Formation	mudstones	1	8/10/19	6.7	−11.1	8.7	41.9	3.6	−1.5	9.7	33.7
SW07	Saw Township	Tilin Formation	mudstones, siltstones	1	8/14/17	29.2	15.2	7.8	51.4	25.1	−21.7	7.8	51.4
SW08	Saw Township	Tabyin Formation	mudstones, siltstones	1	16/16/16	193.8	−23.2	4.9	57.8	201.7	0.7	4.9	57.8
ST04	Saw Township	Tabyin Formation	mudstones, siltstones	1	14/13/15	282	45	8.1	27.2	211.5	24.3	8.1	27.2
Late middle Eocene													
PD	Pondaung Ranges	Pondaung Formation	palaeosols	9	25/71	185.0	0.7	5.8	26.2	4.9	8.6	5.6	27.7
MA-MD*	Kalewa Township	Yaw Formation	mudstones, siltstones, sandstones, siderites	6	140/520	12.6	4.2	3.3	13.8	14.6	1.9	3.3	13.9

*Data from Westerweel *et al.* (2019).

Combined mean directions are also shown. The results are displayed in both *in situ* (IS) and tectonic-corrected (TC) coordinates (applied bedding corrections and site coordinates are listed in Table S1). N, number of studied specimens used for mean direction; n, number of studied core samples; s, number of studied specimens D, mean declination; I, mean inclination; α95, Fisher cone of 95% confidence; k, dispersion parameter.

identified normal overprint with wide unblocking temperatures. Therefore, the magnetostratigraphic age and the close to present-day palaeolatitude determined by Benammi *et al.* (2002) should be discarded.

Our new mean direction for the Pondaung Formation, calculated from 28 samples, is $D = 5.6°$, $I = -3.2°$, $\alpha95 = 6.1°$, $k = 21.1$ in *in situ* coordinates and $D = 5.8°$, $I = 6.6°$, $\alpha95 = 5.6°$, $k = 24.9$ after bedding correction.

Middle Oligocene (Tantkyitaung Pagoda)

From the middle Oligocene Padaung Formation exposed within the large Tantkyitaung Pagoda anticline (TP), 30 fine-grained siltstone samples were progressively demagnetized thermally or by AF, providing univectorial demagnetizations (Fig. 7k). Bulk magnetic susceptibilities of on average ~0.0006 SI but up to ~0.002 SI indicate that these fine-grained mudstones may contain some detrital magnetite. The NRM is also higher than in the Eocene sites with a mean value of around 8.0 mA m^{-1}. Median demagnetization temperatures are in the range ~200–250°C, but the demagnetization plots do not allow a clear separation of two magnetic components. The low unblocking temperature component (130–250°C) is not very different from the high-temperature ChRMs (250–540°C) determined with vectors anchored to the origin, except for a few samples at TP02 showing a ChRM vector that does not pass through the origin. The mean directions in *in situ* coordinates have shallower inclination than the direction expected from the dipole field or the present-day field. Sites TP01 and TP02, from the western limb of the anticline near the fold axis with near subhorizontal bedding, yield a mean declination of ~350°, and the declination of the ChRM at site TP03 on the eastern limb is ~25° (Fig. 9). The strike of bedding at site TP03 is nearly north–south oriented with a similar north–south oriented horizontal ChRM, so the bedding correction does not provide a robust fold test.

The Tantkyitaung Pagoda anticline is located in the hanging wall of a large thrust fault (Fig. S1). The differing declinations could be the result of local deformation. However, the lack of a positive fold test and the very small angle difference between the low-temperature and high-temperature components cast some doubt on this result and we will not use it for plate reconstruction purposes.

Middle Miocene (Kalewa)

All samples in the Natma Formation (NM) are from red to orange mudstones layers interbedded with coarse sandstones, similar to the Pondaung Formation. Samples are usually distributed over thick mudstones beds or several beds at each site. A few tens of centimetres of weathered surface muds needed to be removed to obtain samples in apparently less altered mudstones. From the 27 sites of the middle Miocene Natma Formation, 190 samples were thermally demagnetized and nine samples were AF demagnetized. Magnetic susceptibility is low and homogeneous in the Natma Formation with a geometric mean of 1.7 10^{-4} SI. There is no evidence for sedimentary beds with significant detrital magnetite as observed in the Pondaung Formation and the same pervasive high-temperature overprint recorded by detrital magnetite is not observed in the Natma samples.

A total of 83 samples provided ChRMs above ~200°C of both normal and reverse polarity (Fig. 9) carried by both magnetite and hematite in some samples (Fig. 7l, m). Normal and reverse polarity samples from different sites have similar magnetic properties, supporting a likely primary detrital or early diagenetic remanent magnetization during palaeosol formation. Normal and reverse polarity mean directions are nearly antiparallel with an angular difference of 6.4° compatible with a residual recent field overprint. This is likely to be partially cancelled in the mean combining the normal and reverse polarities yielding $D = 11.5°$, $I = 29.5°$, $\alpha95 = 4.0°$.

Interpretations of the palaeomagnetic results

Considerations on potential biases on the reliability of palaeomagnetic results

The AMS data are typical of a sedimentary fabric in all localities of this study (Fig. 6). They show oblate magnetic fabrics with the minimum axis K_{min} oriented normal to bedding despite the degree of anisotropy being generally low, especially in localities PD and NM, which are mainly fine-grained palaeosols (Fig. 6b, d). The highest anisotropy values are found in site SW08 from the Tabyin Formation (Fig. 6a) and the three sites in the Padaung Formation (Fig. 6c). The typically sedimentary magnetic fabrics suggest that all AMS tensors are likely controlled by sedimentary processes and compaction. Notably, the maximum axis K_{max} is parallel to the main trend of the fold axis within the sampling region, in agreement with a slight tectonic imprint typical for tilted sedimentary sequences in orogenic belts (Borradaile and Henry 1997).

For sites with a well-defined remanent magnetization, GRMs are observed following static AF demagnetization. GRM behaviour is often systematically attributed to greigite (Snowball 1997) but the development of GRMs during static AF can be

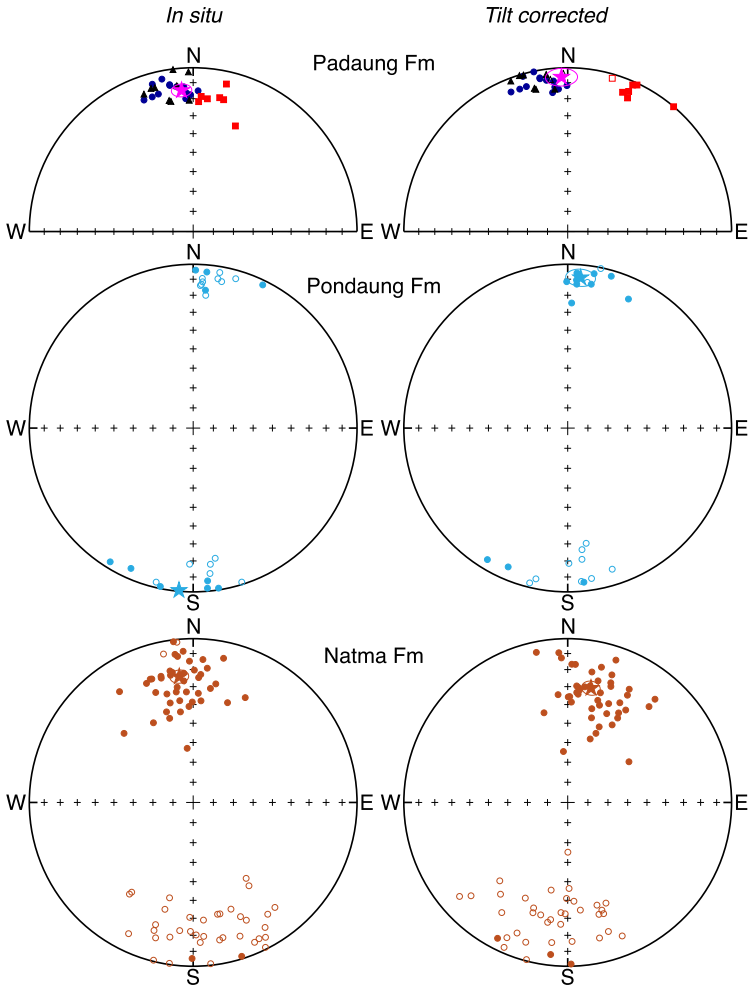

Fig. 9. Equal-area projections of characteristic directions for the Padaung, Pondaung and Natma formations before (*in situ*) and after tilt correction. Legend as in Figure 8.

recorded by uniaxial SD grains of magnetite providing a magnetic fabric to constrain the development of the GRM vectors is present (Roperch and Taylor 1986). The observation of GRMs in static AF demagnetization is thus also evidence for an anisotropy in the orientation of the remanent magnetic carriers. We can discard the presence of greigite in our samples because the GRMs in samples previously thermally demagnetized are much stronger than in non-heated samples. There is also a lack of evidence for greigite in the thermal demagnetization of IRM and greigite is unlikely to survive at depths greater than 2 km (Aubourg *et al.* 2012).

Despite the important thickness of the sedimentary sequence, there is no observed evidence for the resetting of apatite fission track ages in the late Eocene Yaw Formation of the Chindwin Basin (Westerweel *et al.* 2020) and only partial resetting is observed in AFT data from older units of the Chindwin Basin (Zhang *et al.* 2023). This is consistent with the low-temperature gradient measured in boreholes from oil companies (Racey 2018) and sediments in the oil window, rather than in the gas window (Ridd and Racey 2015). Preserved amber has also been found in upper Cretaceous sedimentary rocks near Tilin (Zheng *et al.* 2018). Univectorial ChRMs at some sites such as ST01 and SW08 (Fig. 7) permit us to discard the hypothesis of severe alteration of the magnetic properties due to deep burial for the deepest strata of the basins. By contrast, low-temperature metamorphism affected the Paleogene IBR rocks as shown by the resetting of the

detrital zircon ZHe ages in the same IBR section (Najman *et al.* 2022). This low-temperature metamorphism explains the complex secondary magnetic overprint in these IBR rocks (Supplementary Material 2).

In the Minbu Basin, single well-defined ChRMs are observed at several sites (ST01 and SW08 for sites with the highest stable ChRMs). As discussed previously, we have carefully evaluated and rejected data that are likely to be associated with a recent overprint acquired during the Brunhes normal magnetic polarity chron. The low scatter at the site level supports an acquisition during early diagenesis and compaction, rather than an early acquired detrital remanent magnetization recording palaeosecular variation.

Characteristic remanent magnetization directions

Site-mean palaeomagnetic results with declinations to the north or to the south are unambiguously attributed to, respectively, normal and reverse polarity, because an unlikely near ∼180° tectonic rotation would otherwise be necessary. Site ST01, one of the sites with the most well-defined ChRM vectors, has a mean direction with a SW declination both in *in situ* coordinates and after tilt correction, and the inclination after tilt correction provides the southernmost palaeolatitude for this study. The data from this site are essential and require special discussion. We reject the hypothesis that the magnetization is a secondary magnetization acquired after folding because this would imply a large clockwise rotation since the late Miocene; moreover, we found no evidence for a secondary magnetization in this site. A magnetization acquired after folding would also require rotation of the fold axis, which seems unlikely as the strike of bedding is in agreement with the general trends of folds in the region. Site ST01 is assigned to the Laungshe Formation of Paleocene to early Eocene age based on previous work (Bender 1983), but a more precise age estimate is lacking. As the Earth's magnetic field was almost exclusively of reverse polarity during this time period, the ST01 mean direction is likely of reverse polarity as well and the positive inclination after tilt correction at site ST01 indicates deposition south of the equator. A reverse polarity for this site also yields a clockwise rotation compatible with the palaeomagnetic data from the WPA (Westerweel *et al.* 2019), whereas a normal polarity magnetization would imply a counterclockwise rotation greater than 100°.

The difference between the mean directions at site ST02 and site ST01 suggests that there is a component of local rotation. Site ST02 is located within a more folded area and the overall bedding strike is rotated ∼45° counterclockwise with respect to the general north–south trend of the Minbu Basin, in contrast to the ST01 section that is parallel to this trend.

In summary, we consider that sites ST01, ST02, ST04, SW08 and SW09 have a reverse-polarity early acquired remanence whereas sites SW02, SW07 and SW04 record a normal-polarity ChRM. The reverse-polarity directions are inverted to normal polarity for clarity (Fig. 10c). Site SW09 is from the Kabaw Formation and is the only site that yields a slight counterclockwise rotation.

Palaeolatitudes

The new palaeomagnetic data from this study show some scatter (Figs 8 and 10), which requires further discussion. The latest Paleocene to middle Eocene sites show scatter in declination due to tectonic rotations, which complicates a classic fold test. However, the scatter in inclination is significantly reduced after tilt correction (Fig. 10), supporting the interpretation that magnetizations were acquired prior to folding. The large scatter in inclination of nearly 40° amounts to about 20° when converting these inclinations to palaeolatitudes (Fig. 10d). Thus, such a large variation in inclination is best interpreted as related to northward motion given that the palaeomagnetic sampling covers a >20 Ma time interval (the U–Pb dating of tuffs within the Paunggyi Formation demonstrate volcanic activity at ∼65 Ma; see the 'Late Cretaceous–Paleogene sedimentary basins' subsection). In the time range of ∼65–40 Ma, southern palaeolatitudes and a latitudinal motion of nearly 30° are expected if the BT was fixed with respect to India (Fig. 9a) (see discussion below for the palaeolatitudes of India during the Cenozoic). By contrast, palaeolatitudes higher than 20° N with little latitudinal variation are expected if the BT was fixed with respect to Sibumasu. This interpretation encourages further work on a more comprehensive age control for the Paleocene/Eocene sequence and especially the Laungshe Formation, because the southern palaeolatitude determined at site ST01 from this formation supports an early Paleocene age, rather than a mid-Eocene age, assuming the BT was moving north with India.

Our results are seemingly contradicted by a recent palaeomagnetic study providing a close to present-day palaeolatitude for the BT from the Paleocene Paunggyi Formation in the southern Minbu Basin near Datkon (Li *et al.* 2020). Notably, we sampled the same sites during this study (DK; Supplementary Material S2) and we found that it was impossible to determine stable ChRM results in these rocks. Furthermore, bedding was considered as overturned by Li *et al.* (2020), contrary to our own observations and contrary to the younging direction

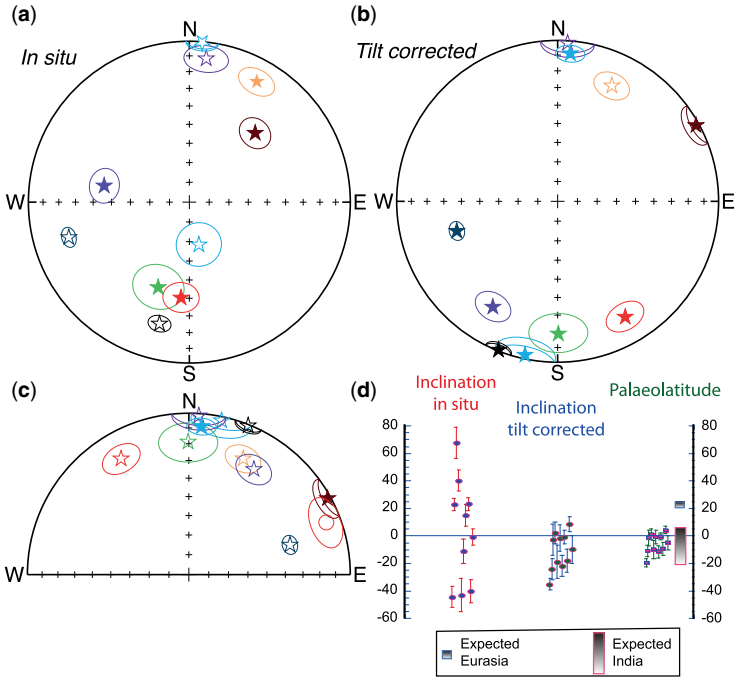

Fig. 10. Equal area plots of estimated site-mean directions (**a**) before and (**b**) after tilt correction. (**c**) Sites with reverse polarity are inverted to normal polarity. (**d**) Scatter in the inclination of Paleocene to Eocene results before and after tilt correction and palaeolatitude calculated from the tilt-corrected mean direction. The error bars in (d) are derived from the site-mean inclination error at 95%. The grey and blue boxes are the expected palaeolatitudes for a site located at 21°N, 94°E for the global apparent polar wander path of India and Eurasia, respectively, at 60–40 Ma based on global APWP from Torsvik *et al.* (2012).

provided by numerical age data from the same location (Cai *et al.* 2020). Based on these arguments, we reject these data and associated conclusions in Li *et al.* (2020).

As we discussed earlier, anisotropy in magnetic susceptibility or remanent magnetization is compatible with compaction, which can generate inclination shallowing adversely affecting palaeolatitude determination. Inclination shallowing of remanent magnetization often occurs in detrital sedimentary rocks and follows a function:

$$\tan(I_{\mathrm{obs}}) = f \tan(I),$$

where I_{obs} is the observed inclination, I is the inclination after shallowing correction and f is the flattening factor, often ranging from 1.0 (no correction) to 0.6 as for much sedimentary data used in Apparent Polar Wander Path (APWP) compilations (Torsvik *et al.* 2012). At low palaeolatitudes, where the inclination is close to zero, this correction is not important. A flattening correction value of 0.6, commonly used with palaeomagnetism in red beds, will just correct an observed inclination of 5° to about 8.3° and the palaeolatitude will only change from 2.5° to 4.2°. Moreover, this inclination shallowing is typically observed in red beds with hematite as a detrital remanent magnetic carrier (Tauxe and Kent 1984). As discussed above, magnetite of early diagenetic origin may not record the flattening associated with detrital magnetization. However, compaction during the thickening of the basin is likely.

We made some measurements of anisotropy of ARM (two samples from site ST01) and IRM (one sample from site ST01 and two samples from site SW08). Magnetic foliation degree in anisotropy of remanent magnetization ranges from 1.2 to 1.46 and is larger than for AMS data. Despite site SW08 having the largest AMS foliation, its near-zero inclination in stratigraphic coordinates will not be changed by shallowing correction. Moreover, several sites have ChRM acquired in the southern hemisphere, and inclination shallowing correction would result in a steeper inclination and more southwardly palaeolatitude. We acknowledge an uncertainty due to inclination shallowing, but that will not change significantly the general outcome of this study. Considering the rapid northward motion

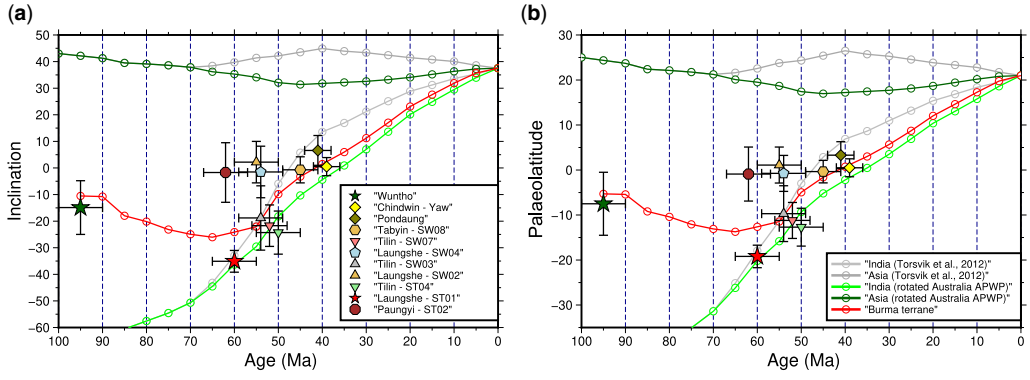

Fig. 11. Plots of (**a**) the observed palaeomagnetic inclinations and (**b**) the corresponding palaeolatitudes v. time compared with the expected inclination and palaeolatitude for a site located at 20°N, 90°E from different models during the Late Cretaceous and Cenozoic either for India or Asia. The grey curves correspond to the expected inclination and palaeolatitude from the APWP (Torsvik *et al.* 2012) for India or Asia. The green curves correspond to the expected inclination and palaeolatitude from the APWP from Australia (Rose *et al.* 2022) rotated and used as the master curve in GPlates. The red curve corresponds to the APWP for the BT proposed in the reconstructions (this study, Fig. 14). Error bars are derived from the site-mean inclination error at 95%.

of India during the Paleocene–Eocene, the uncertainty in the age of the rocks investigated is a greater issue for the tectonic reconstruction and palaeogeography of the region (see discussion below). The resolution of the result in middle Miocene sedimentary rocks of the Natma Formation is not sufficient to quantify the motion of the BT along the Sagaing Fault, but its main value shows the large difference with the palaeomagnetic results in Paleocene and Eocene sedimentary rocks and the significant northward translation of the BT between the Eocene and the Miocene without significant rotation during that time.

Palaeomagnetic constraints on the Late Cretaceous–Paleogene BT palaeogeography

The palaeomagnetic data from this study indicate an equatorial to slightly southern hemispheric position of the BT during the Eocene (~5° N–20° S), but there is significant dispersion in the data (15°–20° in latitude) (Fig. 11), which could be due to age uncertainties. At several sites, the characteristic direction is determined from a selected number of samples, and individual site data are unlikely to provide a robust palaeolatitude determination (Rowley 2019). Palaeomagnetic data that can be considered to correspond to a geomagnetic axial dipole field are usually interpreted following a comparison with the expected data for the major tectonic plates. This is done by compiling reliable palaeomagnetic data for all geologically stable blocks in these plates, from which a global APWP is reconstructed by closing oceans along marine magnetic anomalies in a so-called plate circuit. This global APWP can then be rotated to each continent. We use here as a starting point the commonly used APWP compiled by Torsvik *et al.* (2012), rotated to India and Asia.

The inclinations and associated palaeolatitudes obtained for the BT are compared with those expected from a location at 21° N, 94° E that corresponds to Asia or India (Fig. 11). Although the observed data are closer to those expected for India than for Asia, the palaeolatitudes at several sites are more southerly than expected for India from the APWP from Torsvik *et al.* (2012). However, the APWP for India during the Paleogene is not constrained by data from India (Torsvik *et al.* 2012). There is an excellent and robust reference palaeomagnetic pole from the Deccan Traps volcanism at the K–T boundary but almost no other palaeomagnetic data to define the motion of India during the Cenozoic. An APWP for India can only be obtained from the global palaeomagnetic APWP and plate circuit reconstructions (Besse and Courtillot 1988; Torsvik *et al.* 2012; Vaes *et al.* 2023). Anomalously low palaeolatitudes were observed in Tibet compared to the expected palaeolatitude for Eurasia (Cogne *et al.* 2013). More recent global APWPs (Merdith *et al.* 2021; Vaes *et al.* 2023) provide a generally similar Eocene APWP with only slightly lower palaeolatitudes than the APWP from Torsvik *et al.* (2012) (Fig. S23).

To circumvent this potential problem, we use the new APWP for Australia based on palaeomagnetic results from Cenozoic volcanic rocks in the tectonically stable eastern Australian continent (Hansma and Tohver 2019) and derived from a Bayesian palaeomagnetic Euler pole inversion (Rose *et al.*

2022). Using GPlates and the Global Plate Circuit, this APWP was transferred to Africa and used as the master APWP curve for the Cenozoic. This yields more southerly positions of India and Asia outside the uncertainty range of the palaeomagnetic reference frame from Torsvik *et al.* (2012) (Fig. 11). This global curve appears to partially solve the long-standing low inclination controversy over Tibet in addition to inclination shallowing in red beds (Fig. 11). As the Asian margin is also displaced southward with this Australian APWP, it does not have an impact on the distance between India and Asia.

Based on the available data from early Late Cretaceous rocks in the Wuntho Ranges and late Eocene rocks in the Chindwin Basin, a large ~60° clockwise rotation of the whole BT was initially postulated (Westerweel *et al.* 2019). The general trend in the palaeomagnetic declinations recorded by the latest Paleocene to middle Eocene results from the Laungshe and Tilin Formations is also eastward directed (sites ST01, SW02 and SW07), indicating rotations of intermediate to similar magnitude as the early Late Cretaceous mean direction reported by Westerweel *et al.* (2019). The largest value at site ST01 (Minbu Basin) is coherent with the clockwise rotation found in the Wuntho Ranges and we use these data to construct the tectonic model. However, we acknowledge that the scatter in declination from the other sites also suggests local block rotations (Fig. 8; Fig. S4). The hypothesis of a wholesale clockwise rotation of the BT occurring during the latest Cretaceous to Paleocene time period, as it started to move northward with India, is not fully supported by the results from sites ST02, SW03, SW04 and SW09. Significant deformation is observed in the sampling areas of sites ST02, SW03 and SW04, and their scatter in declinations may be explained by local block rotations. In general, it seems difficult to evaluate the rotation history through time prior to the middle Eocene with the available palaeomagnetic results and age uncertainties. However, from the late Eocene to present, palaeomagnetic data from the late Eocene Chindwin Basin (Westerweel *et al.* 2020), together with data from the Pondaung Ranges and Miocene Natma Formation (this study) clearly indicate that the BT experienced ~2000 km northward motion without any significant tectonic rotation since the late Eocene. The resolution of the Miocene palaeomagnetic results in particular are not sufficient to better constrain the motion of the BT along the Sagaing Fault compared with constraints from structural geology, but its main value is accentuating the large difference with the palaeomagnetic palaeolatitudes from Paleocene and Eocene sedimentary rocks, showing the significant northward translation of the BT between the Eocene and the Miocene without significant rotation.

In summary, the main implications from this palaeomagnetic study are the initial early Late Cretaceous shallow latitude southern hemisphere position of the BT distant from southern Asia, followed by a potential uniform clockwise rotation of the entire BT in the middle Eocene and the onset of a major ~2000 km northward strike-slip translation coeval with India during the late Eocene to the present day. In the following sections, we place these results into a plate reconstruction framework and consider available relevant geological data to propose a tectonic reconstruction model of the BT from its separation from Argoland in the Jurassic to its collision with India and then Asia in the Eocene.

Tectonic reconstructions

Choice of reference frame

There are two types of absolute reference frames in plate tectonic reconstructions: one is the mantle reference frame (Müller *et al.* 2019), usually used in most studies from the EarthByte group developing applications under GPlates, and the other is the palaeomagnetic reference frame. There are several reference frame models available with significant differences between them even for the Cenozoic, as shown in Figure S23. Palaeomagnetic reference frames are likely to better represent the past rotation of the Earth but do not provide constraints on longitude. As the main aim of our study is to discuss palaeomagnetically determined palaeolatitudes, as discussed above, we will use the global curve calculated from the APWP for Australia (Rose *et al.* 2022) in our reconstructions performed with GPlates.

For the BT, we made a composite palaeolatitude model, attempting to fit the overall palaeolatitudinal trend derived from the palaeomagnetic data but not the mean direction of each individual site (Fig. 11).

Reconstruction of South Asian margin

For the reconstructions, we used the global plate block model and relative plate motions proposed as a base with the GPlates software (Müller *et al.* 2018) instead of the global model proposed by Scotese and Wright (2018). We chose a low-latitude position (15–20° N) with a slight counterclockwise rotation for the south Lhasa margin before the India–Asia collision as supported by recent palaeomagnetic data (Bian *et al.* 2022; Ma *et al.* 2022*b*). The choice of the reference frame discussed above results in a lower palaeolatitude for Asia during the Eocene, but this is also the case for India. This has no impact on the distance between the two continents. The South Asian margin prior to the India–Asia collision is slightly curved in our model and not nearly linear as in other reconstructions (Scotese

and Wright 2018) or highly curved as in models where Sumatra does not rotate with the main Indochina Block (Advokaat *et al.* 2018). In terms of lateral extrusion out of the collision zone, our plate model reconstruction for Asia is a conservative model and not too different from GPlates based models (Zahirovic *et al.* 2014; Gibbons *et al.* 2015), allowing for some extrusion and a clockwise rotation of the Khorat Plateau. The displacement along the Red River Fault in the GPlates global model (~340 km) is slightly higher than the ~250 km proposed by Li *et al.* (2017) for the Pacific side of the fault. Large clockwise rotations south of the Ailao–Red River fault in the NW Shan–Thai block (Tong *et al.* 2015, 2021; Li *et al.* 2017; Yan *et al.* 2017) may support the largest estimate (>700 km) from structural geology (Leloup *et al.* 1995) for the western part of the fault. The extrusion of the Indochina block is also consistent with the similar palaeolatitudes for the Lhasa block and the Khorat Plateau prior to the collision in agreement with early tectonic models (Tapponnier *et al.* 1982; Leloup *et al.* 1995). With the exception of the Khorat Plateau, deformation is pervasive and well documented with several large shear zones highlighted on modern topographic maps (Fig. 1) precluding simple reconstruction using rigid blocks (Morley and Wang 2023). The high-grade metamorphism in the Mogok belt of northwestern Sibumasu (Lamont *et al.* 2021) and in the Tengchong block is likely to be the signature of intense Cenozoic deformation and tectonic extrusion (Eroğlu *et al.* 2013).

Choice of the extent of Greater India

The northern extension of Greater India has been the subject of numerous articles, and this scientific question is probably the greatest uncertainty in our understanding of the tectonic reconstructions of the India–Asia collision. Palaeomagnetism applied to fragments of the Greater Indian margin sediments (Tethyan Himalaya) preserved in the collision zone is an ideal method to estimate the size of Greater India (Patzelt *et al.* 1996). Unfortunately, severe deformation of the Tethyan Himalayan sequences and widespread gneiss dome emplacement during the late Oligocene–early Miocene induced magnetization overprints that have not always been properly recognized (Huang *et al.* 2017). Evidence of pyrrhotite as a magnetic carrier clearly allows the detection of such remagnetization (Crouzet *et al.* 2007; Appel *et al.* 2012). However, remagnetization carried by magnetite is often more difficult to characterize (Huang *et al.* 2017; Yi *et al.* 2017). Palaeomagnetic results obtained from Upper Cretaceous and lower Paleogene sedimentary rocks from the Tethyan Himalaya have recently provided very controversial and contradictory configurations of Greater India (Yang *et al.* 2019; Meng *et al.* 2020; Yuan *et al.* 2020).

Primary characteristic magnetizations are likely preserved in Early Cretaceous igneous rocks from the Tethyan Himalaya (Yang *et al.* 2015), but the large rotation of India at that time is such that palaeomagnetic data are not really useful for estimating the size of Greater India. Given the ~60° rotation of India in the Early Cretaceous, determining the size of Greater India is a problem of longitude, rather than latitude, that cannot be constrained via palaeomagnetism.

Another approach therefore is to look at the fit of (Greater) India with Antarctica and Australia as part of Gondwana before rifting apart. Rifting between India and Antarctica and Australia began 130 Myr ago (Heine *et al.* 2004). However, the initial fit between these Gondwana blocks is the subject of much debate and modelling (Gibbons *et al.* 2015; Thompson *et al.* 2019). Recent studies showing a tight fit between India and Antarctica have strong implications for the eastern size of Greater India (Talwani *et al.* 2016; Thompson *et al.* 2019). Geophysical data suggest that the crust in the Bengal region is thin, either an oceanic crust (Talwani *et al.* 2016, 2017) or a very extended continental crust (Sibuet *et al.* 2016; Rangin and Sibuet 2017). Many reconstructions include a continental margin of India that is currently subducted beneath the IBR (Gibbons *et al.* 2015). A tight initial fit between India and Antarctica, as shown in Figure 12, rules out the possibility that the IBR were attached to India prior to rifting (Rangin 2017; Aitchison *et al.* 2019).

Many studies (Gibbons *et al.* 2013, 2015; Zahirovic *et al.* 2014; van Hinsbergen *et al.* 2019; Advokaat and van Hinsbergen 2024) use the Wallaby–Zenith fracture zone as the northern boundary of Greater India (Fig. 12). However, the correlation of Triassic sedimentary rocks of the Langjiexue Group in the northeastern Tethyan Himalaya with Triassic sedimentary rocks of the North Carnarvon Basin suggests that the northern boundary of Greater India could be instead close to the Exmouth Plateau, where a >5 km thick Triassic sedimentary sequence is found (Morón *et al.* 2019). A complex two-phase opening with oceanic crust at ~135 Ma occurred in the Cuvier basin (Reeve *et al.* 2021, 2022) contemporaneous to the rifting between India and Australia. Recent geological studies in the Carnarvon Basin (Bilal and McClay 2022) also consider that break-up between Greater India and NW Australia occurred in the Cuvier Basin and even the Gascoyne Bay. Hence, we thus assume a Greater India that includes the conjugate continental block before the opening of the Cuvier Basin as is the case in other global plate reconstructions (Scotese and Wright 2018).

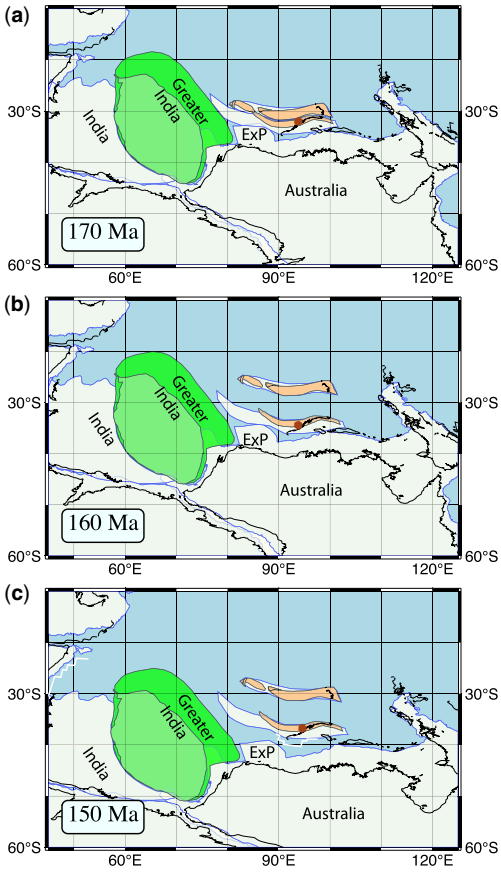

Fig. 12. Late Jurassic plate reconstructions showing the inferred position of the BT with its two stages of rifting from Gondwana. In this tight fit of Gondwana, a small and a large Greater India are shown with different green colours. The CBB block rifted first from the IBR at ~160 Ma. Remains of the inferred Late Jurassic basin between the CBB and IBR are found in the West Belt Ophiolite. The IBR rifted at ~150 Ma. ExP: Exmouth Plateau. The brown hexagon corresponds to the location of Mount Victoria.

An Argoland origin for the BT during the Jurassic–Early Cretaceous

The correlation of the Pane Chaung Formation of the Mount Victoria Block with the Langjiexue Formation of the NE Tethyan Himalayas now provides clear evidence for crustal fragments of Gondwanan origin within the BT (Yao *et al.* 2017; Naing *et al.* 2023).

These Gondwanan crustal ribbon fragments have specifically been referred to as the 'Greater Argoland' archipelago, which would have rifted at ~155 Ma from NW Australia (Hall 2012; Seton *et al.* 2012; I'Anson *et al.* 2019; Morley *et al.* 2020; Advokaat and van Hinsbergen 2024). Despite recent attempts to better define Argoland (Advokaat and van Hinsbergen 2024), it is important to point out that its palaeogeographical evolution during the Mesozoic remains puzzling, and the Argoland blocks that rifted from NW Australia often disappear in several reconstructions for the Cretaceous (for example, see fig. 2 of Delclòs *et al.* 2023). Our reconstructions, alongside results from sedimentology and geochronology, also postulate the existence of a Greater BT in the image of Greater India, which was subducted beneath Asia during the India–Asia collision (Westerweel *et al.* 2020).

A Trans-Tethyan subduction system in the mid-Cretaceous

The correlations of the WPA magmatic arc with the Gangdese Arc and the WBO with the Yarlung–Tsangpo ophiolite belts provide the strongest arguments in favour of the BT as part of the Asian margin. However, although the time concordance is striking, the coincidence of magmatic activity and ophiolite formation along the BT and Lhasa margins does not necessarily prove that the BT was on the same subduction zone as Lhasa. The equatorial palaeolatitude of the WPA in the early Late Cretaceous (Westerweel *et al.* 2019) supports the hypothesis of two distinct magmatic arcs.

An important subduction phase along the BT starting in the mid-Cretaceous is necessary to explain the peak in WPA magmatism (Mitchell *et al.* 2012; Zhang *et al.* 2017*b*; Lin *et al.* 2019; Westerweel *et al.* 2019; Licht *et al.* 2020). This is corroborated by similar trends in mid-Cretaceous magmatic activity and ophiolite emplacement along other proposed intra-oceanic arc segments of this Trans-Tethyan subduction system, such as the Kohistan Arc and the Spontang Ophiolite in the Western Himalayas (Buckman *et al.* 2018; Jagoutz *et al.* 2019). Furthermore, palaeomagnetic data (Zaman and Torii 1999; Martin *et al.* 2020) also indicate that the Kohistan Arc formed at near-equatorial latitudes similar to the WPA. We thus consider that a Trans-Tethyan subduction system is necessary to explain the near-equatorial position of the BT in the mid-Cretaceous (Westerweel *et al.* 2019).

Geological evidence for an early Cenozoic BT–India connection

The near-equatorial to low southern hemisphere palaeolatitude of the BT in the Paleocene–Eocene has strong implications for our interpretation of the geological record. It is thus necessary to consider whether available regional geological information supports the palaeomagnetic data and how it

constrains the position of the blocks in the palaeogeographical reconstructions, in particular its longitude, which is not constrained by palaeomagnetism. Westerweel *et al.* (2019) proposed an easterly position of the BT coming into collision with Sumatra before 40 Ma. By contrast, a more westerly position of the BT closer to India during its northward motion was also proposed by Westerweel *et al.* (2020), because newly acquired palaeomagnetic data indicated an even more southern position of the BT in the Paleocene–middle Eocene than in the late Eocene, which is only compatible with the BT on the Indian Plate. A BT as a forearc sliver of the Sundaland margin, as initially proposed by Westerweel *et al.* (2019), would imply an impossible complete partition of the oblique convergence between the Indian Plate and Sundaland. Furthermore, a BT as a forearc sliver of Sundaland is in conflict with the tectonic history of the Andaman Sea (Morley *et al.* 2020). We also discard the complex tectonic reconstructions putting the BT initially on the Australian Plate (Advokaat and van Hinsbergen 2024) because this reconstruction is based on questionable palaeomagnetic data.

Sedimentary provenance within the BT

The more westerly position of the BT also fits better with the recent evaluation of the potential sources of sediments that filled the thick Paleogene BT basins (Naing *et al.* 2023). These sedimentary archives can provide significant constraints on palaeogeographical models. In recent years, many studies of the BT sedimentary basins have focused on the U–Pb age distribution of detrital zircons (Allen *et al.* 2008; Wang *et al.* 2014; Licht *et al.* 2016, 2019; Zhang *et al.* 2017*b*, 2019*a*, 2023; Aitchison *et al.* 2019; Najman *et al.* 2020, 2022; Arboit *et al.* 2021; Betka *et al.* 2021; Ding *et al.* 2022; Naing *et al.* 2023). We have compiled the published U–Pb DZA dataset using the best ages filtered for discordance as provided in each study. We have not reprocessed the data as was done more recently in Jonell *et al.* (2022), even if the choice of filter can influence the age distribution (Vermeesch 2021). The stratigraphic age of each sample was estimated by considering the published maximum depositional age, the location of the samples within the stratigraphic sections and geological maps.

The erosion of an active magmatic arc should produce sediments that are rich in recent volcanic material. Although not all volcanic arcs produce abundant zircons, and zircon ages may not always accurately reflect the full temporal evolution of a magmatic system, we estimate the percentage of zircons that are younger than the expected stratigraphic age plus 10 Myr as a proxy for nearby arc magmatism within the WPA (Fig. 13a, b). We also use a different approach to the traditional histograms and Kernel density estimates to test the hypothesis of the erosion of the proximal WPA as the main sedimentary source for the BT central basins. Due to the large number of samples (276) and the impossibility of visualizing each of them using pie charts, the relevant information for each sample has been divided into three groups (Fig. 13). Knowing that the presence of zircons with Cretaceous to Cenozoic ages in the sediments is the main argument for attributing the source of the sediments to the WPA magmatic arc, we calculated for each sample the proportion of zircon ages younger than 80 Ma (Fig. 13c, d) and the proportion of zircon ages between 143 and 80 Ma corresponding to the main mid-Cretaceous magmatic activity (Fig. 13e, f). The third group gives the proportion of zircons with pre-Cretaceous ages to check the contribution and nature of the basement source often neglected in previous studies (Fig. 13g, h). For ease of discussion, the data are presented by sampling region, such as the Chindwin Basin, the Minbu Basin, samples close to the magmatic arc, particularly those from boreholes (Zhang *et al.* 2019*a*), and recent sediments from the Irrawaddy. The same approach is taken for the central IBR and Naga region, with a comparison with results from the Bengal Basin and the Andaman Islands. This presentation of U–Pb DZA data also highlights the great variability between samples (Fig. 13), particularly for samples with a low number of zircons, whereas composite samples seems to show little variation on a regional scale (Figs S24 and S25; Naing *et al.* 2023). We thus acknowledge that a limited number of zircons per sample ($\sim<100$) introduces some statistical bias at the sample level but it does not alter the main observations.

Limited Cenozoic magmatic activity within the BT

Tuffs in the Paunggyi formation do confirm volcanism at the Cretaceous–Paleocene boundary (Cai *et al.* 2020). However, during the Eocene, with the exception of a few tuffs, which testify for sporadic magmatic activity concomitant with sedimentation in the basins, most samples contain zircons derived from the erosion of much older rocks, mainly from a mid-Cretaceous magmatic arc and basement rocks. The DZA distributions suggest a source from the Pane Chaung or Lanjiexue Triassic sediments for the pre-Cretaceous zircons (Figs 13 and S25). Furthermore, erosion of an active volcanic arc should produce magnetite-rich sediments (Roperch *et al.* 1994), which is not supported by the magnetic properties of the sediments sampled in this study (Fig. 4). The low magnetite content and magnetic susceptibility dominated by paramagnetic phases in the rocks sampled (Figs 4 and 5)

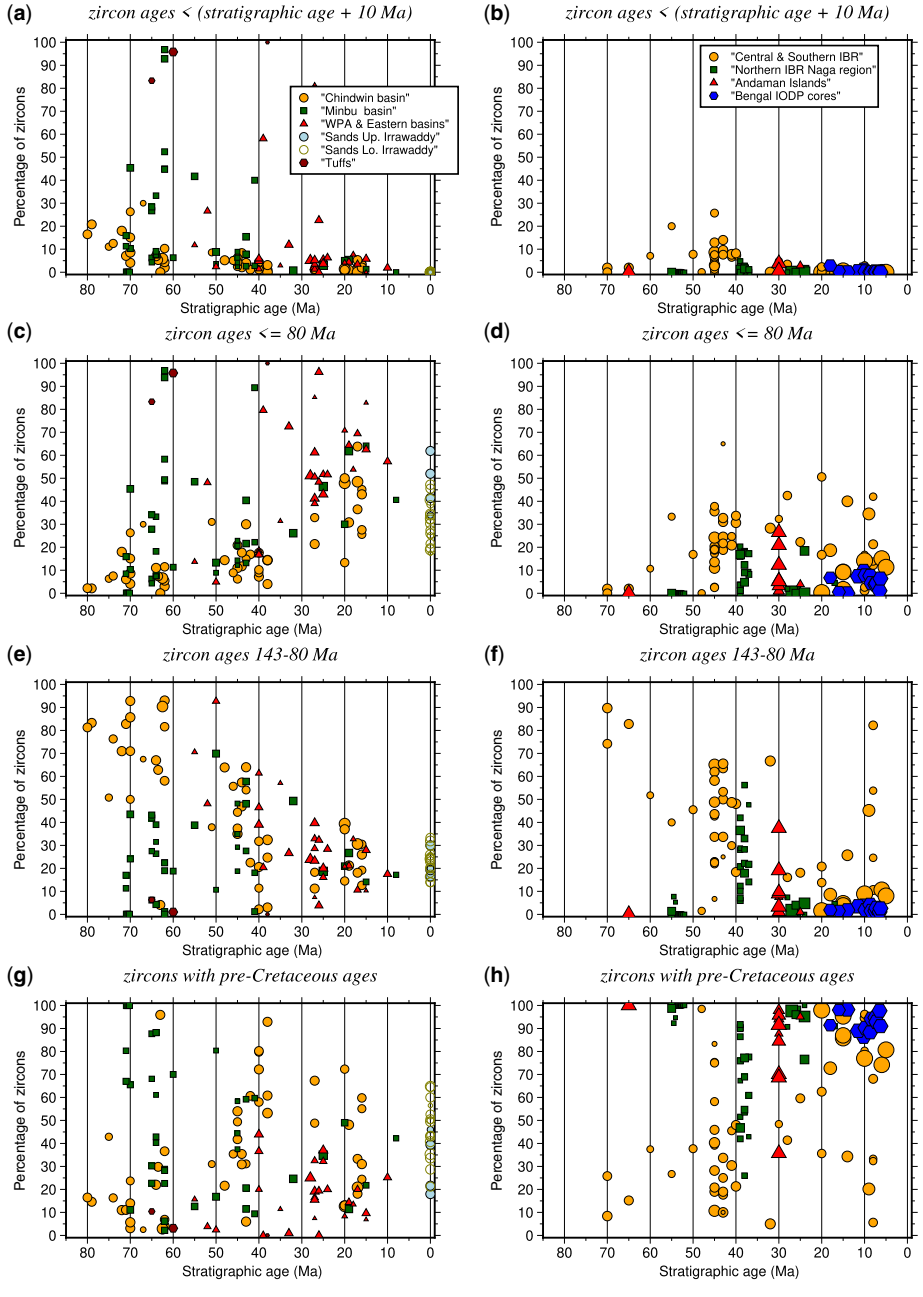

Fig. 13. Plots of the percentage of zircon ages within an age window v. the estimated stratigraphic age of the sample. The sizes of the symbols are proportional to the total number of zircon ages in the sample studied (from less than ~100 up to ~300). Plots in the left column (**a**, **c**, **e**, **g**) are for samples from the CBB block while those in the right column (**b**, **d**, **f**, **h**) are for samples from the central IBR/Naga Hills/Andaman Islands and compared with data from Miocene samples from the Bengal Fan (IODP cores). Source: compilation of numerous previously published DZA studies (Allen *et al.* 2008; Naing *et al.* 2014, 2023; Robinson *et al.* 2014; Wang *et al.* 2014; Garzanti *et al.* 2016; Limonta *et al.* 2017; Blum *et al.* 2018; Cai *et al.* 2020; Licht *et al.* 2019; Morley and Arboit 2019; Zhang *et al.* 2019*a*; Najman *et al.* 2020, 2022; Westerweel *et al.* 2020; Arboit *et al.* 2021; Betka *et al.* 2021; Zhang *et al.* 2021; Bandopadhyay *et al.* 2022; Ding *et al.* 2022; Jonell *et al.* 2022; Najman *et al.* 2022; Zhang *et al.* 2023). Data and location are given in the Supplementary Material.

are more consistent with the exhumation and prolonged transport of sediments from eroded magmatic rocks, basement rocks and reworked sediments from tectonically active zones. The main reliefs of the WPA arc are currently observed in the Wuntho–Banmauk region, with mainly the ~100 Ma WPA batholith with no evidence for a source in basement rocks in sediments from rivers draining the Wuntho Ranges (Licht *et al.* 2020). There are also some isolated volcanoes, such as the Popa volcano, which has an estimated magmatic production of no more than 30 cubic kilometres per Myr (Belousov *et al.* 2018). There is no solid evidence for a major contribution of active volcanism in the WPA recorded during sedimentation (Fig. 13). Low volcanic activity along main topographically high regions of the WPA thus indicates that subduction underneath the Burmese margin was possibly nearly shut down during most of the Paleogene (Fig. 14). Indeed only ~110–90 Ma and sporadic ~42–36 Ma U–Pb zircon ages are present in the Wuntho Ranges volcanic complex (Lin *et al.* 2019; Licht *et al.* 2020). This sporadic igneous activity contradicts tectonic reconstructions where the BT is placed on the margin of Sibumasu or Sumatra in the Cenozoic (e.g. Hall 2012; Zhang *et al.* 2019*b*; Advokaat and van Hinsbergen 2024), as active subduction and volcanism would then be expected along the WPA due to the rapid convergence of India.

An Eocene proto-Bengal basin

The BT closer to India or close to the Sundaland margin during the Eocene has strong implications for the width of the Bengal Basin. In the very wide basin hypothesis, significant differences in sediment sources should be observed on either side of the basin. It is therefore important to assess the type of sediment deposited on each side of the basin to estimate the width of the basin. The Kabaw Formation within the BT central basins, the Falam Formation in the central IBR, the Disang Formation in the Naga Hills all mainly comprise sequences of alternating marine shales and sandstones. It has been difficult to assess an age for these rocks, especially for the central IBR because of an important reworking of Cretaceous fossils (Naing *et al.* 2023). Indeed, Cenozoic zircons have been found in rocks at some sites previously mapped as Cretaceous. U–Pb DZA data are thus the main means to date these sediments. In the Naga Hills region, U–Pb DZA have been recently reported for the late Cretaceous–Eocene Disang Fm, usually interpreted as deposited on the distal Indian continental shelf (Ding *et al.* 2022). The Lower Disang sediments deposited in an open marine environment have only pre-Cretaceous DZA, suggesting a source in the Tethys Himalaya (Ding *et al.* 2022) but also the Triassic Pane Chaung Formation from the IBR. U–Pb DZA data from the Eocene Phokphur Formation in the Naga Hills also indicate a source from either the IBR basement or the Langjiexue Formation (Aitchison *et al.* 2019). Naing *et al.* (2023) consider that the sediments filling the BT central basins and the IBR have two distinct sources, the IBR basement and the WPA, respectively (see fig. 17 from Naing *et al.* (2023); Figs S25, S26 and S27).

In the Upper Disang sediments of the Naga Hills region, likely of late Eocene age from foraminifer evidence (Lokho *et al.* 2020), the distribution of Cretaceous and Cenozoic zircons ages is similar to the one found in equivalent age sediments from the central IBR in Myanmar (Naing *et al.* 2023). Erosion of the WPA is still advocated for a source of sediments in the remote Disang basin from the Naga region (Ding *et al.* 2022). In addition to the similarities in sediment sources from DZA data, large olistoliths of pelagic limestone blocks are present both in the Falam/Chunsung of the central IBR and in Disang sediments deposited within a basin on the eastern margin of India (Sengupta *et al.* 1989; Morley *et al.* 2020). The obvious correlations between the sediments of the Disang Formation, deposited in a basin on the Indian margin, and those found farther south in the central IBR indicate the existence of a basin filled by sediments with similar sources, which constitutes undoubtedly the best geological argument in favour of a close correlation of the BT to India, rather than Sumatra or Indochina. The wide basin from the Indian margin where the Disang sediments were deposited to the central IBR may characterize a wide proto-Bengal basin in the Eocene (Rangin and Sibuet 2017).

The width of the basin during the Eocene was obviously much greater than it is today, but the amount of subduction and shortening below and across the IBR is difficult to estimate. Thermochronological data in Eocene sediments indicate early Miocene zircon (U–Th)/He ages (Najman *et al.* 2020, 2022). Such a reset may be due to burial by a thick upper Eocene–Oligocene sequence or tectonic stacking in the late Oligocene. Since the late Oligocene– early Miocene, the core of the IBR has been uplifted with significant exhumation. There are no good estimates of shortening across the IBR, but the deep earthquakes imaging the subducted crust below the BT (Mon *et al.* 2020) as well as the present-day east–west convergence at a rate of 15–20 mm a^{-1} from GPS data (Lindsey *et al.* 2023) suggest more than 300 km of shortening, mostly during the Neogene.

Tectonic evidence

This positioning of the BT near India is further supported by tectonic evidence east of the BT. First of all, there is a lack of evidence for a suture between

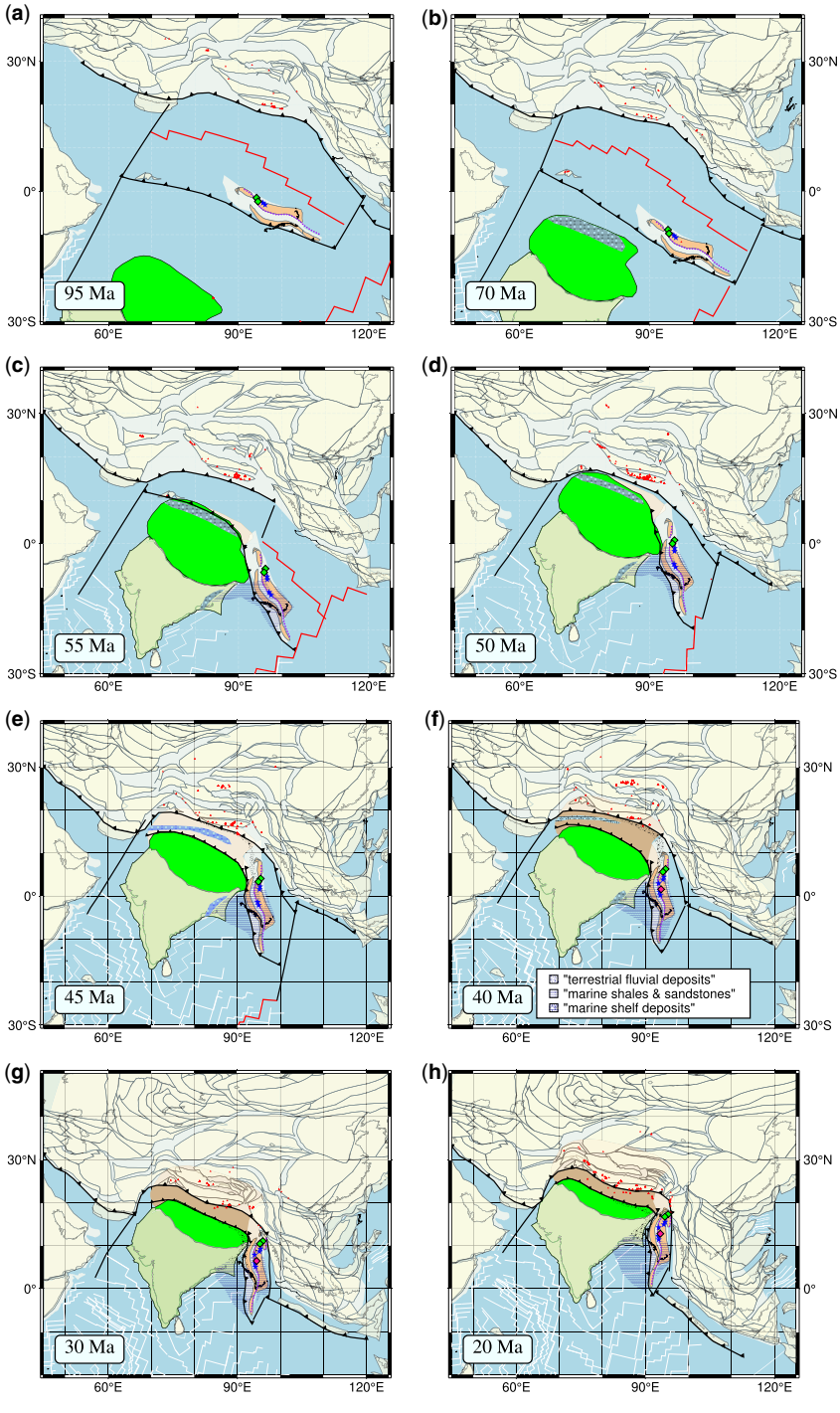

Fig. 14. Plate reconstructions of the BT through time: (**a**)–(**h**) 95, 70, 55, 50, 45, 40, 30 and 20 Ma. The collision of India with Asia is inferred to have occurred at ~50 Ma. At 40 Ma, the deformation front is located within Greater India with subduction of India below this frontal thrust. Major expected sediment depocentres are shown. Reconstructions done according to the reference frame based on data from Australia (see Fig. 11). Red dots are the locations of active magmatism in a ± 2.5 Myr window from the database of Chapman and Kapp (2017).

the BT and Sibumasu, in the form of an ophiolite belt or an accretionary prism (Morley *et al.* 2020), although it is possible that later strike-slip deformation along the Sagaing Fault has obscured this suture. It should be noted that dismembered ophiolite fragments of the Jade Belt and Central Ophiolite Belt lie along the trace of the Sagaing Fault (Htay *et al.* 2017). A second issue concerns geological observations indicating that the Eastern Andaman basins along the margin of Sibumasu experienced east–west extension instead of shortening during the late Eocene–Oligocene (Morley and Alvey 2015; Morley 2017*a*). This precludes the possibility of a major collision and underthrusting event occurring in this region. Finally, significant deformation and uplift within the BT is only observed in the late Oligocene–early Miocene on seismic lines and exhumation ages, with only incipient or no uplift before the late Eocene (Zhang *et al.* 2017*b*, 2019*a*; Licht *et al.* 2019, 2020; Gough *et al.* 2020; Najman *et al.* 2020; Westerweel *et al.* 2020).

Based on the evidence summarized above from both the BT sedimentary basins, WPA volcanic activity, IBR sedimentary provenance and tectonic constraints from Eastern Andaman, we consider a tectonic model with only a reduced amount of subduction of oceanic crust below the BT that supports the BT being close to India instead of a more isolated and eastern position as part of the Australian Plate (Advokaat and van Hinsbergen 2024). In our reconstructions, we also consider the Western Andaman Arc to be part of the BT as the sediments share several sources with those of the CBB and IBR (Naing *et al.* 2023). Thick Paleocene volcanic tuffs are also found in contemporaneous sedimentary sequences in Myanmar and in the Andaman islands, further suggesting nearby volcanic activity at that time from a similar source, in contrast to the complex palaeogeographical setting proposed by Bandopadhyay *et al.* (2022) where these two features are separated.

Plate reconstructions and palaeogeography

In the plate tectonic framework presented above, we propose a series of plate reconstructions according to the palaeolatitudes provided by the BT palaeomagnetic data and the geological constraints, in particular the information from the thick sedimentary archives of the BT.

170–100 Ma

In our reconstructions (Fig. 12) we consider that rifting between the BT and Gondwana occurred in two stages. The first involves the rifting of the CBB with the formation of an ocean basin of Late Jurassic age. Jurassic cherts deposited in this basin are found within the WBO and Nagaland ophiolite belt (Aitchison *et al.* 2019; Naing *et al.* 2023). The IBR ribbon with Mount Victoria Block as the largest element could have rifted from the Australian margin several million years later. Another possibility is that the IBR block may be a thin discontinuous extended crustal ribbon formed during the break-up and only slightly separated from the CBB. In Late Barremian–Early Aptian (~125–120 Ma), we postulate the BT as one element of the Trans-Tethyan subduction system. The CBB may have collided with an existing Trans-Tethyan subduction zone, causing subduction to jump to the south with the formation of a supra subduction zone at ~120 Ma in the Jurassic ocean basin in between the CBB and Mount Victoria block just started the subduction below the CBB. The closure of the postulated ocean basin between the CBB and Mount Victoria block is needed to account for the abundant occurrence of Upper Jurassic radiolarians from deep-marine cherts in the Kalemyo ophiolite (Naing *et al.* 2023) and in the Naga Hills (Aitchison *et al.* 2019) leading to the formation of the WBO and likely followed by a second shift of the subduction zone to the other side of the IBR. The Aptian–Cenomanian Paung Chaung limestones of the BT contain clasts of the Kanpetlet Schists and Pane Chaung Triassic sediments, and unconformably overlie these Triassic units. The Paung Chaung limestones are thus deposited on what becomes a single terrane by the mid-Cretaceous, consisting of the Mount Victoria Block and the CBB and now part of the Trans-Tethyan Arc (Mitchell 2018*g*; Morley *et al.* 2020). In the reconstructions, the IBR and CBB blocks are slightly separated, only to account for the expected shortening occurring mainly during the Neogene. We rule out the possibility that the CBB was on an alternative Trans-Tethyan Arc that rifted from the Lhasa margin instead of Gondwana as part of an extended Xigaze group (Gibbons *et al.* 2015) and that it later collided with the IBR block. This scenario implies subduction of oceanic crust during the Early Cretaceous below the CBB but there is no evidence of Early Cretaceous magmatism in the BT.

95–70 Ma

Following Westerweel *et al.* (2019), the BT is part of the Trans-Tethyan Arc during this time period. At 70 Ma, we speculate that the BT was still on the Trans Tethyan Arc but at a slightly more southern position between 10° and 20° S than at 95 Ma.

~65–50 Ma

The Late Cretaceous–middle Eocene appears to be a key time period for the BT, as our palaeomagnetic

results indicate that the coeval northward motion with India began at this time (Fig. 14), potentially accompanied by a degree of clockwise rotation if we accept that the result at site ST01 is representative of the whole CBB, in agreement with previous data from the WPA (Westerweel *et al.* 2019). We propose that the collision of Greater India with the northern extension of the BT (Greater BT) occurred in the Late Cretaceous–early Paleocene and this collision initiated the final clockwise rotation of the BT. This collision should have been coeval with the thrusting of the WBO on to the Indian passive margin in the northern IBR (Naga Hills). This deformation event in the northern IBR is virtually undocumented along the central and southern IBR, which was shielded from major deformation before the Oligocene. After the collision of Greater India with the northern BT, the BT rotated clockwise, possibly by trench roll back. We speculate that sedimentation initiated in a wide basin extending from the Indian margin to the BT with sources related to the collision of the Greater BT with Greater India. The collision of India with Asia occurred at ~50 Ma, according to our choice of palaeogeography.

45–40 Ma

In this time frame, the entire BT is interpreted to be mainly dragged northward with India based on their similar cumulative northward motion. Except for the northern extension of the BT, most of the BT is still far from the main collision zones and shielded from tectonic deformation, allowing marine sedimentation to occur in most of the area. Sediments from the IBR and the CBB have roughly the same DZA signatures, suggesting the same source (Fig. S25). We speculate the same source of sediments for the thick Eocene sequence in the northern Bay of Bengal as evidenced by multi-channel seismic data (Rangin and Sibuet 2017). In the reconstructions, ~1 cm a^{-1} of dextral convergence is still accepted within the IBR, likely by oblique subduction of the oceanic crust below the BT but at an insufficient rate for active magmatism on the BT. We theorize oblique subduction below Sundaland as the BT is moving north with India, but little information exists for the geological evolution of the area left in between the BT and Sundaland during the Eocene.

30–20 Ma

In the Oligocene–early Miocene, sedimentation begins to show more significant differences on either side of the uplifting IBR chain. To the west, sediments from the Himalayas become important; with pre-Cretaceous zircons that no longer have the Triassic signature of the IBR chain (Betka *et al.* 2021). In the BT central basins, however, the source of Cenozoic sediments corresponds to zircons whose Hf signature becomes negative and is often considered to originate from Sibumasu (Najman *et al.* 2022). Thermochronological data from the early Miocene Letkat sedimentary rocks clearly indicate a sediment source from an area in the Eastern Himalayan Syntaxis of very rapid exhumation (Westerweel *et al.* 2020). The closure of the ocean basin east of the BT led to the formation of the proto-Sagaing Fault and initiation of the opening within the Andaman basin, leading to the set-up of the present-day tectonic regime of Myanmar.

Tectonic implications for India–Asia collision models

Collision of Greater India with the northern Burma terrane

A scenario of an early collision (~60 Ma) of India with the Asian margin is mainly advanced to explain apparent provenance from Asia to India recorded in Paleocene sandstones deposited on the Indian passive margin (An *et al.* 2021). This provides a fundamental clue to constrain the timing of the initial collision (Najman *et al.* 2010, 2017; Hu *et al.* 2016; An *et al.* 2021). With the scenario of a first collision of the BT with India (Fig. 14), and as the BT is likely the main element of the Trans-Tethyan system, the earliest sediments deposited on the Tethyan margin with Late Cretaceous–Paleocene zircon ages may have originated from the BT arc (Trans-Tethyan Arc), rather than the Gangdese and Lhasa margin. This option of a source in the BT, rather than from Lhasa, has never been considered. A source in the Kohistan Arc is also not considered, as it is often proposed that the Kohistan collision occurred first with Asia and then with India, despite palaeomagnetic data suggesting the opposite sequence (Martin *et al.* 2020). We therefore consider that a collision of India with the Trans-Tethyan Arc, composed of the BT and Kohistan, might explain the early arrival of sediments with zircons of Late Cretaceous to Paleocene ages on to the Tethyan margin of India.

Collision of India/BT with Asia

Identifying the origin of the sediments that fill the extensive Eocene sedimentary basins could aid in determining the timing and models of the collision between India and Asia. A contribution from the Gangdese magmatic belt as a source of sediments for the BT central basins was first considered in early studies (Robinson *et al.* 2014). However, in most following studies, except Arboit *et al.* (2021), the filling of the BT central basins has been interpreted as having occurred within an Andean-type

continental margin, with the WPA being an active arc above the continuous subduction of Indian oceanic crust beneath Sundaland (Licht *et al.* 2013, 2019; Wang *et al.* 2014; Zhang *et al.* 2019*a*; Najman *et al.* 2022). The positive ε_{Hf} values found in Mesozoic zircons were then used to reject a source in Sibumasu, leaving the WPA as the sole source of these zircons.

We, however, consider that the WPA, as observed in Myanmar, is unlikely to be a significant source. Sediments should come from areas with active tectonics inducing erosion of an ancient arc and basement rocks, rather than from a subsiding magmatic arc. Indeed, seismic lines and drill cores along the WPA (Zhang *et al.* 2017*b*) indicate that the WPA batholiths are largely covered by Paleogene to Neogene mostly marine sediments of the BT central basins. In our reconstructions (Fig. 14), subduction below the BT is also limited and impeded by the rapid northward motion and the volcanic arc was likely dead during the Eocene. This indicates that the WPA was probably not a major source of sediments for the adjacent major basins. DZA data from Eocene sediments from the central IBR are also quite similar to those of the CBB block (Fig. S25) suggesting that the central IBR was not of significant relief and thus a source of sediments during the Eocene.

For the Oligocene and Miocene, there is already evidence that sediments come from the India–Asia collision zone because the sediments from the Barail Formation in the IBR, the Padaung Formation and the Letkat Formation from the BT central basins have detrital zircons with young ZFT ages (Zhang *et al.* 2019*a*; Betka *et al.* 2021) or apatite with U–Pb ages indicating already very fast exhumation (Westerweel *et al.* 2020) within a region of active tectonics. During the Eocene, erosion of the Gangdese Arc and the domains involved in the collision are likely to have been a major source of sediments that were deposited in a wide proto-Bengal basin from the BT to the Indian margin. From the U–Pb DZA dataset (Figs S24, S25 and S26), it seems difficult to reject that hypothesis. The generally positive ε_{Hf} values from Cretaceous to Eocene zircons found in Eocene BT sediments is not a good argument to assert a WPA origin as zircons from the Gangdese arc also have positive ε_{Hf} values (see Najman *et al.* 2022 for a recent review). The distributions of zircon ages in Eocene sedimentary rocks from the BT are also closely comparable to those found in Eocene sedimentary rocks of the Lhasa margin (Xigaze basin) and Tethyan Himalayas (Ma *et al.* 2022*a*, 2023; Fig. S24). The main difference is a wider peak in mid-Cretaceous ages in the BT (Fig. S24), while the zircon distribution of mid-Cretaceous ages for the Eocene sediments of the Asia margin is better centred on a slightly younger age (~90 Ma), as already shown in Kapp and DeCelles (2019). Cretaceous U–Pb DZA of the BT sediments suggest a contribution of both the WPA and Gangdese arc especially during the Eocene (Fig. S27). Otherwise, the pre-Cretaceous U–Pb DZA distributions in Late Cretaceous to Eocene samples for the CBB, central IBR and Naga Hills regions suggest a sediment source likely from the Triassic Pane Chaung or Langjiexue Formations (Fig. S28; see also Naing *et al.* 2023). However, we should consider that most of the basement rocks from the region share similar Cambrian and Precambrian DZA characteristics – Naga Metamorphic rocks (Aitchison *et al.* 2019), Langjiexue Formation, Pane Chaung Formation (Naing *et al.* 2023), Katha–Gangaw Range (Aung *et al.* 2022) – as most of the terranes (Lhasa, Argoland, Greater India) were probably nearby before their break-up from the northern Gondwanan margin. Future sedimentological studies will need to focus provenance budgets on multiproxy geochronological data (Bracciali 2019; Arboit *et al.* 2021) but also on integrated petrographic, heavy-mineral and geochemical datasets (Liang *et al.* 2022). At this stage, the arguments against the hypothesis that the Eocene sediments of the BT central basins and the IBR cover are partly derived from the India–Asia collision need to be re-evaluated (Arboit *et al.* 2021).

After ~50 Ma, a source of sediments filling the BT central basins and IBR from the erosion of the deforming parts of the northeastern part of Greater India and Greater Burma but also from the Gangdese belt would lend support to a collision of India with Asia at ~50 Ma.

To explain the early collision of India with Asia, van Hinsbergen *et al.* (2012) proposed the existence of a Greater India Basin (GIB). According to their hypothesis, the Tethyan Himalaya block collided with Lhasa at ~60 Ma. The collision between India and Asia was finalized during the Oligocene period. Our interpretation of the source of Eocene sediments filling the BT and Bengal basin is therefore incompatible with the GIB model (Van Hinsbergen *et al.* 2012), as the GIB tectonic setting with a deep-water ocean between India and Asia would prevent sediments from the Gangdese reaching the BT.

BT–Sibumasu collision

In our new model, the main northern Sibumasu block is within the collision zone and extruded with Indochina during the Eocene–Oligocene after the collision of Greater India/Greater Burma with Asia (Fig. 14; Lamont *et al.* 2021).

From the late Oligocene onwards, the displacement of the BT relative to Sundaland is mainly dextral along a proto-Sagaing Fault inducing the opening of the Andaman Sea. The major Miocene

dextral displacement along the Sagaing Fault, which juxtaposes the weakly deformed BT with the uplifted and strongly exhumed Sibumasu margin (Bertrand *et al.* 2001) obscures the earlier tectonic setting. The trace of a past suture between the BT and Sibumasu, in the form of an ophiolite belt or an accretionary prism (Morley *et al.* 2020), remains to be clearly drawn.

Deformation and uplift within the BT is only observed in the late Oligocene – early Miocene based on seismic lines and exhumation ages, with only incipient and limited uplift in the late Eocene (Zhang *et al.* 2017*b*; Najman *et al.* 2020; Westerweel *et al.* 2020). The main uplift phase in the core of the IBR (Najman *et al.* 2020, 2022) occurred during the Miocene.

Thus, geological evidence supports a reconstruction model where the central and southern parts of BT were still separated from Sibumasu until the early Oligocene, resulting in a later final accretion of the central and southern parts of BT with Sibumasu in the late Oligocene–early Miocene, similar to the model of Morley *et al.* (2020). This interpretation is consistent with an earlier collision between Asia and the speculated now underthrusted Greater Burma region, while there is no strong deformation recording a collision within the BT itself.

With this late Oligocene–early Miocene collision event on the eastern side of the BT, the hyper-oblique displacement of India relative to Sibumasu is mainly partitioned by north–south dextral motion along the Sagaing Fault and east–west shortening across the IBR. The exact nature of the plate margin east of the BT during the Eocene remains a major uncertainty in our model, but the western boundary of Sibumasu during the Cenozoic was not a classic Andean-type margin as in most previous models (e.g. Sevastjanova *et al.* 2016; Searle *et al.* 2017; Zhang *et al.* 2019*b*; Li *et al.* 2020).

Palaeobiogeographical importance of the BT on a Trans-Tethyan Arc

The BT contains one of the most prolific sites for Cretaceous fossils preserved in amber anywhere in the world. Therefore, deducing the origin of all these species is important for understanding Asian biodiversity. Palaeolatitude data from the WPA during the Cretaceous (Westerweel *et al.* 2019) provided a geodynamic framework for interpreting the very rich palaeobiodiversity preserved in Myanmar ambers. The rich Burmese record of Cretaceous fossil amber biota contains indications for both Gondwanan and endemic traits within the wide range of species available (e.g. Grimaldi *et al.* 2002; Poinar 2018; Rasnitsyn and Öhm-Kühnle 2018; Liu *et al.* 2020). For these reasons, an isolated ribbon block origin for the BT as part of a Trans-Tethyan subduction system, which incorporated crustal fragments from Gondwana, seems the best way to reconcile the available palaeomagnetic, geological and palaeontological information from the BT.

Huang *et al.* (2021) propose that the BT with its high floristic diversity was a crossroads for India–Asia plant dispersals and that a Trans-Tethyan Arc may also have been an important bridge for important species such as the Dipterocarps to be dispersed from one continent to another (Bansal *et al.* 2022). However, the first middle Paleocene fossil wood specimens from Myanmar also provide evidence for the early presence of multiple taxa of Laurasian affinity in Myanmar (Gentis *et al.* 2023).

The late middle Eocene Pondaung Formation in Central Myanmar contains sites rich in fossils mammals, especially anthropoids primates, older than any known African anthropoid site (Jaeger *et al.* 2019). By examining evidence from anthropoids and other mammalian groups, Chaimanee *et al.* (2024) demonstrate that several dispersal events occurred between South Asia and Afro-Arabia during the middle Eocene to the early Oligocene. The BT may have been a key bridge in the Neotethys Ocean to significantly reduce the distance of overseas dispersal.

Conclusions

This study integrates additional palaeomagnetic datasets for the Paleocene/Eocene of the BT of Myanmar to constrain its palaeolatitudinal motion with previously published results from the early Late Cretaceous and late Eocene (Westerweel *et al.* 2019, 2020).

Despite a scatter in palaeolatitude possibly related to uncertainties in age assignments and the low reliability of some data with a reduced number of samples, these results reveal a systematic trend towards an equatorial to slightly southern hemisphere position of the BT during the Late Cretaceous to Eocene.

Uncertainties remain. Data from the BT are in better agreement with the APWP for India calculated from the Australian APWP than with the APWP global model from Torsvik *et al.* (2012). This observation highlights the need to further study the reliability of current APWPs during the Paleogene.

From the available data, we construct a palaeogeography with the following key features: (1) the BT remained in a southern hemisphere position distant from the southern Asian margin throughout the Late Cretaceous and early Paleogene; (2) the BT was incorporated in the Indian Plate in the latest Paleocene; and (3) it subsequently moved northwards with only minor east–west convergence relative to India along a dextral strike-slip system to its

east, until (4) a late Oligocene–early Miocene oblique collision with the Sundaland margin. These constraints on the tectonic history of the BT and eastern Himalayan orogen provide important new perspectives on the India–Asia collision puzzle, supporting collision models involving the northward-moving Indian continent colliding first with a Trans-Tethyan subduction. Our study suggests that the BT is an essential component of the Trans-Tethyan Arc and that the collision of Greater India with this terrane could explain a very early arrival of sediments with a signature different from that of the Indian margin during the Paleocene, not from the Lhasa margin, but from the northern BT. The collision of Greater India with the Lhasa margin around 50 Ma becomes a region of active tectonics, and sediments produced by the erosion of the uplifting collision zone, potentially including the Gangdese Arc, could be an additional source of sediments filling the basins of the BT from the middle Eocene onwards, even being the early stages of a proto-Bengal basin. This updated palaeogeography model of the India–Asia collision has important implications for understanding the interplay between Asian tectonics and climate, as well as the origin and dispersion of the prolific Burmese pollen and (amber) fossil record. However, despite our collision model being supported by the available geological data, it is also clear that it contains important uncertainties, in particular the postulated disappearance of a Greater Burma block, mainly due to the lack of tectonic constraints from the extremely deformed eastern end of the Himalayan collision zone. Therefore, the collision model and the key role of the BT therein presented here opens up new frontiers for further research across the Himalayan orogen to resolve these uncertainties.

Acknowledgements Special thanks to Alexis Licht for his invaluable help in organizing field trips and numerous discussions during the course of this study. We would like to thank Professor Day Wa Aung from Yangon University for his support for this research project in Myanmar. Magnetic hysteresis data were acquired with the AGM and VSM8600 at the Laboratoire des Sciences du Climat et de l'Environnement (LSCE). We are grateful to Philippe Cullerier for helping with the palaeomagnetic experiments. We thank Eldert Advokaat, Nathan Cogné, François Guillocheau, Amy Gough, France Lagroix, Andrew Mitchell, Chris Morley, Yani Najman, Vincent Perrichot, Anne Replumaz, Ed Sobel and Douwe van Hinsbergen for constructive discussions throughout this study. The palaeogeographical reconstruction and some figures were created using the free software GPlates (http://www.gplates.org), as well as GMT (http://gmt.soest.hawaii.edu/). Finally, we thank John Geissman, Tara Jonell and Chris Morley for their constructive reviews of this article. The whole palaeomagnetic dataset, including the rejected sites, has been uploaded in the Magic database (https://www2.earthref.org/MagIC).

Competing interests The authors declare that they have no known competing financial interests or personal relationships that could have appeared to influence the work reported in this paper.

Author contributions **JW**: conceptualization (equal), data curation (lead), formal analysis (equal), investigation (lead), visualization (equal), writing – original draft (lead), writing – review & editing (equal); **PR**: conceptualization (lead), data curation (equal), formal analysis (equal), investigation (equal), methodology (lead), supervision (lead), validation (lead), visualization (equal), writing – original draft (equal), writing – review & editing (equal); **ZW**: data curation (supporting), investigation (supporting), resources (supporting); **GD-N**: conceptualization (equal), data curation (supporting), formal analysis (equal), funding acquisition (lead), investigation (equal), methodology (supporting), project administration (lead), resources (lead), supervision (equal), validation (equal), writing – original draft (supporting), writing – review & editing (equal).

Funding This research was primarily funded by the European Research Council through ERC Consolidator Grant MAGIC 649081 awarded to GD-N.

Data availability All data generated or analysed during this study are included in this published article (and its Supplementary Material).

References

Acharyya, S.K. 2007. Collisional emplacement history of the Naga-Andaman ophiolites and the position of the eastern Indian suture. *Journal of Asian Earth Sciences*, **29**, 229–242, https://doi.org/10.1016/j.jseaes.2006.03.003

Acharyya, S.K. 2015. Indo-Burma Range: a belt of accreted microcontinents, ophiolites and Mesozoic–Paleogene flyschoid sediments. *International Journal of Earth Sciences*, **104**, 1235–1251, https://doi.org/10.1007/s00531-015-1154-6

Advokaat, E.L. and Van Hinsbergen, D.J.J. 2024. Finding Argoland: reconstructing a microcontinental archipelago from the SE Asian accretionary orogen. *Gondwana Research*, **128**, 161–263, https://doi.org/10.1016/j.gr.2023.10.005

Advokaat, E.L., Marshall, N.T., Li, S., Spakman, W., Krijgsman, W. and van Hinsbergen, D.J.J. 2018. Cenozoic rotation history of Borneo and Sundaland, SE Asia revealed by paleomagnetism, seismic tomography, and kinematic reconstruction. *Tectonics*, **37**, 2486–2512, https://doi.org/10.1029/2018TC005010

Aitchison, J.C., Ao, A. *et al.* 2019. Tectonic evolution of the Western Margin of the Burma microplate based on new fossil and radiometric age constraints. *Tectonics*, **38**, 1718–1741, https://doi.org/10.1029/2018TC005049

Allen, R., Najman, Y. *et al.* 2008. Provenance of the Tertiary sedimentary rocks of the Indo-Burman Ranges, Burma (Myanmar): Burman arc or Himalayan-derived?

Journal of the Geological Society, London, **165**, 1045–1057, https://doi.org/10.1144/0016-76492007-143

An, W., Hu, X., Garzanti, E., Wang, J. and Liu, Q. 2021. New precise dating of the India-Asia collision in the Tibetan Himalaya at 61 Ma. *Geophysical Research Letters*, **48**, e2020GL090641, https://doi.org/10.1029/2020GL090641

Appel, E., Crouzet, C. and Schill, E. 2012. Pyrrhotite remagnetizations in the Himalaya: a review. *Geological Society, London, Special Publications*, **371**, 163–180, https://doi.org/10.1144/SP371.1

Arboit, F., Min, M., Chew, D., Mitchell, A., Drost, K., Badenszki, E. and Daly, J.S. 2021. Constraining the links between the Himalayan belt and the Central Myanmar Basins during the Cenozoic: an integrated multi-proxy detrital geochronology and trace-element geochemistry study. *Geoscience Frontiers*, **12**, 657–676, https://doi.org/10.1016/j.gsf.2020.05.024

Aubourg, C., Pozzi, J.-P. and Kars, M. 2012. Burial, claystones remagnetization and some consequences for magnetostratigraphy. *Geological Society, London, Special Publications*, **371**, 181–188, https://doi.org/10.1144/SP371.4

Aung, M.M., Ding, L. *et al*. 2022. Paleogeographic evolution of Southeast Asia: geochemistry and geochronology of the Katha-Gangaw Range, Northern Myanmar. *Minerals*, **12**, 1632, https://doi.org/10.3390/min12121632

Bandopadhyay, P.C., Van Hinsbergen, D.J.J. *et al*. 2022. Paleogeography of the West Burma Block and the eastern Neotethys Ocean: constraints from Cenozoic sediments shed onto the Andaman-Nicobar ophiolites. *Gondwana Research*, **103**, 335–361, https://doi.org/10.1016/j.gr.2021.10.011

Bannert, D., Sang Lyen, A. and Htay, T. 2012. *The Geology of the Indoburman Ranges in Myanmar*. Geologisches Geologisches Jahrbuch 101, BGR, Hannover.

Bansal, M., Morley, R.J. *et al*. 2022. Southeast Asian Dipterocarp origin and diversification driven by Africa-India floristic interchange. *Science*, **375**, 455–460, https://doi.org/10.1126/science.abk2177

Barber, A.J. and Crow, M.J. 2009. Structure of Sumatra and its implications for the tectonic assembly of Southeast Asia and the destruction of Paleotethys. *Island Arc*, **18**, 3–20, https://doi.org/10.1111/j.1440-1738.2008.00631.x

Belousov, A., Belousova, M., Khin Zaw, Streck, M.J., Bindeman, I., Meffre, S. and Vasconcelos, P. 2018. Holocene eruptions of Mt. Popa, Myanmar: volcanological evidence of the ongoing subduction of Indian Plate along Arakan Trench. *Journal of Volcanology and Geothermal Research*, **360**, 126–138, https://doi.org/10.1016/j.jvolgeores.2018.06.010

Benammi, M., Naing Soe, A. *et al*. 2002. First magnetostratigraphic study of the Pondaung Formation: implications for the age of the Middle Eocene anthropoids of Myanmar. *Journal of Geology*, **110**, 748–756, https://doi.org/10.1086/342868

Bender, F. 1983. *Geology of Burma*. Borntraeger, Berlin.

Bertrand, G. and Rangin, C. 2003. Tectonics of the western margin of the Shan plateau (central Myanmar): implication for the India–Indochina oblique convergence since the Oligocene. *Journal of Asian Earth Sciences*, **21**, 1139–1157, https://doi.org/10.1016/S1367-9120(02)00183-9

Bertrand, G., Rangin, C., Maluski, H. and Bellon, H. 2001. Diachronous cooling along the Mogok Metamorphic Belt (Shan scarp, Myanmar): the trace of the northward migration of the Indian syntaxis. *Journal of Asian Earth Sciences*, **19**, 649–659, https://doi.org/10.1016/S1367-9120(00)00061-4

Besse, J. and Courtillot, V. 1988. Paleogeographic maps of the continents bordering the Indian Ocean since the Early Jurassic. *Journal of Geophysical Research: Solid Earth*, **93**, 11791–11808, https://doi.org/10.1029/JB093iB10p11791

Betka, P.M., Thomson, S.N. *et al*. 2021. Provenance shifts during Neogene Brahmaputra delta progradation tied to coupled climate and tectonic change in the Eastern Himalaya. *Geochemistry, Geophysics, Geosystems*, **22**, 2021GC010026, https://doi.org/10.1029/2021GC010026

Bian, W., Wang, S. *et al*. 2022. Location and shape of the Lhasa terrane prior to India-Asia collision. *GSA Bulletin*, **135**, 2255–2274, https://doi.org/10.1130/B36647.1

Bilal, A. and McClay, K. 2022. Tectonic and stratigraphic evolution of the central Exmouth Plateau, NW Shelf of Australia. *Marine and Petroleum Geology*, **136**, 105447, https://doi.org/10.1016/j.marpetgeo.2021.105447

Blum, M., Rogers, K., Gleason, J., Najman, Y., Cruz, J. and Fox, L. 2018. Allogenic and autogenic signals in the stratigraphic record of the deep-sea Bengal Fan. *Scientific Reports*, **8**, 7973, https://doi.org/10.1038/s41598-018-25819-5

Borradaile, G.J. and Henry, B. 1997. Tectonic applications of magnetic susceptibility and its anisotropy. *Earth-Science Reviews*, **42**, 49–93, https://doi.org/10.1016/S0012-8252(96)00044-X

Bracciali, L. 2019. Coupled zircon-rutile U-Pb Chronology: LA ICP-MS dating, geological significance and applications to sediment provenance in the Eastern Himalayan-Indo-Burman Region. *Geosciences*, **9**, 467, https://doi.org/10.3390/geosciences9110467

Brunnschweiler, R.O. 1966. On the geology of the Indoburman ranges: (Arakan Coast and Yoma, Chin Hills, Naga Hills). *Journal of the Geological Society of Australia*, **13**, 137–194, https://doi.org/10.1080/00167616608728608

Buckman, S., Aitchison, J.C. *et al*. 2018. The Spongtang Massif in Ladakh, NW Himalaya: an Early Cretaceous record of spontaneous, intra-oceanic subduction initiation in the Neotethys. *Gondwana Research*, **63**, 226–249, https://doi.org/10.1016/j.gr.2018.07.003

Butler, R.F. 1992. *Paleomagnetism: Magnetic Domains to Geologic Terranes*. Blackwell.

Cai, F., Ding, L., Laskowski, A.K., Kapp, P., Wang, H., Xu, Q. and Zhang, L. 2016. Late Triassic paleogeographic reconstruction along the Neo–Tethyan Ocean margins, southern Tibet. *Earth and Planetary Science Letters*, **435**, 105–114, https://doi.org/10.1016/j.epsl.2015.12.027

Cai, F., Ding, L. *et al*. 2020. Initiation and evolution of forearc basins in the Central Myanmar Depression. *GSA Bulletin*, **132**, 1066–1082, https://doi.org/10.1130/B35301.1

Chaimanee, Y., Chavasseau, O., Lazzari, V., Soe, A.N., Sein, C. and Jaeger, J. 2024. Early anthropoid primates:

new data and new questions. *Evolutionary Anthropology: Issues, News, and Reviews*, **33**, e22022, https://doi.org/10.1002/evan.22022

Chapman, J.B. and Kapp, P. 2017. Tibetan magmatism database. *Geochemistry, Geophysics, Geosystems*, **18**, 4229–4234, https://doi.org/10.1002/2017GC007217

Cogne, J.-P., Besse, J., Chen, Y. and Hankard, F. 2013. A new Late Cretaceous to Present APWP for Asia and its implications for paleomagnetic shallow inclinations in Central Asia and Cenozoic Eurasian plate deformation. *Geophysical Journal International*, **192**, 1000–1024, https://doi.org/10.1093/gji/ggs104

Crouzet, C., Dunkl, I., Paudel, L., Árkai, P., Rainer, T.M., Balogh, K. and Appel, E. 2007. Temperature and age constraints on the metamorphism of the Tethyan Himalaya in Central Nepal: a multidisciplinary approach. *Journal of Asian Earth Sciences*, **30**, 113–130, https://doi.org/10.1016/j.jseaes.2006.07.014

Crow, M.J. and Khin Zaw 2017. Appendix: geochronology in Myanmar (1964–2017). *Geological Society, London, Memoirs*, **48**, 713–759, https://doi.org/10.1144/M48.32

Cruickshank, R.D. and Ko, K. 2003. Geology of an amber locality in the Hukawng Valley, Northern Myanmar. *Journal of Asian Earth Sciences*, **21**, 441–455, https://doi.org/10.1016/S1367-9120(02)00044-5

Dankers, P.H.M. and Zijderveld, J.D.A. 1981. Alternating field demagnetization of rocks, and the problem of gyromagnetic remanence. *Earth and Planetary Science Letters*, **53**, 89–92, https://doi.org/10.1016/0012-821X(81)90029-7

Delclòs, X., Peñalver, E. *et al*. 2023. Amber and the Cretaceous Resinous Interval. *Earth-Science Reviews*, **243**, 104486, https://doi.org/10.1016/j.earscirev.2023.104486

Dickinson, W.R. and Gehrels, G.E. 2009. Use of U–Pb ages of detrital zircons to infer maximum depositional ages of strata: a test against a Colorado Plateau Mesozoic database. *Earth and Planetary Science Letters*, **288**, 115–125, https://doi.org/10.1016/j.epsl.2009.09.013

Ding, L., Goswami, T.K., Cai, F.L., Baral, U., Sarmah, R.K. and Bezbaruah, D. 2022. Detrital zircon U–Pb ages of Tertiary sequences (Palaeocene-Miocene): Inner Fold Belt and Belt of Schuppen, Indo-Myanmar Ranges, India. *Geological Journal*, **57**, 5191–5206, https://doi.org/10.1002/gj.4446

Eroğlu, S., Siebel, W., Danišík, M., Pfänder, J.A. and Chen, F. 2013. Multi-system geochronological and isotopic constraints on age and evolution of the Gaoligongshan metamorphic belt and shear zone system in western Yunnan, China. *Journal of Asian Earth Sciences*, **73**, 218–239, https://doi.org/10.1016/j.jseaes.2013.03.031

Fareeduddin. 2015. Structure and petrology of the Nagaland-Manipur Hill Ophiolite Melange Zone, NE India: a fossil Tethyan subduction channel at the India–Burma plate boundary. *Episodes*, **38**, https://doi.org/10.18814/epiiugs/2015/v38i4/82426

Fisher, R. 1953. Dispersion on a sphere. *Proceedings of the Royal Society of London Series A: Mathematical and Physical Sciences*, **217**, 295–305, https://doi.org/10.1098/rspa.1953.0064

Gardiner, N.J., Searle, M.P., Robb, L.J. and Morley, C.K. 2015. Neo-Tethyan magmatism and metallogeny in Myanmar – an Andean analogue? *Journal of Asian Earth Sciences*, **106**, 197–215, https://doi.org/10.1016/j.jseaes.2015.03.015

Gardiner, N.J., Hawkesworth, C.J., Robb, L.J., Whitehouse, M.J., Roberts, N.M.W., Kirkland, C.L. and Evans, N.J. 2017. Contrasting granite metallogeny through the zircon record: a case study from Myanmar. *Scientific Reports*, **7**, 748, https://doi.org/10.1038/s41598-017-00832-2

Garzanti, E. 2019. The Himalayan Foreland Basin from collision onset to the present: a sedimentary-petrology perspective. *Geological Society, London, Special Publications*, **483**, 65–122, https://doi.org/10.1144/SP483.17

Garzanti, E., Wang, J-G., Vezzoli, G. and Limonta, M. 2016. Tracing provenance and sediment fluxes in the Irrawaddy River basin (Myanmar). *Chemical Geology*, **440**, 73–90, https://doi.org/10.1016/j.chemgeo.2016.06.010

Gentis, N., Licht, A., De Franceschi, D., Win, Z., Aung, D.W., Dupont-Nivet, G. and Boura, A. 2023. First fossil woods and palm stems from the mid Paleocene of Myanmar and their implications for biogeography and wood anatomy. *American Journal of Botany*, **111**, e16259, https://doi.org/10.1002/ajb2.16259

Gibbons, A.D., Whittaker, J.M. and Müller, R.D. 2013. The breakup of East Gondwana: assimilating constraints from Cretaceous ocean basins around India into a best-fit tectonic model: the Enderby Basin/East Gondwana breakup. *Journal of Geophysical Research: Solid Earth*, **118**, 808–822, https://doi.org/10.1002/jgrb.50079

Gibbons, A.D., Zahirovic, S., Müller, R.D., Whittaker, J.M. and Yatheesh, V. 2015. A tectonic model reconciling evidence for the collisions between India, Eurasia and intra-oceanic arcs of the central-eastern Tethys. *Gondwana Research*, **28**, 451–492, https://doi.org/10.1016/j.gr.2015.01.001

Godin, L., Grujic, D., Law, R.D. and Searle, M.P. 2006. Channel flow, ductile extrusion and exhumation in continental collision zones: an introduction. *Geological Society, London, Special Publications*, **268**, 1–23, https://doi.org/10.1144/GSL.SP.2006.268.01.01

Gough, A., Hall, R. and BouDagher-Fadel, M.K. 2020. Mid-Cenozoic fluvio-deltaic to marine environments of the Salin Sub-basin, Central Myanmar. *Journal of Asian Earth Sciences*, **90**, 104143, https://doi.org/10.1016/j.jseaes.2019.104143

Grimaldi, D.A., Engel, M.S. and Nascimbene, P.C. 2002. Fossiliferous Cretaceous Amber from Myanmar (Burma): its rediscovery, biotic diversity, and paleontological significance. *American Museum Novitates*, **3361**, 1–71, https://doi.org/10.1206/0003-0082(2002)361<0001:FCAFMB>2.0.CO;2

Hall, R. 2012. Late Jurassic–Cenozoic reconstructions of the Indonesian region and the Indian Ocean. *Tectonophysics*, **570–571**, 1–41, https://doi.org/10.1016/j.tecto.2012.04.021

Hansma, J. and Tohver, E. 2019. Paleomagnetism of Oligocene hot spot volcanics in Central Queensland, Australia. *Journal of Geophysical Research: Solid Earth*, **124**, 6280–6296, https://doi.org/10.1029/2019JB017639

Haproff, P.J., Zuza, A.V. *et al*. 2019. Geologic framework of the northern Indo-Burma Ranges and lateral correlation of Himalayan-Tibetan lithologic units across the

eastern Himalayan syntaxis. *Geosphere*, **15**, 856–881, https://doi.org/10.1130/GES02054.1

Heine, C., Müller, R.D. and Gaina, C. 2004. Reconstructing the lost eastern Tethys Ocean Basin: convergence history of the SE Asian margin and marine gateways. *In*: Clift, P., Kuhnt, W., Wang, P. and Hayes, D. (eds) *Continent-Ocean Interactions Within East Asian Marginal Seas Geophysical Monograph Series*, **149**, 37–54, American Geophysical Union, https://doi.org/10.1029/149GM03

Htay, H., Khin Zaw and Oo, T.T. 2017. Chapter 6. The mafic–ultramafic (ophiolitic) rocks of Myanmar. *Geological Society, London, Memoirs*, **48**, 117–141, https://doi.org/10.1144/M48.6

Hrouda, F. 1982. Magnetic anisotropy of rocks and its application in geology and geophysics. *Geophysical Surveys*, **5**, 37–82, https://doi.org/10.1007/BF01450244

Hu, X., Garzanti, E., Moore, T. and Raffi, I. 2015. Direct stratigraphic dating of India-Asia collision onset at the Selandian (middle Paleocene, 59 ± 1 Ma). *Geology*, **43**, 859–862, https://doi.org/10.1130/G36872.1

Hu, X., Garzanti, E., Wang, J., Huang, W., An, W. and Webb, A. 2016. The timing of India-Asia collision onset–facts, theories, controversies. *Earth-Science Reviews*, **160**, 264–299, https://doi.org/10.1016/j.earscirev.2016.07.014

Huang, H., Pérez-Pinedo, D. *et al*. 2021. At a crossroads: the late Eocene flora of central Myanmar owes its composition to plate collision and tropical climate. *Review of Palaeobotany and Palynology*, **291**, 104441, https://doi.org/10.1016/j.revpalbo.2021.104441

Huang, W., Lippert, P.C. *et al*. 2017. Remagnetization of the Paleogene Tibetan Himalayan carbonate rocks in the Gamba area: implications for reconstructing the lower plate in the India-Asia collision: carbonates were remagnetized in Gamba. *Journal of Geophysical Research: Solid Earth*, **122**, 808–825, https://doi.org/10.1002/2016JB013662

I'Anson, A., Elders, C. and McHarg, S. 2019. Marginal fault systems of the Northern Carnarvon Basin: evidence for multiple Palaeozoic extension events, North-West Shelf, Australia. *Marine and Petroleum Geology*, **101**, 211–229, https://doi.org/10.1016/j.marpetgeo.2018.11.040

Jackson, A., Jonkers, A.R.T. and Walker, M.R. 2000. Four centuries of geomagnetic secular variation from historical records. *Philosophical Transactions of the Royal Society A: Mathematical, Physical and Engineering Sciences*, **358**, 957–990, https://doi.org/10.1098/rsta.2000.0569

Jackson, M. and Worm, H.-U. 2001. Anomalous unblocking temperatures, viscosity and frequency-dependent susceptibility in the chemically-remagnetized Trenton limestone. *Physics of the Earth and Planetary Interiors*, **126**, 27–42, https://doi.org/10.1016/S0031-9201(01)00242-4

Jaeger, J.-J., Chavasseau, O. *et al*. 2019. New Eocene primate from Myanmar shares dental characters with African Eocene crown anthropoids. *Nature Communications*, **10**, 3531, https://doi.org/10.1038/s41467-019-11295-6

Jagoutz, O., Royden, L., Holt, A.F. and Becker, T.W. 2015. Anomalously fast convergence of India and Eurasia caused by double subduction. *Nature Geoscience*, **8**, 475–478, https://doi.org/10.1038/ngeo2418

Jagoutz, O., Bouilhol, P., Schaltegger, U. and Müntener, O. 2019. The isotopic evolution of the Kohistan Ladakh arc from subduction initiation to continent arc collision. *Geological Society, London, Special Publications*, **483**, 165–182, https://doi.org/10.1144/SP483.7

Jelinek, V. 1981. Characterization of the magnetic fabric of rocks. *Tectonophysics*, **79**, T63–T67, https://doi.org/10.1016/0040-1951(81)90110-4

Jonell, T.N., Giosan, L. *et al*. 2022. No modern Irrawaddy River until the late Miocene-Pliocene. *Earth and Planetary Science Letters*, **584**, 117516, https://doi.org/10.1016/j.epsl.2022.117516

Jouault, C., Perrichot, V. and Nel, A. 2021. New flat wasps from mid-Cretaceous Burmese amber deposits highlight the bethylid antiquity and paleobiogeography (Hymenoptera: Chrysidoidea). *Cretaceous Research*, **123**, 104772, https://doi.org/10.1016/j.cretres.2021.104772

Kapp, P. and DeCelles, P.G. 2019. Mesozoic–Cenozoic geological evolution of the Himalayan-Tibetan orogen and working tectonic hypotheses. *American Journal of Science*, **319**, 159–254, https://doi.org/10.2475/03.2019.01

Kellett, D.A., Grujic, D., Coutand, I., Cottle, J. and Mukul, M. 2013. The South Tibetan detachment system facilitates ultra rapid cooling of granulite-facies rocks in Sikkim Himalaya. *Tectonics*, **32**, 252–270, https://doi.org/10.1002/tect.20014

Kirschvink, J.L. 1980. The least-squares line and plane and the analysis of palaeomagnetic data. *Geophysical Journal International*, **62**, 699–718, https://doi.org/10.1111/j.1365-246X.1980.tb02601.x

Kissel, C., Barrier, E., Laj, C. and Lee, T-Q. 1986. Magnetic fabric in 'undeformed' marine clays from compressional zones. *Tectonics*, **5**, 769–781, https://doi.org/10.1029/TC005i005p00769

Khin, K. and Myitta, B. 1999. Marine transgression and regression in Miocene sequences of northern Pegu (Bago) Yoma, Central Myanmar. *Journal of Asian Earth Sciences*, **17**, 369–393, https://doi.org/10.1016/S0743-9547(98)00065-8

Khin Zaw, Meffre, S. *et al*. 2014. The oldest anthropoid primates in SE Asia: evidence from LA-ICP-MS U–Pb zircon age in the Late Middle Eocene Pondaung Formation, Myanmar. *Gondwana Research*, **26**, 122–131, https://doi.org/10.1016/j.gr.2013.04.007

Lamont, T.N., Searle, M.P. *et al*. 2021. Late Eocene-Oligocene granulite facies garnet-sillimanite migmatites from the Mogok Metamorphic belt, Myanmar, and implications for timing of slip along the Sagaing Fault. *Lithos*, **386–387**, 106027, https://doi.org/10.1016/j.lithos.2021.106027

Leloup, P.H., Lacassin, R. *et al*. 1995. The Ailao Shan-Red River shear zone (Yunnan, China), Tertiary transform boundary of Indochina. *Tectonophysics*, **251**, 3–84, https://doi.org/10.1016/0040-1951(95)00070-4

Li, S., Advokaat, E.L., van Hinsbergen, D.J.J., Koymans, M., Deng, C. and Zhu, R. 2017. Paleomagnetic constraints on the Mesozoic-Cenozoic paleolatitudinal and rotational history of Indochina and South China: review and updated kinematic reconstruction. *Earth-Science Reviews*, **171**, 58–77, https://doi.org/10.1016/j.earscirev.2017.05.007

Li, S., van Hinsbergen, D.J.J., Deng, C., Advokaat, E.L. and Zhu, R. 2018. Paleomagnetic constraints from the Baoshan area on the deformation of the Qiangtang-Sibumasu terrane around the Eastern Himalayan Syntaxis. *Journal of Geophysical Research: Solid Earth*, **123**, 977–997, https://doi.org/10.1002/2017JB015112

Li, Z., Ding, L. *et al*. 2020. Kinematic evolution of the West Burma block during and after India-Asia collision revealed by paleomagnetism. *Journal of Geodynamics*, **134**, 101690, https://doi.org/10.1016/j.jog.2019.101690

Liang, W., Garzanti, E., Hu, X., Resentini, A., Vezzoli, G. and Yao, W. 2022. Tracing erosion patterns in South Tibet: balancing sediment supply to the Yarlung Tsangpo from the Himalaya v. Lhasa Block. *Basin Research*, **34**, 411–439, https://doi.org/10.1111/bre.12625

Licht, A., France-Lanord, C., Reisberg, L., Fontaine, C., Soe, A.N. and Jaeger, J.-J. 2013. A palaeo Tibet–Myanmar connection? Reconstructing the Late Eocene drainage system of central Myanmar using a multi-proxy approach. *Journal of the Geological Society, London*, **170**, 929–939, https://doi.org/10.1144/jgs2012-126

Licht, A., Reisberg, L., France-Lanord, C., Naing Soe, A. and Jaeger, J.-J. 2016. Cenozoic evolution of the central Myanmar drainage system: insights from sediment provenance in the Minbu Sub-Basin. *Basin Research*, **28**, 237–251, https://doi.org/10.1111/bre.12108

Licht, A., Dupont-Nivet, G., Win, Z., Hnin Swe, H., Roperch, P. and Al, E. 2019. Paleogene evolution of the Burmese forearc basin and implications for the history of India-Asia convergence. *GSA Bulletin*, **131**, 730–748, https://doi.org/10.1130/B35002.1

Licht, A., Win, Z. *et al*. 2020. Magmatic history of central Myanmar and implications for the evolution of the Burma Terrane. *Gondwana Research*, **87**, 303–319, https://doi.org/10.1016/j.gr.2020.06.016

Limonta, M., Resentini, A., Carter, A., Bandopadhyay, P.C. and Garzanti, E. 2017. Chapter 10. Provenance of Oligocene Andaman sandstones (Andaman–Nicobar Islands): Ganga–Brahmaputra or Irrawaddy derived? *Geological Society, London, Memoirs*, **47**, 141–152, https://doi.org/10.1144/M47.10

Lin, T-H., Mitchell, A.H.G., Chung, S-L., Tan, X-B., Tang, J-T., Oo, T. and Wu, F-Y. 2019. Two parallel magmatic belts with contrasting isotopic characteristics from southern Tibet to Myanmar: zircon U–Pb and Hf isotopic constraints. *Journal of the Geological Society, London*, **176**, 574–587, https://doi.org/10.1144/jgs2018-072

Lindsey, E.O., Wang, Y. *et al*. 2023. Active subduction and strain partitioning in western Myanmar revealed by a dense survey GNSS network. *Earth and Planetary Science Letters*, **622**, 118384, https://doi.org/10.1016/j.epsl.2023.118384

Liu, C-Z., Zhang, C. *et al*. 2016. Petrology and geochemistry of mantle peridotites from the Kalaymyo and Myitkyina ophiolites (Myanmar): implications for tectonic settings. *Lithos*, **264**, 495–508, https://doi.org/10.1016/j.lithos.2016.09.013

Liu, Y., Tihelka, E., Yamamoto, S., Yin, Z., Huang, D., Tian, L. and Cai, C. 2020. The first fossil record of the rove beetle subfamily Protopselaphinae (Coleoptera: Staphylinidae) from mid-Cretaceous Burmese amber. *Cretaceous Research*, **110**, 104416, https://doi.org/10.1016/j.cretres.2020.104416

Lokho, K., Aitchison, J.C., Whiso, K., Lhoupenyi, D., Zhou, R. and Raju, D.S.N. 2020. Eocene foraminifers of the Naga Hills of Manipur, Indo-Myanmar Range (IMR): implications on age and basin evolution. *Journal of Asian Earth Sciences*, **191**, 104259, https://doi.org/10.1016/j.jseaes.2020.104259

Ma, X., Attia, S., Cawood, T., Cao, W., Xu, Z. and Li, H. 2022*a*. Arc tempos of the Gangdese batholith, southern Tibet. *Journal of Geodynamics*, **149**, 101897, https://doi.org/10.1016/j.jog.2022.101897

Ma, X., Xu, Z., Lusk, A.D., Erdmann, S., Chen, X. and Ma, S. 2023. Late Cretaceous tectonothermal events of the Gangdese belt, southern Tibet. *Geosphere*, **19**, 933–956, https://doi.org/10.1130/GES02602.1

Ma, Y., Wang, Q. *et al*. 2022*b*. Location of the Lhasa terrane in the Late Cretaceous and its implications for crustal deformation. *Palaeogeography, Palaeoclimatology, Palaeoecology*, **588**, 110821, https://doi.org/10.1016/j.palaeo.2021.110821

Martin, C.R., Jagoutz, O. *et al*. 2020. Paleocene latitude of the Kohistan–Ladakh arc indicates multistage India–Eurasia collision. *Proceedings of the National Academy of Sciences*, **117**, 29487–29494, https://doi.org/10.1073/pnas.2009039117

Maung, H. 1987. Transcurrent movements in the Burma–Andaman Sea region. *Geology*, **15**, 911, https://doi.org/10.1130/0091-7613(1987)15<911:TMITBS>2.0.CO;2

Maurin, T. and Rangin, C. 2009. Structure and kinematics of the Indo-Burmese Wedge: recent and fast growth of the outer wedge. *Tectonics*, **28**, TC2010, https://doi.org/10.1029/2008TC002276

McFadden, P.L. and McElhinny, M. 1988. The combined analysis of remagnetisation circles and direct observation in palaeomagnetism. *Earth and Planetary Science Letters*, **87**, 161–172, https://doi.org/10.1016/0012-821X(88)90072-6

Meng, J., Gilder, S.A., Li, Y., Wang, C. and Liu, T. 2020. Expanse of Greater India in the late Cretaceous. *Earth and Planetary Science Letters*, **542**, 116330, https://doi.org/10.1016/j.epsl.2020.116330

Merdith, A.S., Williams, S.E. *et al*. 2021. Extending full-plate tectonic models into deep time: linking the Neoproterozoic and the Phanerozoic. *Earth-Science Reviews*, **214**, 103477, https://doi.org/10.1016/j.earscirev.2020.103477

Metcalfe, I. 2013. Gondwana dispersion and Asian accretion: tectonic and palaeogeographic evolution of eastern Tethys. *Journal of Asian Earth Sciences*, **66**, 1–33, https://doi.org/10.1016/j.jseaes.2012.12.020

Metcalfe, I. 2017. Tectonic evolution of Sundaland. *Bulletin of the Geological Society of Malaysia*, **63**, 35, https://doi.org/10.7186/bgsm63201702

Mitchell, A.H.G. 1981. Phanerozoic plate boundaries in mainland SE Asia, the Himalayas and Tibet. *Journal of the Geological Society, London*, **138**, 109–122, https://doi.org/10.1144/gsjgs.138.2.0109

Mitchell, A.H.G. 1993. Cretaceous–Cenozoic tectonic events in the western Myanmar (Burma)–Assam region. *Journal of the Geological Society, London*, **150**, 1089–1102, https://doi.org/10.1144/gsjgs.150.6.1089

Mitchell, A. 2018*a*. Chapter 13 – Hukawng Basin, the Amber Mines, and the *Orbitolina* Limestone. *In*: *Geological Belts, Plate Boundaries, and Mineral Deposits in Myanmar*. Elsevier, 433–438, https://doi.org/10.1016/B978-0-12-803382-1.00013-4

Mitchell, A. 2018*b*. Chapter 14 – Jade Mines–Loimaw Uplift. *In*: *Geological Belts, Plate Boundaries, and Mineral Deposits in Myanmar*. Elsevier, 439–460, https://doi.org/10.1016/B978-0-12-803382-1.00014-6

Mitchell, A. 2018*c*. Chapter 15 – Kumon Range. *In*: *Geological Belts, Plate Boundaries, and Mineral Deposits in Myanmar*. Elsevier, 461–465, https://doi.org/10.1016/B978-0-12-803382-1.00015-8

Mitchell, A. 2018*d*. Chapter 9 – Popa–Loimye Magmatic Arc. *In*: *Geological Belts, Plate Boundaries, and Mineral Deposits in Myanmar*. Elsevier, 277–323, https://doi.org/10.1016/B978-0-12-803382-1.00009-2

Mitchell, A. 2018*e*. Chapter 8 – Tagaung–Myitkyina Belt and Katha–Gangaw Range. *In*: *Geological Belts, Plate Boundaries, and Mineral Deposits in Myanmar*. Elsevier, 253–273, https://doi.org/10.1016/B978-0-12-803382-1.00008-0

Mitchell, A. 2018*f*. Chapter 11 – The Indo-Burman Ranges and the Arakan Coastal Lowland. *In*: *Geological Belts, Plate Boundaries, and Mineral Deposits in Myanmar*. Elsevier, 351–389, https://doi.org/10.1016/B978-0-12-803382-1.00011-0

Mitchell, A. 2018*g*. *Geological Belts, Plate Boundaries, and Mineral Deposits in Myanmar*. Elsevier.

Mitchell, A., Chung, S-L., Oo, T., Lin, T-H. and Hung, C-H. 2012. Zircon U–Pb ages in Myanmar: magmatic–metamorphic events and the closure of a neo-Tethys ocean? *Journal of Asian Earth Sciences*, **56**, 1–23, https://doi.org/10.1016/j.jseaes.2012.04.019

Mon, C.T., Gong, X. *et al*. 2020. Insight into major active faults in Central Myanmar and the related geodynamic sources. *Geophysical Research Letters*, **47**, e2019GL086236, https://doi.org/10.1029/2019GL086236

Mon, C.T., Yang, S., Ren, C., He, Y., Thant, M. and Sein, K. 2023. New insight into the subducted Indian Plate beneath Central Myanmar based on seismic activity and focal mechanisms analysis. *Seismological Research Letters*, **94**, 2337–2347, https://doi.org/10.1785/0220220381

Morishita, T., Soe, H.M. *et al*. 2023. Origin and evolution of ultramafic rocks along the Sagaing Fault, Myanmar. *Journal of Earth Science*, **34**, 122–132, https://doi.org/10.1007/s12583-021-1435-x

Morley, C.K. 2017*a*. Chapter 4. Cenozoic rifting, passive margin development and strike-slip faulting in the Andaman Sea: a discussion of established v. new tectonic models. *Geological Society, London, Memoirs*, **47**, 27–50, https://doi.org/10.1144/M47.4

Morley, C.K. 2017*b*. Syn-kinematic sedimentation at a releasing splay in the northern Minwun Ranges, Sagaing Fault zone, Myanmar: significance for fault timing and displacement. *Basin Research*, **29**, 684–700, https://doi.org/10.1111/bre.12201

Morley, C.K. and Alvey, A. 2015. Is spreading prolonged, episodic or incipient in the Andaman Sea? Evidence from deepwater sedimentation. *Journal of Asian Earth Sciences*, **98**, 446–456, https://doi.org/10.1016/j.jseaes.2014.11.033

Morley, C.K. and Arboit, F. 2019. Dating the onset of motion on the Sagaing fault: evidence fromdetrital zircon and titanite U-Pb geochronology from the North-Minwun Basin, Myanmar. *Geology*, **47**, 581–585, https://doi.org/10.1130/G46321.1

Morley, C.K. and Wang, Y. 2023. The Cenozoic hyper-oblique collision zone of Indochina: a re-appraisal of escape tectonics. *Earth-Science Reviews*, **243**, 104453, https://doi.org/10.1016/j.earscirev.2023.104453

Morley, C.K., Naing, T.T., Searle, M. and Robinson, S.A. 2020. Structural and tectonic development of the Indo-Burma ranges. *Earth-Science Reviews*, **200**, 102992, https://doi.org/10.1016/j.earscirev.2019.102992

Morley, C.K., Chantraprasert, S., Kongchum, J. and Chenoll, K. 2021. The West Burma Terrane, a review of recent paleo-latitude data, its geological implications and constraints. *Earth-Science Reviews*, **220**, 103722, https://doi.org/10.1016/j.earscirev.2021.103722

Morley, C.K., Chantraprasert, S., Chenoll, K., Sootlek, P. and Jitmahantakul, S. 2023. Interaction of thin-skinned detached faults and basement-involved strike-slip faults on a transform margin: the Moattama Basin, Myanmar. *Geological Society, London, Special Publications*, **524**, 165–190, https://doi.org/10.1144/SP524-2021-90

Morón, S., Cawood, P.A., Haines, P.W., Gallagher, S.J., Zahirovic, S., Lewis, C.J. and Moresi, L. 2019. Paleozoic to Triassic continental-scale sediment provenance of the Canning, Officer and Northern Carnarvon Basins, Western Australia. *In*: Keep, M. and Moss, E.J. (eds) *The Sedimentary Basins of Western Australia V*. Proceedings of the Petroleum Exploration Society of Australia Symposium, Perth, WA, 20.

Müller, R.D., Cannon, J. *et al*. 2018. GPlates: building a virtual earth through deep time. *Geochemistry, Geophysics, Geosystems*, **19**, 2243–2261, https://doi.org/10.1029/2018GC007584

Müller, R.D., Zahirovic, S. *et al*. 2019. A global plate model including lithospheric deformation along major rifts and orogens since the triassic. *Tectonics*, **38**, 1884–1907, https://doi.org/10.1029/2018TC005462

Nagappa, Y. 1959. Foraminiferal biostratigraphy of the Cretaceous-Eocene succession in the India-Pakistan-Burma region. *Micropaleontology*, **5**, 145–177, https://doi.org/10.2307/1484208

Naing, T.T., Bussien, D.A., Winkler, W.H., Nold, M. and Von Quadt, A. 2014. Provenance study on Eocene–Miocene sandstones of the Rakhine Coastal Belt, Indo-Burman Ranges of Myanmar: geodynamic implications. *Geological Society, London, Special Publications*, **386**, 195–216, https://doi.org/10.1144/SP386.10

Naing, T.T., Robinson, S.A. *et al*. 2023. Age, depositional history and tectonics of the Indo-Myanmar Ranges, Myanmar. *Journal of the Geological Society, London*, **180**, jgs2022-091, https://doi.org/10.1144/jgs2022-091

Najman, Y., Appel, E. *et al*. 2010. Timing of India-Asia collision: geological, biostratigraphic, and palaeomagnetic constraints. *Journal of Geophysical Research*, **115**, B12416, https://doi.org/10.1029/2010JB007673

Najman, Y., Jenks, D. *et al*. 2017. The Tethyan Himalayan detrital record shows that India–Asia terminal collision occurred by 54 Ma in the Western Himalaya. *Earth and Planetary Science Letters*, **459**, 301–310, https://doi.org/10.1016/j.epsl.2016.11.036

Najman, Y., Mark, C., Barfod, D.N., Carter, A., Parrish, R., Chew, D. and Gemignani, L. 2019. Spatial and temporal trends in exhumation of the Eastern Himalaya and syntaxis as determined from a multitechnique detrital thermochronological study of the Bengal Fan. *GSA Bulletin*, **131**, 1607–1622, https://doi.org/10.1130/B35031.1

Najman, Y., Sobel, E.R. *et al*. 2020. The exhumation of the Indo-Burman Ranges, Myanmar. *Earth and Planetary Science Letters*, **530**, 115948, https://doi.org/10.1016/j.epsl.2019.115948

Najman, Y., Sobel, E.R. *et al*. 2022. The timing of collision between Asia and the West Burma Terrane, and the development of the Indo-Burman Ranges. *Tectonics*, **41**, e2021TC007057, https://doi.org/10.1029/2021TC007057

Oo, T., Hlaing, T. and Htay, N. 2002. Permian of Myanmar. *Journal of Asian Earth Sciences*, **20**, 683–689, https://doi.org/10.1016/S1367-9120(01)00074-8

Oryan, B., Betka, P.M. *et al*. 2023. New GNSS and geological data from the Indo-Burman subduction zone indicate active convergence on both a locked megathrust and the Kabaw Fault. *Journal of Geophysical Research: Solid Earth*, **128**, e2022JB025550, https://doi.org/10.1029/2022JB025550

Panda, D., Kundu, B., Gahalaut, V.K. and Rangin, C. 2018. Crustal deformation, spatial distribution of earthquakes and along strike segmentation of the Sagaing Fault, Myanmar. *Journal of Asian Earth Sciences*, **166**, 89–94, https://doi.org/10.1016/j.jseaes.2018.07.029

Panda, D., Kundu, B., Gahalaut, V.K. and Rangin, C. 2020. India-Sunda plate motion, crustal deformation, and seismic hazard in the Indo-Burmese Arc. *Tectonics*, **39**, e2019TC006034, https://doi.org/10.1029/2019TC006034

Patzelt, A., Li, H., Wang, J. and Appel, E. 1996. Palaeomagnetism of Cretaceous to Tertiary sediments from southern Tibet: evidence for the extent of the northern margin of India prior to the collision with Eurasia. *Tectonophysics*, **259**, 259–284.

Pivnik, D.A., Nahm, J., Tucker, R.S., Smith, G.O., Nyein, K., Nyunt, M. and Maung, P.H. 1998. Polyphase deformation in a fore-arc/back-arc basin, Salin Subbasin, Myanmar (Burma). *AAPG Bulletin*, **82**, 1837–1856.

Poinar, G. 2018. Burmese amber: evidence of Gondwanan origin and Cretaceous dispersion. *Historical Biology*, **31**, 1304–1309, https://doi.org/10.1080/08912963.2018.1446531

Prévot, M. 1981. Some aspects of magnetic viscosity in subaerial and submarine volcanic rocks. *Geophysical Journal International*, **66**, 169–192, https://doi.org/10.1111/j.1365-246X.1981.tb05952.x

Racey, A. 2018. Chapter 12 - Exploration history and petroleum geology of offshore Myanmar. *In*: Mitchell, A. (ed.) *Geological Belts, Plate Boundaries, and Mineral Deposits in Myanmar*. Elsevier, 391–431, https://doi.org/10.1016/B978-0-12-803382-1.00012-2

Rangin, C. 2017. Chapter 3. Active and recent tectonics of the Burma Platelet in Myanmar. *Geological Society, London, Memoirs*, **48**, 53–64, https://doi.org/10.1144/M48.3

Rangin, C. 2018. *The Western Sunda Basins and the India/Asia Collision: An Atlas*. Geotecto.

Rangin, C. and Sibuet, J.-C. 2017. Structure of the northern Bay of Bengal offshore Bangladesh: evidences from new multi-channel seismic data. *Marine and Petroleum Geology*, **84**, 64–75, https://doi.org/10.1016/j.marpetgeo.2017.03.020

Rangin, C., Maurin, T. and Masson, F. 2013. Combined effects of Eurasia/Sunda oblique convergence and East-Tibetan crustal flow on the active tectonics of Burma. *Journal of Asian Earth Sciences*, **76**, 185–194, https://doi.org/10.1016/j.jseaes.2013.05.018

Rasnitsyn, A.P. and Öhm-Kühnle, C. 2018. Three new female *Aptenoperissus* from mid-Cretaceous Burmese amber (Hymenoptera, Stephanoidea, Aptenoperissidae): unexpected diversity of paradoxical wasps suggests insular features of source biome. *Cretaceous Research*, **91**, 168–175, https://doi.org/10.1016/j.cretres.2018.06.004

Reeve, M.T., Magee, C., Bastow, I.D., McDermott, C., Jackson, C.A.-L., Bell, R.E. and Prytulak, J. 2021. Nature of the Cuvier Abyssal Plain crust, offshore NW Australia. *Journal of the Geological Society, London*, **178**, jgs2020-172, https://doi.org/10.1144/jgs2020-172

Reeve, M.T., Magee, C., Jackson, C.A.-L., Bell, R.E. and Bastow, I.D. 2022. Stratigraphic record of continental breakup, offshore NW Australia. *Basin Research*, **34**, 1220–1243, https://doi.org/10.1111/bre.12656

Replumaz, A. and Tapponnier, P. 2003. Reconstruction of the deformed collision zone Between India and Asia by backward motion of lithospheric blocks. *Journal of Geophysical Research: Solid Earth*, **108**, https://doi.org/10.1029/2001JB000661

Replumaz, A., Negredo, A.M., Guillot, S. and Villaseñor, A. 2010. Multiple episodes of continental subduction during India/Asia convergence: insight from seismic tomography and tectonic reconstruction. *Tectonophysics*, **483**, 125–134, https://doi.org/10.1016/j.tecto.2009.10.007

Replumaz, A., Guillot, S., Villaseñor, A. and Negredo, A.M. 2013. Amount of Asian lithospheric mantle subducted during the India/Asia collision. *Gondwana Research*, **24**, 936–945, https://doi.org/10.1016/j.gr.2012.07.019

Ridd, M.F. and Racey, A. 2015. Chapter 4. Onshore petroleum geology of Myanmar: Central Burma Depression. *Geological Society, London, Memoirs*, **45**, 21–50, https://doi.org/10.1144/M45.04

Roberts, A.P. 2015. Magnetic mineral diagenesis. *Earth-Science Reviews*, **151**, 1–47, https://doi.org/10.1016/j.earscirev.2015.09.010

Robinson, R.A.J., Brezina, C.A. *et al*. 2014. Large rivers and orogens: the evolution of the Yarlung Tsangpo–Irrawaddy system and the Eastern Himalayan Syntaxis. *Gondwana Research*, **26**, 112–121, https://doi.org/10.1016/j.gr.2013.07.002

Roperch, P. and Taylor, G.K. 1986. The importance of gyromagnetic remanence in alternating field demagnetization. Some new data and experiments on GRM and RRM. *Geophysical Journal International*, **87**, 949–965, https://doi.org/10.1111/j.1365-246X.1986.tb01978.x

Roperch, P., Chabernaud, T. and Calza, F. 1994. Magnetic properties of a volcanic-rich sedimentary sequence in the intra-arc Aoba Basin. *Proceedings of the Ocean Drilling Program, Scientific Results*, **134**, 491–507.

Rowley, D.B. 2019. Comparing paleomagnetic study means with apparent wander paths: a case study and paleomagnetic test of the Greater India Versus Greater Indian Basin Hypotheses. *Tectonics*, **38**, 722–740, https://doi.org/10.1029/2017TC004802

Rose, I.R., Zhang, Y. and Swanson-Hysell, N.L. 2022. Bayesian paleomagnetic Euler pole inversion for paleogeographic reconstruction and analysis. *Journal of Geophysical Research: Solid Earth*, **127**, https://doi.org/10.1029/2021JB023890

Royden, L.H., Burchfiel, B.C. and van der Hilst, R.D. 2008. The geological evolution of the Tibetan Plateau. *Science*, **321**, 1054–1058, https://doi.org/10.1126/science.1155371

Scotese, C.R. and Wright, N. 2018. PALEOMAP paleodigital elevation models (PaleoDEMS) for the Phanerozoic. Paleomap Project, https://www.earthbyte.org/paleodem-resource-scotese-and-wright-2018/

Searle, M.P., Noble, S.R., Cottle, J.M., Waters, D.J., Mitchell, A.H.G., Hlaing, T. and Horstwood, M.S.A. 2007. Tectonic evolution of the Mogok metamorphic belt, Burma (Myanmar) constrained by U–Th–Pb dating of metamorphic and magmatic rocks. *Tectonics*, **26**, https://doi.org/10.1029/2006TC002083

Searle, M.P., Morley, C.K., Waters, D.J., Gardiner, N.J., Htun, U.K., Nu, T.T. and Robb, L.J. 2017. Chapter 12. Tectonic and metamorphic evolution of the Mogok Metamorphic and Jade Mines belts and ophiolitic terranes of Burma (Myanmar). *Geological Society, London, Memoirs*, **48**, 261–293, https://doi.org/10.1144/M48.12

Searle, M.P., Garber, J.M., Hacker, B.R., Htun, K., Gardiner, N.J., Waters, D.J. and Robb, L.J. 2020. Timing of syenite-charnockite magmatism and ruby-and sapphire metamorphism in the Mogok valley region, Myanmar. *Tectonics*, **39**, e2019TC005998, https://doi.org/10.1029/2019TC005998

Searle, M.P., Palin, R.M., Gardiner, N.J., Htun, K. and Wade, J. 2023. The Burmese Jade Mines belt: origins of jadeitites, serpentinites and ophiolitic peridotites and gabbros. *Journal of the Geological Society, London*, **180**, jgs2023-004, https://doi.org/10.1144/jgs2023-004

Sengupta, S., Acharyya, S.K., Van Den Hul, H.J. and Chattopadhyay, B. 1989. Geochemistry of volcanic rocks from the Naga Hills Ophiolites, northeast India and their inferred tectonic setting. *Journal of the Geological Society, London*, **146**, 491–498, https://doi.org/10.1144/gsjgs.146.3.0491

Seton, M., Müller, R.D. *et al*. 2012. Global continental and ocean basin reconstructions since 200 Ma. *Earth-Science Reviews*, **113**, 212–270, https://doi.org/10.1016/j.earscirev.2012.03.002

Sevastjanova, I., Hall, R., Rittner, M., Paw, S.M.T.L., Naing, T.T., Alderton, D.H. and Comfort, G. 2016. Myanmar and Asia united, Australia left behind long ago. *Gondwana Research*, **32**, 24–40, https://doi.org/10.1016/j.gr.2015.02.001

Shen, F., Royden, L.H. and Burchfiel, B.C. 2001. Large-scale crustal deformation of the Tibetan Plateau. *Journal of Geophysical Research: Solid Earth*, **106**, 6793–6816, https://doi.org/10.1029/2000JB900389

Sibuet, J.-C., Klingelhoefer, F., Huang, Y-P., Yeh, Y-C., Rangin, C., Lee, C-S. and Hsu, S-K. 2016. Thinned continental crust intruded by volcanics beneath the northern Bay of Bengal. *Marine and Petroleum Geology*, **77**, 471–486, https://doi.org/10.1016/j.marpetgeo.2016.07.006

Singh, A.K., Chung, S-L., Bikramaditya, R.K. and Lee, H.Y. 2017. New U–Pb zircon ages of plagiogranites from the Nagaland–Manipur Ophiolites, Indo-Myanmar Orogenic Belt, NE India. *Journal of the Geological Society, London*, **174**, 170–179, https://doi.org/10.1144/jgs2016-048

Snowball, I.F. 1997. Gyroremanent magnetization and the magnetic properties of greigite-bearing clays in southern Sweden. *Geophysical Journal International*, **129**, 624–636, https://doi.org/10.1111/j.1365-246X.1997.tb04498.x

Socquet, A., Goffé, B., Pubellier, M. and Rangin, C. 2002. Le métamorphisme Tardi-Crétacé à Éocène des zones internes de la chaı^ne Indo-Birmane (Myanmar occidental): implications géodynamiques. *Comptes Rendus Geoscience*, **334**, 573–580, https://doi.org/10.1016/S1631-0713(02)01796-0

Socquet, A., Vigny, C., Chamot-Rooke, N., Simons, W., Rangin, C. and Ambrosius, B. 2006. India and Sunda plates motion and deformation along their boundary in Myanmar determined by GPS. *Journal of Geophysical Research: Solid Earth*, **111**, B05406, https://doi.org/10.1029/2005JB003877

Steckler, M.S., Mondal, D.R. *et al*. 2016. Locked and loading megathrust linked to active subduction beneath the Indo-Burman Ranges. *Nature Geoscience*, **9**, 615–618, https://doi.org/10.1038/ngeo2760

Talwani, M., Desa, M.A., Ismaiel, M. and Sree Krishna, K. 2016. The Tectonic origin of the Bay of Bengal and Bangladesh: the Tectonic Origin of the Bay of Bengal. *Journal of Geophysical Research: Solid Earth*, **121**, 4836–4851, https://doi.org/10.1002/2015JB012734

Talwani, M., Krishna, K.S., Ismaiel, M. and Desa, M.A. 2017. Comment on a paper by Sibuet *et al.* (2016) entitled 'Thinned continental crust intruded by volcanics beneath the northern Bay of Bengal'. *Marine and Petroleum Geology*, **88**, 1123–1125, https://doi.org/10.1016/j.marpetgeo.2016.12.009

Tapponnier, P., Peltzer, G., Le Dain, A.Y., Armijo, R. and Cobbold, P. 1982. Propagating extrusion tectonics in Asia: new insights from simple experiments with plasticine. *Geology*, **10**, 611–616, https://doi.org/10.1130/0091-7613(1982)10<611:PETIAN>2.0.CO;2

Tauxe, L. and Kent, D.V. 1984. Properties of a detrital remanence carried by haematite from study of modern river deposits and laboratory redeposition experiments. *Geophysical Journal of the Royal Astronomical Society*, **76**, 543–561, https://doi.org/10.1111/j.1365-246X.1984.tb01909.x

Thein, M. 2015. The Pre-Tertiary carbonate rocks exposed at the NE margin of the Central Myanmar Basin and their development history. *Journal of the Myanmar Geosciences Society*, **6**, 1–22.

Thein, M. and Maung, M. 2017. Chapter 8. The Eastern (Back-arc) Basin of Central Myanmar: basement rocks, lithostratigraphic units, palaeocurrents, provenance and developmental history. *Geological Society, London, Memoirs*, **48**, 169–183, https://doi.org/10.1144/M48.8

Thompson, J.O., Moulin, M., Aslanian, D., de Clarens, P. and Guillocheau, F. 2019. New starting point for the

Indian Ocean: second phase of breakup for Gondwana. *Earth-Science Reviews*, **191**, 26–56, https://doi.org/10.1016/j.earscirev.2019.01.018

Tong, Y-B., Yang, Z., Zheng, L-D., Xu, Y-L., Wang, H., Gao, L. and Hu, X-Z. 2013. Internal crustal deformation in the northern part of Shan-Thai Block: new evidence from paleomagnetic results of Cretaceous and Paleogene redbeds. *Tectonophysics*, **608**, 1138–1158, https://doi.org/10.1016/j.tecto.2013.06.031

Tong, Y-B., Yang, Z., Wang, H., Gao, L., An, C-Z., Zhang, X-D. and Xu, Y-C. 2015. The Cenozoic rotational extrusion of the Chuan Dian Fragment: new paleomagnetic results from Paleogene red-beds on the southeastern edge of the Tibetan Plateau. *Tectonophysics*, **658**, 46–60, https://doi.org/10.1016/j.tecto.2015.07.007

Tong, Y., Yang, Z., Pei, J., Wang, H., Wu, Z. and Li, J. 2021. Crustal clockwise rotation of the Southeastern Edge of the Tibetan Plateau since the Late Oligocene. *Journal of Geophysical Research: Solid Earth*, **126**, e2020JB020153, https://doi.org/10.1029/2020JB020153

Torsvik, T.H., Van der Voo, R. *et al*. 2012. Phanerozoic polar wander, palaeogeography and dynamics. *Earth-Science Reviews*, **114**, 325–368, https://doi.org/10.1016/j.earscirev.2012.06.007

Tun, S.T. and Watkinson, I.M. 2017. Chapter 19. The Sagaing Fault, Myanmar. *Geological Society, London, Memoirs*, **48**, 413–441, https://doi.org/10.1144/M48.19

Ueno, K., Thein, M. and Barber, A.J. 2016. Permian fusuline fauna from the Minwun Range, Central Myanmar. Paper presented at the 5th Symposium of the International Geosciences Programme (IGCP), Yangon, Myanmar, 27–28.

United Nations 1978. *Geology and Exploration Geochemistry of the Pinlebu-Banmauk area, Sagaing Division, northern Burma*. Geological Survey and Exploration Project, United Nations Development Programme, Technical Report UN/B URi72/002, No 2.

Vaes, B., Van Hinsbergen, D.J.J. *et al*. 2023. A global apparent polar wander path for the last 320 Ma calculated from site-level paleomagnetic data. *Earth-Science Reviews*, **245**, 104547, https://doi.org/10.1016/j.earscirev.2023.104547

Van Hinsbergen, D.J.J., Kapp, P., Dupont-Nivet, G., Lippert, P.C., DeCelles, P.G. and Torsvik, T.H. 2011. Restoration of Cenozoic deformation in Asia and the size of Greater India. *Tectonics*, **30**, TC5003, https://doi.org/10.1029/2011TC002908

Van Hinsbergen, D.J., Lippert, P.C., Dupont-Nivet, G., McQuarrie, N., Doubrovine, P.V., Spakman, W. and Torsvik, T.H. 2012. Greater India Basin hypothesis and a two-stage Cenozoic collision between India and Asia. *Proceedings of the National Academy of Sciences*, **109**, 7659–7664, https://doi.org/10.1073/pnas.1117262109

van Hinsbergen, D.J.J., Lippert, P.C., Li, S., Huang, W., Advokaat, E.L. and Spakman, W. 2019. Reconstructing Greater India: paleogeographic, kinematic, and geodynamic perspectives. *Tectonophysics*, **760**, 69–94, https://doi.org/10.1016/j.tecto.2018.04.006

Vannay, J.-C., Grasemann, B., Rahn, M., Frank, W., Carter, A., Baudraz, V. and Cosca, M. 2004. Miocene to Holocene exhumation of metamorphic crustal wedges in the NW Himalaya: evidence for tectonic extrusion coupled to fluvial erosion. *Tectonics*, **23**, 2002TC001429, https://doi.org/10.1029/2002TC001429

Vermeesch, P. 2021. On the treatment of discordant detrital zircon U–Pb data. *Geochronology*, **3**, 247–257, https://doi.org/10.5194/gchron-3-247-2021

Vigny, C., Socquet, A. *et al*. 2003. Present-day crustal deformation around Sagaing fault, Myanmar. *Journal of Geophysical Research: Solid Earth*, **108**, https://doi.org/10.1029/2002JB001999

Wang, J-G., Wu, F-Y., Tan, X-C. and Liu, C-Z. 2014. Magmatic evolution of the Western Myanmar Arc documented by U–Pb and Hf isotopes in detrital zircon. *Tectonophysics*, **612–613**, 97–105, https://doi.org/10.1016/j.tecto.2013.11.039

Wang, J-G., Wu, F-Y., Garzanti, E., Hu, X., Ji, W-Q., Liu, Z-C. and Liu, X-C. 2016. Upper Triassic turbidites of the northern Tethyan Himalaya (Langjiexue Group): the terminal of a sediment-routing system sourced in the Gondwanide Orogen. *Gondwana Research*, **34**, 84–98, https://doi.org/10.1016/j.gr.2016.03.005

Wang, Y., Wang, Y. *et al*. 2022. Kinematics and $^{40}Ar/^{39}Ar$ geochronology of the Lincang-Inthanon tectonic belt: implication for Cenozoic tectonic extrusion of SE Asia. *GSA Bulletin*, **134**, 2854–2866, https://doi.org/10.1130/B36187.1

Wessel, P., Luis, J.F., Uieda, L., Scharroo, R., Wobbe, F., Smith, W.H.F. and Tian, D. 2019. The Generic Mapping Tools Version 6. *Geochemistry, Geophysics, Geosystems*, **20**, 5556–5564, https://doi.org/10.1029/2019GC008515

Westerweel, J., Roperch, P. *et al*. 2019. Burma Terrane part of the Trans-Tethyan arc during collision with India according to palaeomagnetic data. *Nature Geoscience*, **12**, 863–868, https://doi.org/10.1038/s41561-019-0443-2

Westerweel, J., Licht, A. *et al*. 2020. Burma Terrane Collision and Northward Indentation in the Eastern Himalayas recorded in the Eocene–Miocene Chindwin Basin (Myanmar). *Tectonics*, **39**, https://doi.org/10.1029/2020TC006413

Xing, L. and Qiu, L. 2020. Zircon U Pb age constraints on the mid-Cretaceous Hkamti amber biota in northern Myanmar. *Palaeogeography, Palaeoclimatology, Palaeoecology*, **558**, 109960, https://doi.org/10.1016/j.palaeo.2020.109960

Yan, Y., Huang, B., Zhao, J., Zhang, D., Liu, X., Charusiri, P. and Veeravinantanakul, A. 2017. Large southward motion and clockwise rotation of Indochina throughout the Mesozoic: paleomagnetic and detrital zircon U–Pb geochronological constraints. *Earth and Planetary Science Letters*, **459**, 264–278, https://doi.org/10.1016/j.epsl.2016.11.035

Yang, T., Ma, Y. *et al*. 2015. New insights into the India–Asia collision process from Cretaceous paleomagnetic and geochronologic results in the Lhasa terrane. *Gondwana Research*, **28**, 625–641, https://doi.org/10.1016/j.gr.2014.06.010

Yang, T., Jin, J. *et al*. 2019. Precollisional latitude of the Northern Tethyan Himalaya from the paleocene redbeds and its implication for Greater India and the India–Asia collision. *Journal of Geophysical Research: Solid Earth*, **124**, 10777–10798, https://doi.org/10.1029/2019JB017927

Yao, W., Ding, L., Cai, F., Wang, H., Xu, Q. and Zaw, T. 2017. Origin and tectonic evolution of upper Triassic Turbidites in the Indo-Burman ranges, West Myanmar. *Tectonophysics*, **721**, 90–105, https://doi.org/10.1016/j.tecto.2017.09.016

Yi, Z., Appel, E. and Huang, B. 2017. Comment on 'Remagnetization of the Paleogene Tibetan Himalayan carbonate rocks in the Gamba area: implications for reconstructing the lower plate in the India–Asia collision' by Huang et al. *Journal of Geophysical Research: Solid Earth*, **122**, 4852–4858, https://doi.org/10.1002/2017JB014353

Yuan, J., Yang, Z. *et al*. 2020. Rapid drift of the Tethyan Himalaya terrane before two-stage India–Asia collision. *National Science Review*, **8**, nwaa173, https://doi.org/10.1093/nsr/nwaa173

Yui, T-F., Fukoyama, M., Iizuka, Y., Wu, C-M., Wu, T-W., Liou, J.G. and Grove, M. 2013. Is Myanmar jadeitite of Jurassic age? A result from incompletely recrystallized inherited zircon. *Lithos*, **160–161**, 268–282, https://doi.org/10.1016/j.lithos.2012.12.011

Zahirovic, S., Seton, M. and Müller, R.D. 2014. The Cretaceous and Cenozoic tectonic evolution of Southeast Asia. *Solid Earth*, **5**, 227–273, https://doi.org/10.5194/se-5-227-2014

Zahirovic, S., Matthews, K.J., Flament, N., Müller, R.D., Hill, K.C., Seton, M. and Gurnis, M. 2016. Tectonic evolution and deep mantle structure of the eastern Tethys since the latest Jurassic. *Earth-Science Reviews*, **162**, 293–337, https://doi.org/10.1016/j.earscirev.2016.09.005

Zaman, H. and Torii, M. 1999. Palaeomagnetic study of Cretaceous red beds from the eastern Hindukush ranges, northern Pakistan: palaeoreconstruction of the Kohistan-Karakoram composite unit before the India–Asia collision. *Geophysical Journal International*, **136**, 719–738, https://doi.org/10.1046/j.1365-246x.1999.00757.x

Zhang, B., Zhang, J., Zhong, D., Yang, L., Yue, Y. and Yan, S. 2012. Polystage deformation of the Gaoligong metamorphic zone: Structures, $^{40}Ar/^{39}Ar$ mica ages, and tectonic implications. *Journal of Structural Geology*, **37**, 1–18, https://doi.org/10.1016/j.jsg.2012.02.007

Zhang, J., Xiao, W., Windley, B.F., Cai, F., Sein, K. and Naing, S. 2017*a*. Early Cretaceous wedge extrusion in the Indo-Burma Range accretionary complex: implications for the Mesozoic subduction of Neotethys in SE Asia. *International Journal of Earth Sciences*, **106**, 1391–1408, https://doi.org/10.1007/s00531-017-1468-7

Zhang, P., Mei, L., Hu, X., Li, R., Wu, L., Zhou, Z. and Qiu, H. 2017*b*. Structures, uplift, and magmatism of the Western Myanmar Arc: constraints to mid-Cretaceous–Paleogene tectonic evolution of the western Myanmar continental margin. *Gondwana Research*, **52**, 18–38, https://doi.org/10.1016/j.gr.2017.09.002

Zhang, P., Najman, Y. *et al*. 2019*a*. Palaeodrainage evolution of the large rivers of East Asia, and Himalayan-Tibet tectonics. *Earth-Science Reviews*, **192**, 601–630, https://doi.org/10.1016/j.earscirev.2019.02.003

Zhang, P., Jiang, S-Y., Donelick, R.A., Li, R., Soares, C.J. and Mei, L. 2023. Frontal expansion of an accretionary wedge under highly oblique plate convergence: Southern Indo-Burman Ranges, Myanmar. *GSA Bulletin*, **135**, 2348–2374, https://doi.org/10.1130/B36560.1

Zhang, X., Chung, S-L., Lai, Y-M., Ghani, A.A., Murtadha, S., Lee, H-Y. and Hsu, C. 2019*b*. A 6000-km-long Neo-Tethyan arc system with coherent magmatic flare-ups and lulls in South Asia. *Geology*, **47**, 573–576, https://doi.org/10.1130/G46172.1

Zhang, X., Chung, S-L. *et al*. 2021. Tracing Argoland in eastern Tethys and implications for India-Asia convergence. *GSA Bulletin*, **133**, 1712–1722, https://doi.org/10.1130/B35772.1

Zhang, Y-C., Aung, K.P. *et al*. 2020. Middle Permian fusulines from the Thitsipin Formation of Shan State, Myanmar and their palaeobiogeographical and palaeogeographical implications. *Papers in Palaeontology*, **6**, 293–327, https://doi.org/10.1002/spp2.1298

Zheng, D., Chang, S-C. *et al*. 2018. A Late Cretaceous amber biota from central Myanmar. *Nature Communications*, **9**, 3170, https://doi.org/10.1038/s41467-018-05650-2